University of Colorado, Boulder
CU Scholar

Chemical & Biological Engineering Graduate Theses & Dissertations

Chemical & Biological Engineering

Spring 1-1-2012

Investigation of Kinetic Theory for Rapid Flows of Polydisperse and/or Continuous Particle Size Distributions

John Aaron Murray
University of Colorado at Boulder, john.a.murray@colorado.edu

Follow this and additional works at: http://scholar.colorado.edu/chbe_gradetds

 Part of the Chemical Engineering Commons

Recommended Citation
Murray, John Aaron, "Investigation of Kinetic Theory for Rapid Flows of Polydisperse and/or Continuous Particle Size Distributions" (2012). *Chemical & Biological Engineering Graduate Theses & Dissertations*. Paper 27.

This Thesis is brought to you for free and open access by Chemical & Biological Engineering at CU Scholar. It has been accepted for inclusion in Chemical & Biological Engineering Graduate Theses & Dissertations by an authorized administrator of CU Scholar. For more information, please contact cuscholaradmin@colorado.edu.

INVESTIGATION OF KINETIC THEORY FOR RAPID FLOWS OF POLYDISPERSE AND CONTINUOUS PARTICLE SIZE DISTRIBUTIONS

by

JOHN AARON MURRAY

B.S. in Chemical Engineering, Rose-Hulman Institute of Technology, 2009

A thesis submitted to the

Faculty of the Graduate School of the

University of Colorado in partial fulfillment

of the requirement for the degree of

Master of Science

Department of Chemical and Biological Engineering

2012

This thesis entitled:
Investigation of Kinetic Theory for Rapid Flows of Polydisperse and/or Continuous Particle Size Distributions
written by John Aaron Murray
has been approved by the Department of Chemical and Biological Engineering

Christine M. Hrenya, Professor

Arthi Jayaraman, Assistant Professor

Alan W. Weimer, Professor

August 2012

The final copy of this thesis has been examined by the signatories, and we find that both the content and the form meet acceptable presentation standards of scholarly work in the above mentioned discipline

Murray, John Aaron (M.S., Chemical and Biological Engineering)

Investigation of Kinetic Theory for Rapid Flows of Polydisperse and Continuous Particle Size Distributions

Dissertation directed by Professor Christine M. Hrenya

Natural and industrial granular flows often consist of several particle sizes, approximately forming a *continuous* particle size distribution (PSD). Continuous PSDs are ubiquitous, though existing kinetic-theory-based, hydrodynamic models for rapid granular flows are limited to a *discrete* number of species, many restricted to only two particle species. The objective of this effort is threefold: (i) to determine the importance of finite-volume (non-dilute) effects of solid particles in binary mixtures, (ii) to determine the minimum number of discrete particle species needed to accurately approximate a continuous PSD, and (iii) to validate discrete approximations of continuous PSDs applied to a kinetic-theory-based model via comparison with MD simulations.

With regard to the first objective, the recent kinetic theory (KT) model proposed by Garzó, Hrenya and Dufty (GHD) [Phys. Rev. E 76, 31303 and 031304 (2007)], is used as the basis for this work. This theory is derived rigorously from the Enskog equation, and thus can be applied to moderately dense concentrations. To demonstrate the significance of the dense-phase treatment relative to its dilute counterpart, the ratio of dense-to-dilute predictions of all relevant transport coefficients and equations of state are plotted over a range of physical parameters (volume fraction, coefficients of restitution, material density ratio, diameter ratio, and mixture composition). Results reveal the deviation between the two treatments can become quite large (> 100%) even at moderate values of the physical parameters. Such information is useful when choosing which theory is most applicable to a given situation, since the dilute theory offers

relative simplicity and the dense theory offers significantly improved accuracy for even fairly low concentrations (~1 order of magnitude difference for a volume fraction of $\phi = 0.1$).

Focusing on the second objective, the number of *discrete* species required to accurately approximate a *continuous* PSD is determined in two separate studies. The first study includes an examination of several transport coefficients of a KT model that depend only on the physical parameters of the granular mixture. The focus of the second study is the prediction of solids fraction and granular temperature profiles for granular mixtures in bounded conduction, which includes the effects of segregation unlike the first study. With regard to the former, several analytic (Gaussian and lognormal) and experimental (coal and lunar soil simulants) distributions are investigated. Single-valued transport coefficients (pressure, shear viscosity, etc.) of the granular mixture given by the polydisperse theory of Garzó, Hrenya and Dufty [Phys. Rev. E 76, 31303 and 031304 (2007)] are compared using an increasing number of species s to approximate the given PSD. These discrete approximations are determined by matching the first $2s$ moments of the approximation and the given continuous distribution. Relatively few species (~3) are required to approximate moderately wide distributions (Gaussian, lognormal), whereas the widest distributions (lunar soil simulants) require a larger, though still moderate, number of species (~7). With regard to the second method used to study discrete approximations of continuous PSDs, discrete approximations of Gaussian and lognormal distributions only are examined. In this study, the solids fraction and granular temperature profiles for a bounded conduction system are compared using an increasing number of species s to approximate the given PSD. This comparison is carried out for a moderately dilute, highly elastic system ($\phi = 0.05$, $\alpha = 0.99$). Unlike the first study, this segregating system involves transport coefficients that are not single-valued (e.g., ordinary and thermal diffusion). Because the transport coefficients

involved with a segregating system are different than those associated with the study of single-valued transport coefficients, one cannot be certain *a priori* whether or not the minimum number of species needed for the discrete approximations from the two studies will agree. However, results of this effort show that both methods for establishing a discrete approximation of a continuous PSD yield similar values with respect to the Gaussian and lognormal distributions analyzed.

Regarding the third objective, a comparison between kinetic theory predictions and MD simulations for a simple shear flow of both Gaussian and lognormal PSDs reveal essentially no loss of accuracy stemming from the polydisperse theory itself (as compared to theories for monodisperse systems) or from the discrete approximations of continuous PSDs used in the polydisperse theory. Also, a comparison between kinetic theory predictions and MD simulations of solids fraction and granular temperature profiles for a bounded conduction system shows that kinetic theory predictions maintain accuracy in a system known to exhibit moderate levels of species segregation.

DEDICATION

To Mom and Dad,
who have always guided me in the right direction

ACKNOWLEDGEMENTS

I am very grateful for the funding support provided by the Department of Energy (DE-FC26-07NT43098) and the National Science Foundation (CBET-0318999). Also, I am appreciative of the funding support by the Department of Energy (DE-FC26-07NT43098) and the National Aeronautics and Space Administration (NNX09AD07A).

Several individuals had a hand in the work presented in here. First, I would like to thank Christine Hrenya, an advisor who truly offered guidance, insight, and inspiration throughout the culmination of my research. Also, I would like to thank Vicente Garzó, Sofiane Benyahia, and Phillip Metzger for the several fruitful discussions and collaborative works. Thanks to Larry Shadle of DOE NETL for providing the bidisperse gasifier data, Rodney Fox for providing code to obtain the discrete approximations, and, of course, the past and present members of the Hrenya Research Group for the continued assistance and support.

TABLE OF CONTENTS

LIST OF FIGURES

LIST OF TABLES

CHAPTER 1

INTRODUCTION

1.1 Motivation

Rapid solids flows are quite prevalent in both nature (e.g., landslides, planetary rings) and industry (e.g., pharmaceutical processing, high-velocity fluidized beds), though much remains to be understood. Predicting the behavior of a rapid solids flow is similar to that of a molecular gas in the sense that collisions are assumed binary and instantaneous. However, granular flows depend on several other physical aspects, such as dissipative collisions which have no molecular counterpart, and polydispersity, which is the focus of this thesis work. The vast majority of previous work on polydispersity has been limited to binary mixtures. Extending beyond this limit will allow for a better understanding of natural and industrial granular flows.

Polydisperse mixtures contain multiple particle species of different sizes and/or masses, many times resulting in a continuous particle size distribution (PSD). For an example of a continuous PSD observed in nature, see Figure 1.1, which shows a PSD of a lunar soil simulant. It is important to note that the PSD of lunar regolith (i.e., lunar soil) spans several orders of magnitude. Such polydispersity not only impacts the continuum flow quantities like solid-phase stress, but also gives rise to a phenomenon with no monodisperse counterpart, namely species segregation or the de-mixing of unlike particles [1-4]. Depending on the desired application, particle segregation may be a desired or an undesired effect. Consequently, an accurate model of a polydisperse solids mixture lends itself to a variety of non-trivial applications, such as the design of coal and/or biomass gasifiers for energy production. In this thesis work, particular

attention is given to *continuous* PSDs, as there are numerous practical applications and relatively few previous works compared to that of binary mixtures.

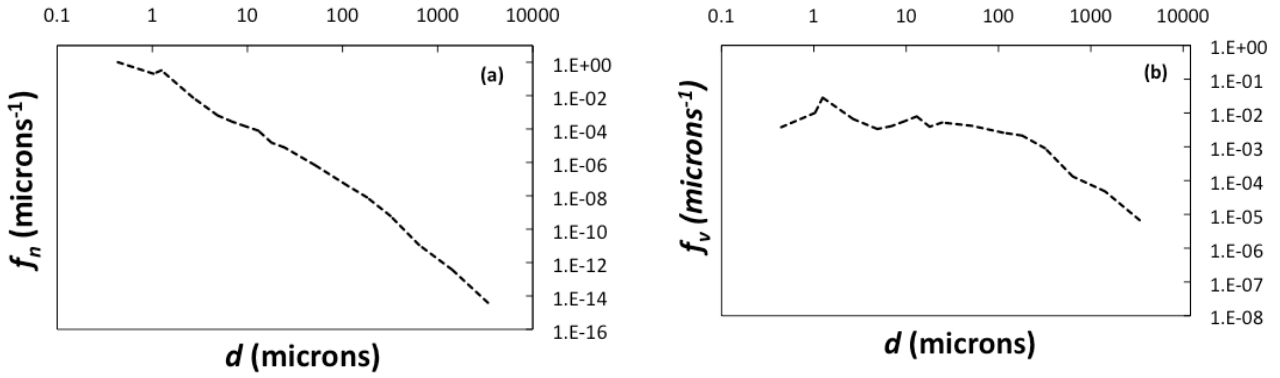

Figure 1.1: Frequency distributions of lunar soil simulant (OB-1) in terms of a **(a)** number (f_n) and **(b)** mass (f_v) basis.

1.2 Modeling of Polydisperse, Rapid Granular Flows

The mathematical modeling of the behavior of a rapid solids flow is possible using two different approaches. The first approach, known as a molecular dynamics (MD) simulation, is to consider every particle in the system, and impose the laws of motion to each particle as it progresses through space and time. Another approach, known as a continuum model, or more specifically a kinetic-theory (KT) based model, utilizes local averaging to obtain Navier-Stokes-like equations. Because of the pros and cons associated with each approach mentioned, the method of choice depends on the application. Namely, because MD simulations track every particle position and velocity, providing extremely detailed results with relatively few assumptions. However, MD simulations are very computationally expensive, such that application to granular flows on an industrial scale is not currently feasible. Continuum models do not involve the tracking of particles, but instead involve the solution of hydrodynamic (locally-averaged) variable; the averaging which leads to the governing equations to constitutive quantities, which require constitutive models. The constitutive models are derived based on the

kinetic theory analogy. Consequently, continuum models are applicable to large-scale systems and offer relative ease in computation. However, due to the averaging procedure and the subsequent requirement for constitutive relations, a KT model involves more assumptions than MD simulation.

1.2.1 Kinetic Theory Models

1.2.1.1 Assumptions and Comparison

The scope of current research pertains to polydisperse mixtures of inelastic grains (i.e., negligible fluid phase) engaging in instantaneous, binary collisions (i.e., rapid flows). Numerous previous contributors have proposed continuum theories for such systems (for recent review, see Ref. [4]), and the application of these theories has led to a better understanding of the mechanisms by which de-mixing occurs [5, 6-13]. Nevertheless, the improvement of existing models remains an active area of research due to differences in the derivation process. More specifically, one or both of the following simplifications have been incorporated in the vast majority of previous models: Maxwellian velocity distribution [14-17, 25], and/or an equipartition of energy [18, 19]. (The theories proposed by Rahaman et al. [17] as well as Iddir and Arastoopour [25] assumed a Maxwellian velocity distribution between unlike particles only.) The aforementioned assumptions are strictly true for systems of perfectly elastic spheres in a uniform steady state [20], but not so for inelastic grains. Furthermore, numerous studies have demonstrated the influence of non-equipartition on species segregation [7-9, 12, 13]. Currently, only one *s*-component continuum model, proposed by Garzó, Hrenya, and Dufty [21, 22], has been derived without assuming a Maxwellian velocity distribution, an equipartition of energy, or a dilute system of particles. The former will be referred to as GHD theory and will be the continuum model of focus in this thesis work due to its wide range of applicability. For the

specific governing equations, constitutive relations, and transport coefficients, see Table 1.1 with additional expressions in Appendix A.

1.2.1.2 Application to Continuous PSDs: Need for Discrete Approximation to Continuous PSD in KT Predictions

A common feature of current hydrodynamic models is their restriction to a *discrete* number, s, of particle species. This restriction stems from the starting kinetic equations, which are cast as a single-particle velocity distribution function for a given particle species, where each species has a unique set of physical properties (i.e., size and/or material density and/or restitution coefficient). Consequently, current hydrodynamic models cannot be directly applied to a continuous PSD. Instead, the continuous PSD must first be approximated as a discrete distribution of s particle diameters and associated relative solids volume fractions (i.e., composition). Using a larger number of particle species in a discrete approximation of a continuous PSD will lead to a more accurate estimation; however, solving the associated governing equations and constitutive relations (see Table 1.1) becomes much more computationally expensive as the number of particle species is increased. Therefore, determining the appropriate number of particle species to maintain a balance between accuracy and computational expense is of great interest here.

1.2.2 Previous Polydisperse KT and MD Studies

Though several kinetic-theory (KT) based models for rapid granular flows of s-component mixtures are available [21, 22, 23-25], studies involving the flow of mixtures containing 3 or more particle species are scarce, especially compared to their binary counterparts. Iddir, Arastoopour, and Hrenya [26] analyzed the kinetic-theory-based predictions of Iddir and Arastoopour [25] for both binary and ternary mixtures. Predictions of rheological

behavior for binary mixtures were compared to both molecular dynamics (MD) and experimental data, but similar comparisons for the ternary system were not possible due to the lack of such data. With regard to continuous distributions, Remy, Khinast, and Glasser [27] investigated how the degree of polydispersity of a granular mixture within a bladed mixer affects flow and segregation. MD simulations were carried out for 4 different systems: binary, ternary, 5 particles, and 11 particles. Because this flow is not considered a rapid granular flow, a kinetic-theory-based model could not be included in the comparison. Dahl *et al*. [18-30] used MD simulations of simple shear flow and bounded conduction to analyze the behavior of rapid granular flows comprised of continuous PSDs, though to date no KT predictions of this data have been performed.

Table 1.1: Governing equations and constitutive relations of GHD theory. The quantities within the table are defined as follows: α_{ij} (coefficient of restitution between species i and j), d_{ij} (average diameter of species i and j), D_{ij} (mutual (ordinary) diffusion coefficient relating species i and j, D_{ij}^{F} (mass mobility coefficient relating species i and j), D_{i}^{T} (thermal diffusion coefficient of species i), $D_{q,i}$ (dufour coefficient of species i), $\underline{F_i}$ (external force acting on species i, η (shear viscosity), η^{c} (collisional contribution to shear viscosity), η_j^{k} (kinetic contribution of species j to shear viscosity), $\underline{j_{oi}}$ (mass flux of species i), κ (bulk viscosity), λ (conductivity), L_{ij} (thermal mobility coefficient relating species i and j), m (average mass amongst particle species), m_i (mass of species i), μ_{ij} ($m_i/(m_i + m_j)$), n (number density of overall system), n_i (number-based density of species i), p (granular pressure), $\underline{\underline{P}}$ (pressure tensor), $\underline{q}$ (heat flux), θ_i ($m_i T/(mT_i)$), ρ (material density), T (number-based mixture granular temperature), T_i (granular temperature of species i), $\underline{U}$ (mass-based mixture velocity), ζ (overall cooling rate), $\zeta^{(0)}$ (zeroth-order cooling rate), ζ_u (first-order cooling rate), $\zeta^{(1,1)}$ ((1,1) contribution to first-order cooling rate), $\zeta^{(1,0)}$ ((1,0) contribution to first-order cooling rate). Because $\underline{F_i} = 0$ for this work, the quantities D_{ij}^{F} and L_{ij} are not considered. See Appendix A for all additional expressions. Also, see Garzó, Hrenya, and Dufty [21, 22], with corrections in Murray, Garzó, and Hrenya [31], for further details.

Balance Equations		
Mass	$\frac{Dn_i}{Dt} + n_i \underline{\nabla}\cdot \underline{U} = -\frac{1}{m_i}\underline{\nabla}\cdot \underline{j_{oi}}$	**Eq. 1.1**
Momentum	$\rho\frac{D\underline{U}}{Dt} = -\underline{\nabla}\cdot \underline{\underline{P}} + \sum_{i=1}^{s} n_i \underline{F_i}$	**Eq. 1.2**
Granular Energy	$\frac{3}{2} n \frac{DT}{Dt} = -\underline{\nabla}\cdot\ \underline{q}\ - \underline{\underline{P}} : \underline{\nabla U} - \frac{3}{2} nT\ \zeta\ + \frac{3}{2} T \sum_{i=1}^{s} \frac{1}{m_i} \underline{\nabla}\cdot \underline{j_{oi}} + \sum_{i=1}^{s} \frac{1}{m_i} \underline{F_i}\cdot \underline{j_{oi}}$	**Eq. 1.3**
Flux Laws		
Mass	$\underline{j_{oi}} = -\sum_{j=1}^{s} m_i m_j \frac{n_j}{\rho}\ D_{ij}\ \underline{\nabla}\ln(n_j) - \rho\ D_i^{T}\ \underline{\nabla}\ln T - \sum_{j=1}^{s}\ D_{ij}^{F}\ \underline{F}_j$	**Eq. 1.4**
Heat	$\underline{q} = -\lambda \underline{\nabla} T - \sum_{i=1}^{s}\sum_{j=1}^{s} T^2 D_{q,ij} \underline{\nabla}\ln(n_i) - \sum_{i=1}^{s}\sum_{j=1}^{s} L_{ij} \underline{F_i}$	**Eq. 1.5**
Pressure	$\underline{\underline{P}} = \ p\ \underline{\underline{\delta}} - \ \eta\ \left[\left(\underline{\nabla U} + (\underline{\nabla U})^{T}\right) - \frac{2}{3}(\underline{\nabla}\cdot \underline{U})\underline{\underline{\delta}}\right] - \ \kappa\ (\underline{\nabla}\cdot \underline{U})\underline{\underline{\delta}}$	**Eq. 1.6**
Cooling Rate	$\zeta = \zeta^{(0)} + \zeta_U \underline{\nabla}\cdot \underline{U}$	**Eq. 1.7**

Transport Coefficients

Zeroth-Order Cooling Rate

$$\zeta_i^{(0)} = \frac{8\sqrt{\pi}}{3}\sqrt{\frac{2T}{m}}\sum_{j=1}^{s}\chi_{ij}^{(0)} n_j \mu_{ji}\, d_{ij}^2 \left(\frac{\theta_i+\theta_j}{\theta_i\theta_j}\right)^{1/2}\left(1+\alpha_{ij}\right)\left[1-\frac{\mu_{ji}}{2}\left(1+\alpha_{ij}\right)\left(\frac{\theta_i+\theta_j}{\theta_j}\right)\right] \quad \textbf{Eq. 1.8}$$

Shear Viscosity

$$\sum_{j=1}^{s}\left(\tau_{ij}-\tfrac{1}{2}\zeta^{(0)}\delta_{ij}\right)\eta_j^k = n_i T_i + \sum_{j=1}^{s}\tfrac{2\pi}{15} m_i n_i n_j \mu_{ji} d_{ij}^3 \chi_{ij}^{(0)}\left(1+\alpha_{ij}\right)\left[\mu_{ji}\left(3\alpha_{ij}-1\right)\left(\frac{T_i}{m_i}+\frac{T_j}{m_j}\right)-\frac{4\left(T_i-T_j\right)}{\left(m_i+m_j\right)}\right] \quad \textbf{Eq. 1.9}$$

$$\eta^c = \left[\tfrac{4\pi}{15}\sum_{i=1}^{s}\sum_{j=1}^{s} n_j d_{ij}^3 \chi_{ij}^{(0)}\mu_{ji}\left(1+\alpha_{ij}\right)\eta_i^k\right] + \tfrac{3}{5}\kappa^c \quad \textbf{Eq. 1.10}$$

$$\eta = \eta^c + \sum_{j=1}^{s}\eta_j^k \quad \textbf{Eq. 1.11}$$

Pressure

$$p = nT + \frac{2\pi}{3}\sum_{i=1}^{s}\sum_{j=1}^{s}\mu_{ji}\left(1+\alpha_{ij}\right)d_{ij}^3\,\chi_{ij}^{(0)} n_i\, n_j\, T_i \quad \textbf{Eq. 1.12}$$

First-Order Cooling Rate

$$\zeta^{(1,1)} = \tfrac{\sqrt{\pi}}{2}\frac{\left(2T/m\right)^{3/2}}{nT}\sum_{i=1}^{s}\sum_{j=1}^{s} e_{i,D} n_i n_j d_{ij}^2 \chi_{ij}^{(0)} m_j \mu_{ij}\left(1-\alpha_{ij}^2\right)\frac{\theta_j^{1/2}}{\theta_i^{3/2}\left(\theta_i+\theta_j\right)^{1/2}} \quad \textbf{Eq. 1.13}$$

$$\zeta^{(1,0)} = \tfrac{-2\pi}{3nT}\sum_{i=1}^{s}\sum_{j=1}^{s} n_i n_j \mu_{ji} d_{ij}^3 \chi_{ij}^{(0)}\left(1-\alpha_{ij}^2\right)T_i \quad \textbf{Eq. 1.14}$$

$$\zeta_u = \zeta^{(1,0)} + \zeta^{(1,1)} \quad \textbf{Eq. 1.15}$$

Bulk Viscosity

$$\kappa = \kappa^c = \frac{2\sqrt{\pi}}{9}\sum_{i=1}^{s}\sum_{j=1}^{s}\mu_{ij}\, m_j\, n_i\, n_j\sqrt{\frac{2T}{m}} d_{ij}^4\, \chi_{ij}^{(0)}\left(1+\alpha_{ij}\right)\left(\frac{\theta_i+\theta_j}{\theta_i\theta_j}\right)^{1/2} \quad \textbf{Eq. 1.16}$$

Conductivity for i = 1-s

$$\lambda^c = \sum_{i=1}^{s}\sum_{j=1}^{s}\frac{1}{8}\left(1+\alpha_{ij}\right)m_j\mu_{ij}d_{ij}\chi_{ij}^{(0)}\left\{\frac{4\pi}{5}\left(1-\alpha_{ij}\right)\left(\mu_{ij}-\mu_{ji}\right)n_i\left[\frac{2}{m_j}\lambda^k+\frac{5T_i}{m_i m_j T}\rho D_j^T\right]-\frac{\sigma_{ij}C_{ij}^T}{T}\right. \quad \textbf{Eq. 1.17}$$

$$\left.+\frac{16\pi}{5}n_i\left[\frac{2\mu_{ij}}{m_j}\lambda_j^k-\frac{5T_i}{m_i m_j T}\left(2\mu_{ij}-\mu_{ji}\right)\rho D_j^T\right]\right\}$$

$$\lambda = \lambda^k + \lambda^c \quad \textbf{Eq. 1.18}$$

$$\lambda^k = \sum_{i=1}^{s}\lambda_i + \frac{5}{2T}\frac{\rho T_i}{m_i}D_i^T \quad \textbf{Eq. 1.19}$$

$$\sum_{j=1}^{s}\left(\gamma_{ij}-2\zeta^{(0)}\delta_{ij}\right)\lambda_j = \bar{\lambda}_i \quad \textbf{Eq. 1.20}$$

Thermal Diffusion for i = 1-s

$$\sum_{j=1}^{s}\left(\nu_{ij}-\zeta^{(0)}\delta_{ij}\right)D_j^T = \frac{-p\rho_i}{\rho^2}\left(1-\frac{\rho n_i T_i}{\rho_i p}\right)+\frac{2\pi}{3}\frac{n_i}{\rho}\sum_{j=1}^{s} n_j\mu_{ij}\chi_{ij}^{(0)}d_{ij}^3 T_j\left(1+\alpha_{ij}\right) \quad \textbf{Eq. 1.21}$$

Mutual (Ordinary) Diffusion for i = 1-s and j =1-s

$$\sum_{\ell=1}^{s}\left(\nu_{i\ell}-\frac{1}{2}\zeta^{(0)}\delta_{i\ell}\right)\frac{m_\ell}{m_i}D_{\ell j} = \frac{\rho^2}{m_i m_j}\frac{\partial\zeta^{(0)}}{\partial n_j}D_i^T+\frac{\rho}{m_i m_j}\frac{\partial}{\partial n_j}\left(n_i T_i\right)-\frac{n_i}{m_j}\frac{\partial p}{\partial n_j}$$
$$+\frac{2\pi}{3}\frac{\rho n_i}{m_j}\sum_{\ell=1}^{s}\chi_{i\ell}^{(0)}d_{i\ell}^3\mu_{\ell i}\left(1+\alpha_{ij}\right)\left\{\left(\frac{T_i}{m_i}+\frac{T_\ell}{m_\ell}\right)\left[\delta_{j\ell}+\frac{1}{2}\frac{n_\ell}{n_j}\left(\frac{n_j}{\chi_{i\ell}}\frac{\partial\chi_{i\ell}}{\partial n_j}+I_{ij\ell}\right)\right]+\frac{n_\ell}{m_\ell}\frac{\partial T_\ell}{\partial n_j}\right\} \quad \textbf{Eq. 1.22}$$

Dufour Coefficient for i = 1-s and j =1-s

$$D_{q,ij}^c = \sum_{p=1}^{s}\frac{1}{8}\left(1+\alpha_{ip}\right)m_p\mu_{ip}d_{ip}^3\chi_{ip}^{(0)}\left\{\frac{4\pi}{5}\left(1-\alpha_{ip}\right)\left(\mu_{ip}-\mu_{pi}\right)n_i\left[\frac{2}{m_p}D_{q,pj}^k+5\frac{T_i}{T^2}\frac{m_j n_j}{\rho m_i}D_{pj}\right]-\frac{\sigma_{ij}}{T^2}C_{ipj}^T\right. \quad \textbf{Eq. 1.23}$$

$$\left.+\frac{16\pi}{5}n_i\left[\frac{2\mu_{pi}}{m_p}D_{q,pj}^k-5\left(2\mu_{ip}-\mu_{pi}\right)\frac{T_i}{T^2}\frac{n_j m_j}{\rho m_i}D_{pj}\right]\right\}$$

$$D_{q,ij} = D_{q,ij}^k + D_{q,ij}^c \quad \textbf{Eq. 1.24}$$

$$D_{q,\ell j}^k = d_{q,\ell j}+\frac{5}{2T^2}\frac{m_j n_j T_\ell}{\rho}D_{\ell j} \quad \textbf{Eq. 1.25}$$

$$\sum_{\ell=1}^{s}\left(\gamma_{i\ell}-\frac{3}{2}\zeta^{(0)}\delta_{i\ell}\right)d_{q,\ell j} = \bar{d}_{q,ij} \quad \textbf{Eq. 1.26}$$

1.3 Thesis Objectives

The underlying objective of this work is to further develop and validate a kinetic theory model for rapid, polydisperse solids flows, with a special emphasis on systems with a continuous distribution of particle sizes. The focus of this investigation is three-fold:

(i) to determine the importance of finite-volume (non-dilute) effects of solid particles in binary mixtures,

(ii) to determine the minimum number of discrete particle species needed to accurately approximate a continuous PSD, and

(iii) to validate discrete approximations of continuous PSDs applied to a kinetic-theory-based model via comparison with MD simulations of both segregating and non-segregating systems.

With respect to the first objective, GHD predictions of transport coefficients are compared to an earlier dilute-limit version of the same theory [32] over a range of physical parameters. With regard to the second objective, the number of species required for an accurate discrete approximation of a continuous PSD using GHD theory is determined in two separate studies. One focuses on the comparison of a subset of the KT transport coefficients (ie., single-valued transport coefficients); therefore, the study depends only on the physical parameters of the system and not the system geometry. The second study focuses on a system known to exhibit segregation (ie., bounded conduction), allowing for an investigation where system geometry may be influential. Lastly, the third objective was accomplished via comparison of the GHD predictions, determined in the second objective, to MD data.

Literature Cited

1. Curtis, J.S. and B. van Wachem, *Modeling particle-laden flows: A research outlook.* AIChE Journal, 2004. **50**(11): p. 2638-2645.
2. Muzzio, F.J., T. Shinbrot, and B.J. Glasser, *Powder technology in the pharmaceutical industry: the need to catch up fast.* Powder Technology, 2002. **124**(1-2): p. 1-7.
3. Sundaresan, S., *Some outstanding questions in handling of cohesionless particles.* Powder Technology, 2001. **115**(1): p. 2-7.
4. Hrenya, C.M., *Kinetic theory for granular materials: Polydispersity*, in *Computational Gas-Solids Flows and Reacting Systems: Theory, Methods and Practice*, S.P., M. Syamlal, and T. O'Brien, Editor. 2011, IGI Global: Hershey, PA.
5. Ottino, J. and D. Khakhar, *Mixing and segregation of granular materials.* Annual Review of Fluid Mechanics, 2000. **32**(1): p. 55-91.
6. Hsiau, S. and M. Hunt, *Granular thermal diffusion in flows of binary-sized mixtures.* Acta Mechanica, 1996. **114**(1): p. 121-137.
7. Brey, J., M. Ruiz-Montero, and F. Moreno, *Energy partition and segregation for an intruder in a vibrated granular system under gravity.* Physical Review Letters, 2005. **95**(9): p. 98001.
8. Galvin, J., S. Dahl, and C. Hrenya, *On the role of non-equipartition in the dynamics of rapidly flowing granular mixtures.* Journal of Fluid Mechanics, 2005. **528**: p. 207-232.
9. Garzó, V., *Segregation in granular binary mixtures: Thermal diffusion.* Europhysics Letters, 2006. **75**: p. 521.
10. Schröter, M., et al., *Mechanisms in the size segregation of a binary granular mixture.* Physical Review E, 2006. **74**(1): p. 11307.
11. Wildman, R., et al., *A comparison of the predictions of a simple kinetic theory with experimental and numerical results for a vibrated granular bed consisting of nearly elastic particles of two sizes.* Physics of Fluids, 2006. **18**: p. 073301.
12. Yoon, D. and J. Jenkins, *The influence of different species granular temperatures on segregation in a binary mixture of dissipative grains.* Physics of Fluids, 2006. **18**: p. 073303.
13. Liu, X., M. Metzger, and B. Glasser, *Couette flow with a bidisperse particle mixture.* Physics of Fluids, 2007. **19**: p. 073301.
14. Jenkins, J. and F. Mancini, *Balance laws and constitutive relations for plane flows of a dense, binary mixture of smooth, nearly elastic, circular disks.* Journal of Applied Mechanics, 1987. **54**: p. 27.
15. Mathiesen, V., et al., *Experimental and computational study of multiphase gas/particle flow in a CFB riser.* AIChE journal, 1999. **45**(12): p. 2503-2518.
16. Huilin, L., D. Gidaspow, and E. Manger, *Kinetic theory of fluidized binary granular mixtures.* Physical Review E, 2001. **64**(6): p. 61301.
17. Rahaman, M.F., J. Naser, and P.J. Witt, *An unequal granular temperature kinetic theory: description of granular flow with multiple particle classes.* Powder Technology, 2003. **138**(2-3): p. 82-92.
18. Jenkins, J. and F. Mancini, *Kinetic theory for binary mixtures of smooth, nearly elastic spheres.* Physics of Fluids A: Fluid Dynamics, 1989. **1**: p. 2050.
19. Arnarson, B. and J. Willits, *Thermal diffusion in binary mixtures of smooth, nearly elastic spheres with and without gravity.* Physics of Fluids, 1998. **10**: p. 1324.

20. Chapman, S. and T. Cowling, *The mathematical theory of non-uniform gases.* Cambridge: Cambridge University, 1970.

21. Garzó, V., C.M. Hrenya, and J.W. Dufty, *Enskog theory for polydisperse granular mixtures. II. Sonine polynomial approximation.* Physical Review E, 2007. **76**(3): p. 031304.
22. Garzó, V., J.W. Dufty, and C.M. Hrenya, *Enskog theory for polydisperse granular mixtures. I. Navier-Stokes order transport.* Physical Review E, 2007. **76**(3): p. 031303.
23. Zamankhan, P., *Kinetic theory of multicomponent dense mixtures of slightly inelastic spherical particles.* Physical Review E, 1995. **52**(5): p. 4877-4891.
24. Mathiesen, V., et al., *Experimental and computational study of multiphase gas/particle flow in a CFB riser.* AIChE Journal, 1999. **45**(12): p. 2503-2518.
25. Iddir, H. and H. Arastoopour, *Modeling of multitype particle flow using the kinetic theory approach.* AIChE Journal, 2005. **51**(6): p. 1620-1632.
26. Iddir, H., H. Arastoopour, and C.M. Hrenya, *Analysis of binary and ternary granular mixtures behavior using the kinetic theory approach.* Powder Technology, 2005. **151**(1- 3): p. 117-125.
27. Remy, B., J.G. Khinast, and B.J. Glasser, *Polydisperse granular flows in a bladed mixer: Experiments and simulations of cohesionless spheres.* Chemical Engineering Science, 2011. **66**(9): p. 1811-1824.
28. Dahl, S., R. Clelland, and C.M. Hrenya, *Three-dimensional, rapid shear flow of particles with continuous size distributions.* Powder Technology, 2003. **138**(1): p. 7-12.
29. Dahl, S., R. Clelland, and C.M. Hrenya, *The effects of continuous size distributions on the rapid flow of inelastic particles.* Physics of Fluids, 2002. **14**: p. 1972.
30. Dahl, S. and C.M. Hrenya, *Size segregation in rapid, granular flows with continuous size distributions.* Physics of Fluids, 2004. **16**: p. 1.
31. Murray, J.A., V. Garzó, and C.M. Hrenya, *Enskog theory for polydisperse granular mixtures. III. Comparison of dense and dilute transpornt coefficients and equations of state for a binary mixture.* Powder Technology, 2012. **220**: p. 24-36.
32. Garzó, V. and J.W. Dufty, *Hydrodynamics for a granular mixture at low density*. Physics of Fluids, 2002 **14**: 1476–1490.

CHAPTER 2

COMPARISON OF DENSE AND DILUTE TRANSPORT COEFFICIENTS AND EQUATIONS OF STATE FOR A BINARY MIXTURE[a]

2.1 Introduction

The objective of this chapter is to assess the impact of a dense-phase treatment on the hydrodynamic description of granular, binary mixtures relative to a previous dilute-phase treatment. Though kinetic theory is not applicable for packed systems or multiple, enduring particle contacts, the "dense-phase" treatment considered here allows for volume fractions as high as $\phi = 0.5$. As mentioned in Section 1.2.1.1, GHD theory [1, 2] is an s-component continuum model applicable to dilute and moderately dense rapid granular flows. An analogous model, referred to as GD theory [3], was derived in the exact same manner as GHD theory, however a dilute, binary system of particles was assumed [3]. Therefore, with GHD theory in its binary limit, an apples-to-apples comparison between dilute and non-dilute treatments of transport coefficients is possible. Each theory gives rise to a set of zeroth-order closures known as equations of state, as well as constitutive relations for first-order contributions to fluxes, or more specifically the associated transport coefficients. The equations of state and transport coefficients are functions of the hydrodynamic variables: number densities (n_i), mass-based mixture velocity ($\underline{U}$), and number-based mixture granular temperature (T). Although the predictions for the equations of state and transport coefficients from the two theories are expected to match at low volume fractions (i.e., dilute systems), a non-negligible difference is expected at higher concentrations, though the level of discrepancy between the two has not yet

[a] Murray, J.A., V. Garzó, and C.M. Hrenya, *Enskog theory for polydisperse granular mixtures. III. Comparison of dense and dilute transport coefficients and equations of state for a binary mixture.* Powder Technology, 2012. **220**: p. 24-36.

been reported for polydisperse systems.

The focus of this work is to analyze binary mixtures, where the two particle species differ in mass and/or size. Motivation for this study is threefold: (i) to assess importance of dense-phase corrections to hydrodynamic description of mixtures proposed by Garzó, Hrenya, and Dufty [1, 2] compared to the previous dilute-phase description [3], and more specifically to determine rules-of-thumb for the volume fraction at which such dense-phase descriptions become non-negligible, (ii) to examine the behavior of the GHD equations of state and transport coefficients over a range of physical parameters, and (iii) to provide a complete, self-contained set of the GHD expressions (see Table 1.1 with additional expressions in Appendix A). This latter goal also provides an opportunity to display the expressions in a form more suitable for computational purposes.

To accomplish the first two objectives, the equations of state and transport coefficients were evaluated over a range of volume fractions, coefficients of restitution, and mixture properties (diameter ratio, mass ratio, and volume fraction ratio). The results indicate that the discrepancy between transport coefficients and equations of state predicted by each theory at a volume fraction of $\phi = 0.1$ can vary from a factor of 1.05 to a factor of 10. As the volume fraction becomes fairly dense ($\phi = 0.5$), the predicted discrepancy increases to a factor of at least 1.7 and as large as a factor of 120. Hence, though the derivation of the constitutive relations for a dilute flow and the resulting constitutive expressions are simpler than its moderately dense counterpart, the difference between the two theories is non-negligible at low to moderate volume fractions. In Table 1.1, with additional expressions in Appendix A, a complete, self-contained set of the GHD constitutive relations for the mass flux, heat flux, pressure tensor, and cooling rate can be found. Also, a description for how this theory is compared to GD is offered in Section 2.2.

The results, which are contained in Section 2.3, indicate stark differences between the dilute and dense treatments. The chapter is closed in Section 2.4 with a brief summary of the main results obtained here.

2.2 Quantitative Approach: Comparison of Dilute and Dense-Phase Expressions for Hard Spheres

In order to assess the importance of dense-phase corrections to the continuum theory for rapid granular flows of binary mixtures, the equations of state and transport coefficients obtained from the GHD and GD theories were compared over a range of volume fractions and coefficients of restitution for a given set of mixture properties (diameter ratio, size ratio, and volume fraction ratio). To illustrate the differences in a straightforward manner, each quantity is examined as a ratio of the GHD value (dilute through moderately dense) to the GD value (dilute limit), giving rise to a non-dimensional quantity. These non-dimensional ratios were plotted as functions of volume fraction and coefficients of restitution, holding all other mixture properties constant. Representing the transport coefficients and equations of state in this manner reveals the relative magnitudes of the dense- and dilute-phase predictions. Recall the complete set of equations of state and transport coefficients for GHD theory are given in Table 1.1 ($\zeta^{(0)}$, ζ_u, D_{ij}, D_i^T, D_{ij}^F, λ, $D_{q,i}$, L_{ij}, p, η, κ) with additional expressions in Appendix A.

It is important to note that some transport coefficients (L_{ij}, D_{ij}^F) were not considered in the dilute theory (GD), and thus these quantities are not considered here. Moreover, two of the transport coefficients, namely ζ_u and κ, are zero in the dilute limit, and thus the corresponding ratios of the moderately dense (GHD) value to the dilute (GD) value diverge. Accordingly, only the GHD predictions of these quantities are shown. Thus, the comparison between the GHD and GD theory predictions presented here involves the seven remaining quantities: $\zeta^{(0)}$, D_{ij}, D_i^T, λ,

$D_{q,i}$, p, η.

2.2.1 Mixture Parameters

The continuum description of a binary mixture of inelastic hard spheres is a function of the following dimensional parameters: species masses (m_1, m_2), species diameters (d_1, d_2), species 1 volume fraction (ϕ_1), overall volume fraction ($\phi = \phi_1 + \phi_2$), and coefficients of restitution (α_{11}, α_{22}, $\alpha_{12} = \alpha_{21}$). (Note that the number densities and volume fractions are related by $\phi_i = n_i \pi d_i^3/6$.) The subscripts 1 and 2 denote the two species in the binary mixture. For purposes of simplicity, the coefficients of restitution have been assumed to be the same for all combinations of collisions (i.e., $\alpha_{11} = \alpha_{22} = \alpha_{12} = \alpha$). In terms of the ratio of moderately dense (GHD) to dilute (GD) predictions for each quantity, the parameter space is reduced to the following dimensionless inputs: mass ratio (m_1/m_2), diameter ratio (d_1/d_2), overall volume fraction (ϕ), volume fraction ratio of species 1 relative to the total (ϕ_1/ϕ), and coefficient of restitution α. Hereafter, the ratio ϕ_1/ϕ will be referred to as the (mixture) composition of species 1. Recall that the GHD and GD theories allow for a non-equipartition of energy, and thus several of the aforementioned closures involve the species granular temperatures, T_1 and T_2. It is important to point out that these quantities are not hydrodynamic variables (i.e., they do not require the solution of species energy balances; for a detailed explanation, see Ref. [2]) and instead are determined by the set of equations defining the zeroth-order cooling rate.

2.2.2 Parameter Space Evaluated

Table 2.1 summarizes the three cases (equal size and different mass, equal mass and different size, and different size and mass) used to compare the GHD and GD theories, and the wide ranges of input parameters used in each case study. Though the transport coefficients and equations of state may vary quantitatively from case to case, the general trends show little

variation. For sake of brevity, the upcoming section will focus on one representative case, namely that of different size and equal material densities (i.e., different mass) in order to quantify how the newly acquired GHD predictions differ from the dilute-phase counterpart (GD).

Table 2.1: Range of input parameters used in analysis of binary mixture via GHD theory.

Case Description	d_1/d_2	m_1/m_2	ϕ_1/ϕ	α
Equal Sizes	1	1-10	0.25-0.75	0.50-0.99
Equal Masses	1-10	1	0.25-0.75	0.50-0.99
Different diameters, different masses	2	0.10-10	0.50	0.75

2.2.3 Case Presented: Different-Sized Particles with Same Material Densities

Many industrial and natural granular flows are comprised of one material (i.e., same material density), but different-sized particles. In the case presented here, the diameter of species 1 was twice that of species 2 (i.e., $d_1/d_2 = 2$), and both species had the same material density (i.e., $m_1/m_2 = 8$). For the sake of consistency, the composition of each species was held constant at 50% by volume for this analysis (i.e., $\phi_1/\phi = \phi_2/\phi = 0.5$). The ratio of GHD to GD predictions of each quantity evaluated was plotted over a range of volume fractions from dilute to moderately dense ($\phi = 10^{-8} – 0.5$) while holding the coefficient of restitution constant. Also, each quantity was varied over a range of coefficients of restitution from relatively inelastic to nearly elastic (α = 0.5–0.99) while holding the overall volume fraction constant. The results of this case study are presented in the upcoming section.

2.3 Results and Discussion

The overall objective was to analyze each transport coefficient and equation of state over a range of parameters for the newly-developed GHD theory. By comparing these results to the

predictions from the dilute (GD) theory [3], it was possible to demonstrate the need for a moderately dense-phase correction, as detailed below.

2.3.1 Cooling Rate: Zeroth-Order and First-Order Contributions

As indicated by Figure 2.1, the dense-to-dilute ratio of the zeroth-order cooling rate ($\zeta^{(0)}$) is much more sensitive to changes in volume fraction than coefficient of restitution. Such behavior can be explained via the dependency of the zeroth-order cooling rate on the pair correlation function at contact, χ_{ij}. This factor accounts for the volume exclusion effects between like particles (χ_{11}) and unlike particles (χ_{12}). In the dilute limit, the spatial correlation factor equals one (i.e., $\chi_{11} = \chi_{12} = 1$). When the zeroth-order cooling rate of GHD theory is then divided by its dilute counterpart, the resulting function is strongly dependent on the spatial correlation factor. Because χ_{ij} is sensitive to changes in overall volume fraction, it is then reasonable that the dimensionless zeroth-order cooling rate ratio exhibits the same sensitivity. More specifically, the results shown in Figure 2.1a indicate that $\zeta^{(0)}$ predicted by GHD theory is more than 5 times greater than its dilute counterpart for a fairly dense system (ϕ = 0.5) and more than 2 times greater for ϕ = 0.3. Even at ϕ =0.2, a discrepancy of 27% is found between the dilute- and dense-phase predictions.

Unlike the zeroth-order contribution to the cooling rate, the trans- port coefficient associated with the first-order contribution is zero in the dilute limit. Therefore, a ratio comparison of the dense-to-dilute predictions is not possible. The results given in Figure 2.2 represent the first-order contribution to the cooling rate (which is non-dimension- al), which approaches zero as volume fraction diminishes. As evident from this figure, ζ_u is quite sensitive to changes in both volume fraction (Figure 2.2a) and coefficient of restitution (Figure 2.2b).

Also, the results for this case indicate that the magnitude of the first-order contribution increases as the system becomes denser and less elastic.

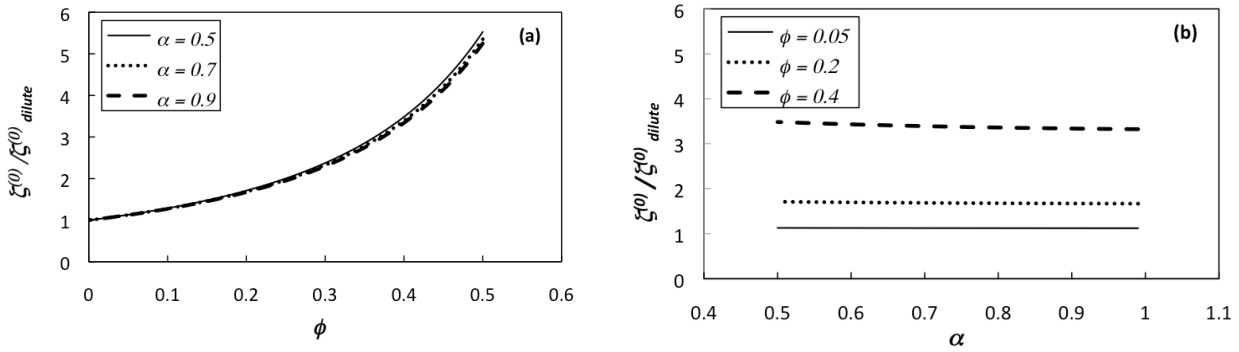

Figure 2.1: Zeroth-order cooling rate: ratio of moderately dense (GHD) to dilute (GD) predictions as a function of (a) overall volume fraction and (b) coefficient of restitution.

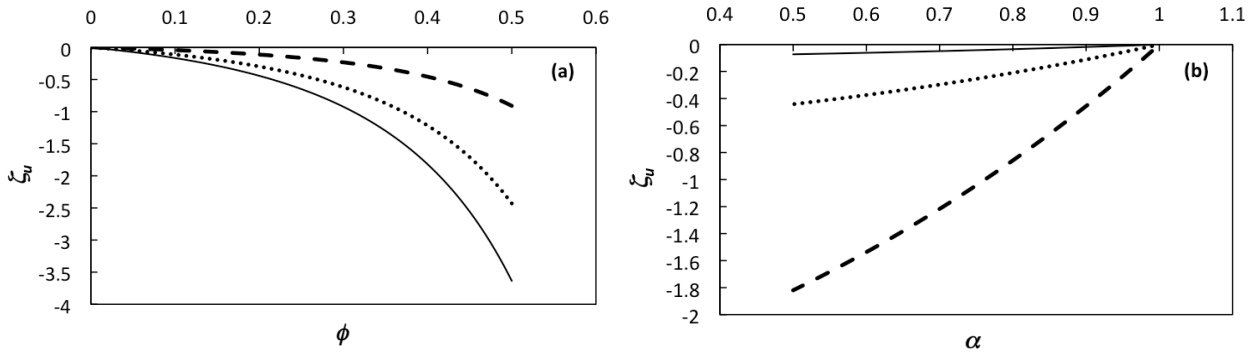

Figure 2.2: Transport coefficient associated with first-order cooling rate: moderately dense (GHD) predictions as a function of (a) overall volume fraction and (b) coefficient of restitution. See legends presented in Figure 2.1.

2.3.2 Momentum Flux: Pressure, Shear Viscosity, and Bulk Viscosity

Now moving on to results associated with the momentum flux, Figure 2.3 indicates that the dense-to-dilute ratio of granular pressure is more sensitive to changes in volume fraction (Figure 2.3a) than coefficient of restitution (Figure 2.3b). Also, this ratio increases monotonically with both volume fraction and coefficient of restitution. For a moderately dense system (ϕ = 0.4), GHD theory predicts that the granular pressure is about 5 times greater than dilute (GD) theory. Even at lower volume fractions (ϕ = 0.1), the moderately dense-phase prediction is greater than

its dilute counterpart by 40%.

Shear viscosity, results of which are given in Figure 2.4, behaves in a similar manner to granular pressure (Figure 2.3). A monotonic increase is exhibited with respect to both volume fraction (Figure 2.4a) and coefficient of restitution (Figure 2.4b). The GHD prediction is about 5 times larger than the GD prediction for moderately dense systems (ϕ = 0.4). However, the discrepancy at lower volume fractions (ϕ = 0.1) decreases to approximately 5% (Figure 2.4a).

As mentioned previously, the bulk viscosity is zero in the dilute limit. Therefore the results for bulk viscosity, given in Figure 2.5, are those obtained from the moderately dense theory (GHD) alone, instead ratios of dense-to-dilute predictions. Furthermore, these GHD-based bulk viscosities are non-dimensionalized. It is evident from this figure that the prediction of bulk viscosity via GHD theory increases significantly in magnitude as the system becomes moderately dense, whereas little variation results from changes in particle elasticity.

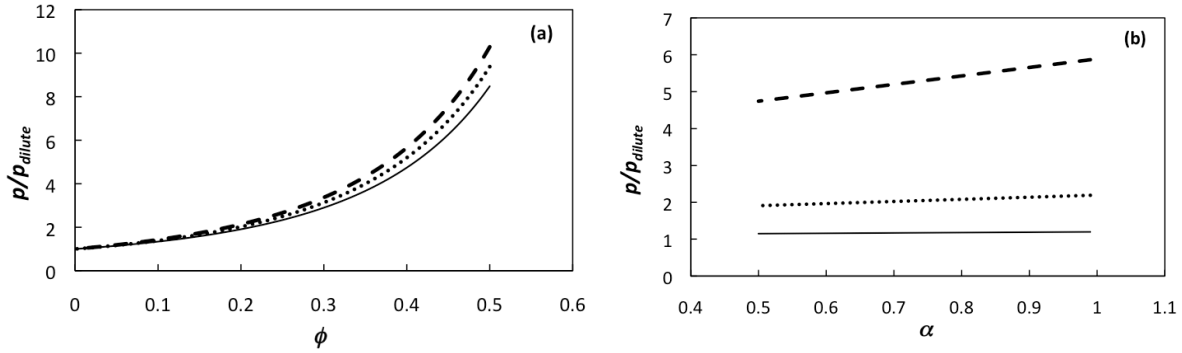

Figure 2.3: Transport coefficient associated with pressure: moderately dense (GHD) predictions as a function of (a) overall volume fraction and (b) coefficient of restitution. See legends presented in Figure 2.1.

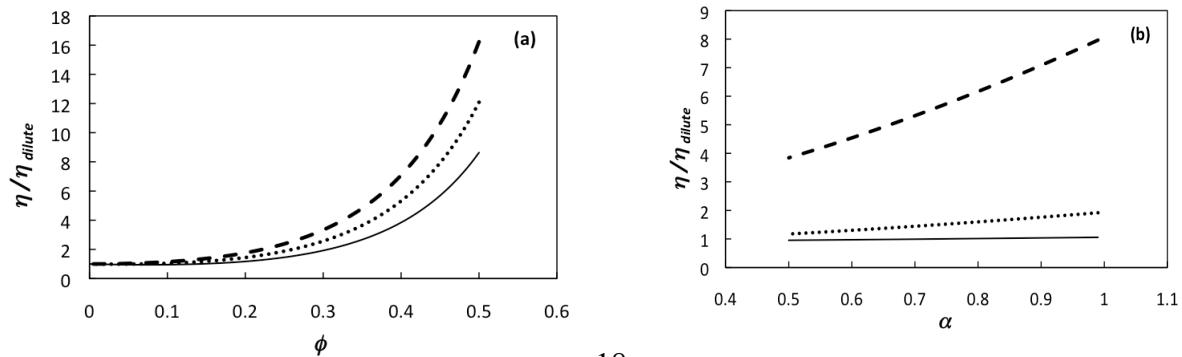

Figure 2.4: Transport coefficient associated with shear stress: moderately dense (GHD) predictions as a function of (a) overall volume fraction and (b) coefficient of restitution. See legends presented in Figure 2.1.

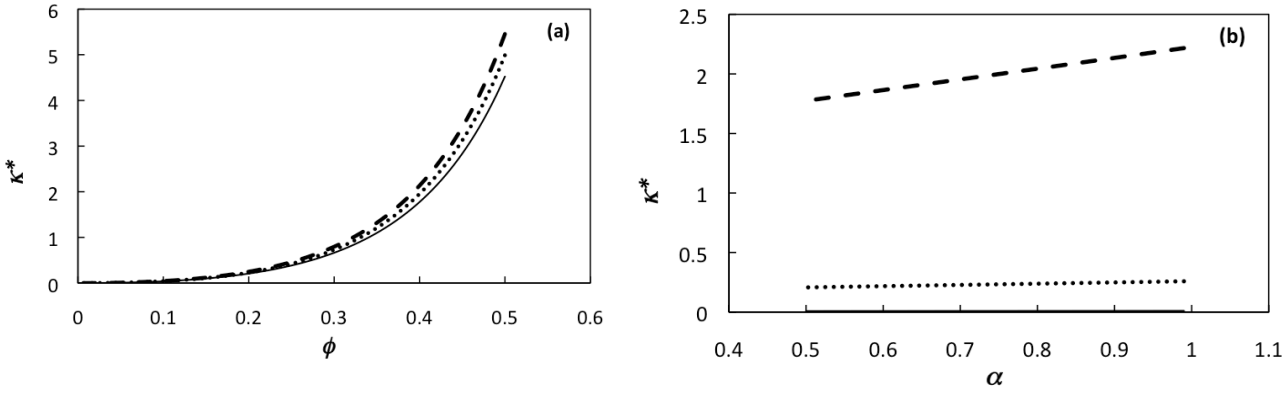

Figure 2.5: Transport coefficient associated with bulk viscosity: moderately dense (GHD) predictions as a function of (a) overall volume fraction and (b) coefficient of restitution. See legends presented in Figure 2.1.

2.3.3 Mass Flux: Mutual Diffusion and Thermal Diffusion

The mutual and thermal diffusion coefficients (D_{ij}, D_i^T) are elements of the constitutive equation for the mass flux. The dimensionless mutual diffusion can be described by two quantities ($D_{11}/D_{11,\ dilute}$ and $D_{22}/D_{22,\ dilute}$), whereas the dimensionless thermal diffusion can be described by a single quantity ($D^T_1/D^T_{1,dilute}$). Note that the dilute (GD) mutual and thermal diffusion coefficients presented by Garzó and Dufty [3] are defined using different spatial gradients than those used in the dense (GHD) theory. Nonetheless, a conversion is made such that both dense and dilute theories use the same representations for the fluxes, namely those shown in Murray, Garzó, and Hrenya [4], thereby ensuring an apples-to-apples comparison.

An examination of the dense-to-dilute ratio of the mutual diffusion coefficient elements (Figs. 2.6 and 2.7) reveals a more complicated behavior of these quantities. Because D_{11}, dilute approaches zero for inelastic systems (at $\alpha = 0.52$), the coefficient of restitution was varied

between 0.6 and 0.99 (Figure 2.6b). As shown in Figure 2.6a, $D_{11}/D_{11,dilute}$ is non-monotonic with respect to the volume fraction in less elastic systems (α = 0.5), reaching a maximum ratio between the dense and dilute predictions of 20 at a volume fraction of 0.37. As the system becomes more elastic, $D_{11}/D_{11,dilute}$ shifts from positive to negative. A change in the sign, as well as magnitude, between dense and dilute predictions of the mutual diffusion coefficient D_{11} may provide insight into counter intuitive species segregation [5-8].

The results for $D_{22}/D_{22,\ dilute}$, which are displayed in Figure 2.7, reveal increasing discrepancies between predictions as volume fraction increases and restitution coefficient decreases. In other words, GHD and GD theories display a larger discrepancy in denser, less elastic systems. For a relatively inelastic and dense system (α = 0.5 and ϕ = 0.5), the GHD prediction is about half of its dilute counterpart (Figure 2.7a). However, it is significant to note the minor differences that exist between the dense and dilute predictions for the mutual diffusion coefficient D_{22} near the elastic limit (α = 0.9) over a range of volume fractions from $\phi = 10^{-8}$ to 0.5 (Figure 2.7a, $D_{22}/D_{22,\ dilute} \sim 1$). GHD and GD theories display a larger discrepancy in denser, less elastic systems. For a relatively inelastic and dense system (α = 0.5, ϕ = 0.4), the moderately dense-phase theory prediction is about half of its dilute counterpart (Figure 2.7a). Comparing dense- and dilute-phase predictions for the individual elements D_{11} and D_{22} shows the relative importance of each contribution to the mutual diffusion. At a moderately low volume fraction and high coefficient of restitution (ϕ = 0.1, α = 0.9), the discrepancies for GHD and GD theory predictions are about 70% and 5% for D_{11} and D_{22}, respectively. The dilute theory does not consider the finite size of the particles, which is the main difference between dense and dilute predictions. The discrepancy between D_{11} and $D_{11,\ dilute}$ is larger than the discrepancy between D_{22} and $D_{22,\ dilute}$ because D_{11} is directly related to the size of species 1, whereas D_{22} is

proportional to the size of species 2 (recall $d_1/d_2 = 2$ for the case examined). Neither dilute quantities contains species size, therefore, the self-diffusion coefficient of a relatively large particle compared to its dilute counterpart will be greater than that of its smaller counterpart.

The results for thermal diffusion (Figure 2.8) indicate that the ratio of dense-to-dilute predictions is extremely sensitive to changes in volume fraction compared to the coefficient of restitution. These general trends were also observed in the cooling rate and momentum flux relations (Figs. 2.1, 2.3–2.5). The quantity $D^T_1/D^T_{1,\ dilute}$ is nearly linear when plotted as a function of volume fraction, regardless the restitution coefficient (Figure 2.8a). In a moderately dense system ($\phi = 0.4$), the results of Figure 2.8a indicate that the dilute (GD) theory prediction of D^T_1 is 5 times larger than predicted by GHD theory. At a much lower volume fraction of 0.1, the dilute (GD) theory prediction is larger than the moderately dense-phase (GHD) theory prediction by 20% (Figure 2.8a).

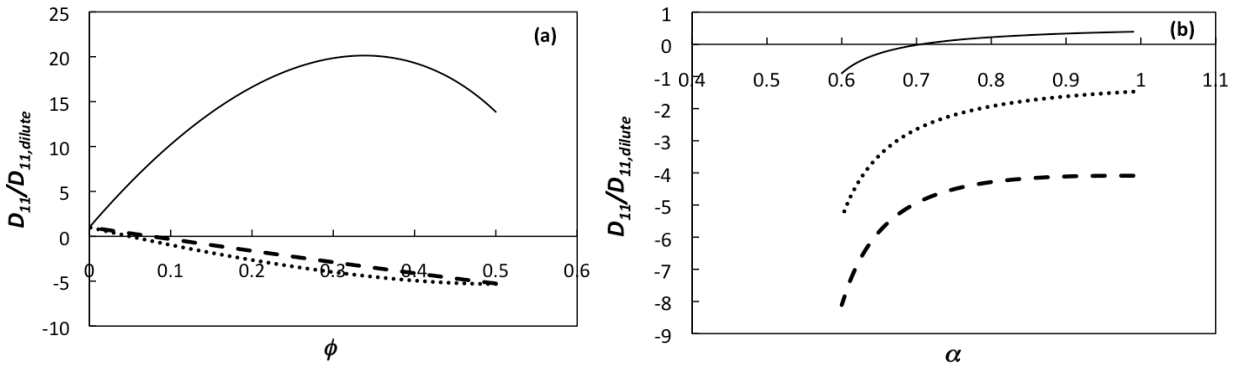

Figure 2.6: Transport coefficient associated with mutual diffusion, D_{11}: moderately dense (GHD) predictions as a function of (a) overall volume fraction and (b) coefficient of restitution. See legends presented in Figure 2.1.

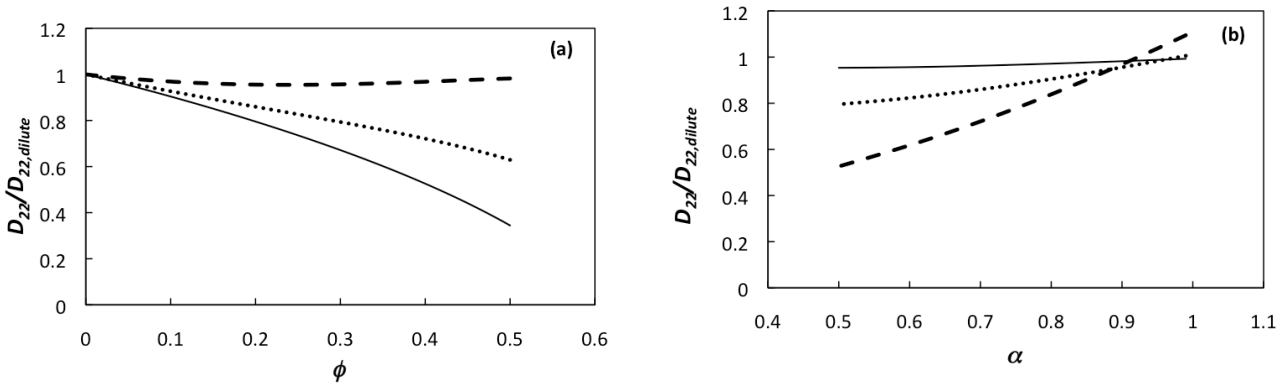

Figure 2.7: Transport coefficient associated with mutual diffusion, D_{22}: moderately dense (GHD) predictions as a function of (a) overall volume fraction and (b) coefficient of restitution. See legends presented in Figure 2.1.

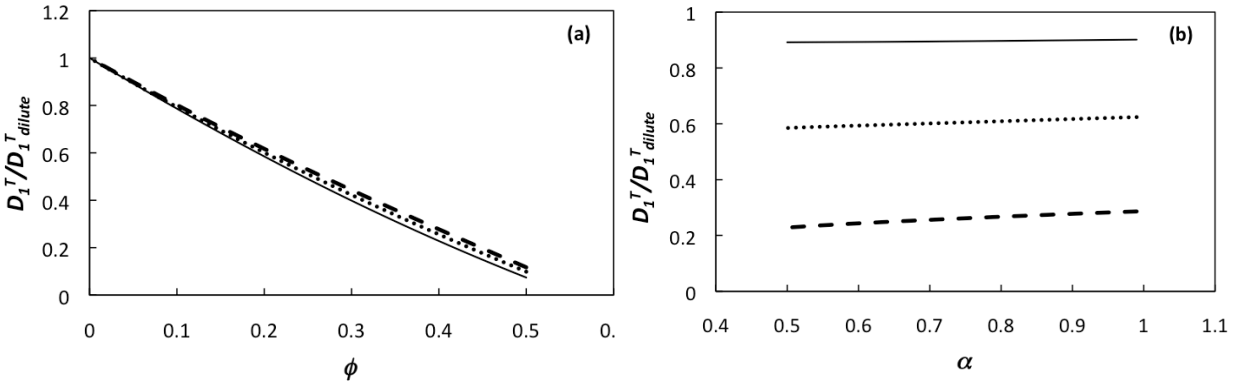

Figure 2.8: Transport coefficient associated with thermal diffusion: moderately dense (GHD) predictions as a function of (a) overall volume fraction and (b) coefficient of restitution. See legends presented in Figure 2.1.

2.3.4 Heat Flux: Thermal Conductivity, Dufour Coefficient

Heat flux is characterized by the thermal conductivity and the Dufour coefficients $D_{q,i}$. Figure 2.9 shows that the dense-to-dilute ratio of thermal conductivity increases monotonically with respect to both volume fraction and coefficient of restitution. In an elastic, moderately dense system ($\phi = 0.4$), results (Figure 2.9a) indicate that the prediction of thermal conductivity from GHD theory is 4 times larger than that of its dilute (GD) counterpart. For systems of lower densities ($\phi = 0.1$), the discrepancies range from 1% ($\alpha = 0.9$) to 6% ($\alpha = 0.5$) (Figure 2.9a).

Similar to the mutual diffusion coefficient, the dilute form of the Dufour coefficient takes on a zero value at certain α, thereby making the dense-to-dilute value diverge at this value of α. Because this value occurs at a practical value of $\alpha = 0.63$ (whereas $D_{11,dilute}$ diverges at $\alpha = 0.52$), the dense and dilute predictions of the dimensionless Dufour coefficient $D^*_{q,1}$ were instead plotted separately against the coefficient of restitution (Figure 2.10b and c). As expected, the dilute prediction of the Dufour coefficient is independent of the volume fraction (Figure 2.10c).

The differences in magnitude between dilute and moderately dense predictions are non-trivial for both $D_{q,1}$ and $D_{q,2}$. More specifically, the discrepancies that exist between the predictions of $D_{q,1}$ and $D_{q,1,dilute}$ are up to 2 orders of magnitude in some cases (Figure 2.10). For a moderately dense, inelastic system ($\phi = 0.5$, $\alpha = 0.7$), the dense-phase prediction is over 100 times greater than its dilute counterpart (Figure 2.10a). Even at a much lower volume fraction ($\phi = 0.01$), the discrepancy between dense and dilute predictions is at least 30%. The differences between dense and dilute predictions of $D_{q,2}$, shown in Figure 2.11, are less pronounced than $D_{q,1}$, however, still quite significant. In fact, results indicate at least a 20% discrepancy between predictions at a volume fraction $\phi = 0.1$ (Figure 2.11a). As for the mutual and thermal diffusion coefficients, the dilute (GD) Dufour coefficient presented in Ref. [3] is defined using different spatial gradients than those used in the dense (GHD) theory. As done before, a conversion has been applied to compare the Dufour coefficients by using the same representation for the heat flux.

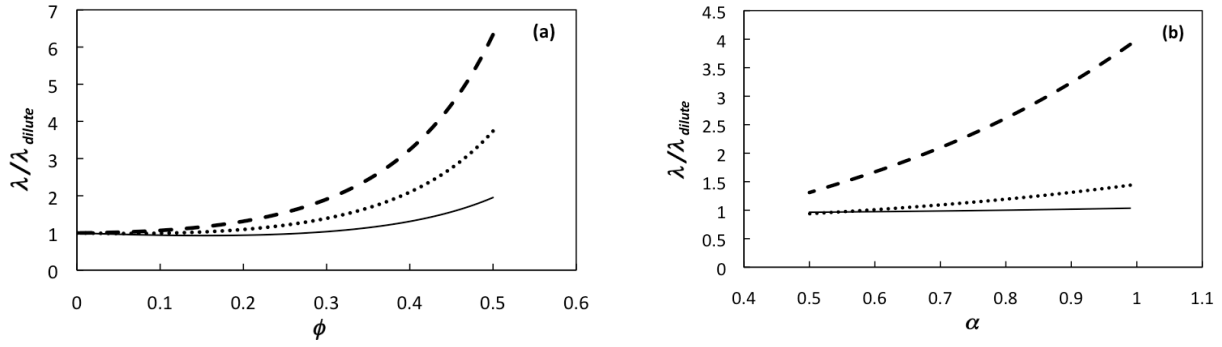

Figure 2.9: Transport coefficient associated with thermal conductivity: moderately dense (GHD) predictions as a function of (a) overall volume fraction and (b) coefficient of restitution. See legends presented in Figure 2.1.

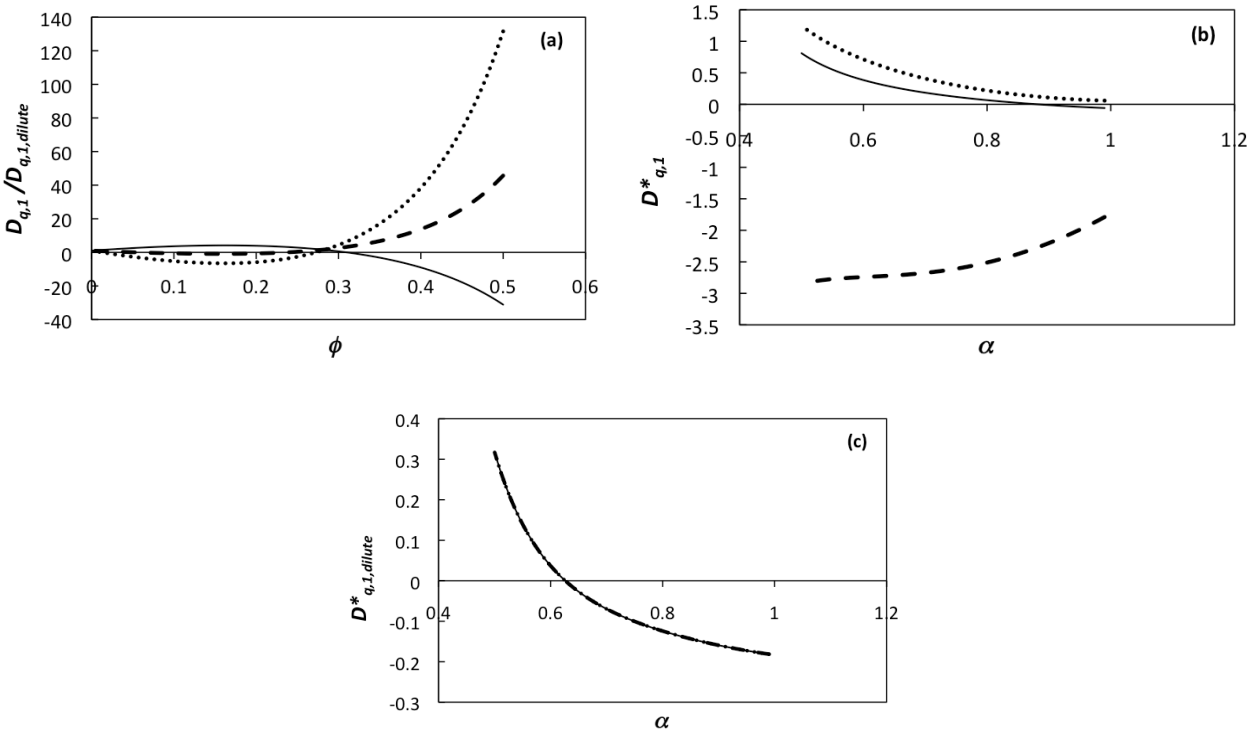

Figure 2.10: Transport coefficient associated with Dufour coefficient (1): moderately dense (GHD) predictions as a function of (a) overall volume fraction (b) dimensionless Dufour (1) with respect to coefficient of restitution and (c) dimensionless Dufour (1) with respect to coefficient of restitution. See legends presented in Figure 2.1.

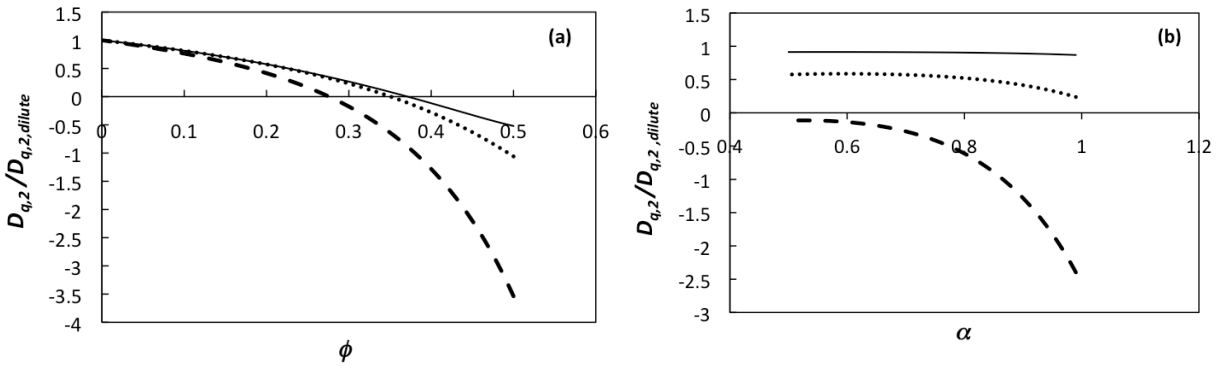

Figure 2.11: Transport coefficient associated with Dufour coefficient (2): moderately dense (GHD) predictions as a function of (a) overall volume fraction and (b) coefficient of restitution. See legends presented in Figure 2.1.

2.4 Concluding Remarks

To date, the understanding of particle segregation within polydisperse, rapid granular flows is somewhat limited due to a wide array of complexities that arise during the associated derivation of continuum theories. As previously mentioned, the two most common simplifications used in previous theories have been a Maxwellian velocity distribution and an equipartition of energy. This study focuses on two particular theories, neither of which assumes the above conditions. The first was proposed by Garzó and Dufty [3] for binary, dilute mixtures (referred to as GD theory), and the second was recently pro- posed by Garzó, Hrenya and Dufty [1, 2] for binary, moderately dense mixtures (referred to as GHD theory). In order to gage the importance of this dense-phase extension, the transport coefficients and equations of state predicted by GHD theory were compared to their dilute counterparts (GD theory). Furthermore, although not the focus of this study, it is worthwhile to mention that the CPU time required to evaluate the dense-phase coefficients was typically three times the requirement for its dilute counterpart.

A systematic comparison was carried out for three different cases (equal size and different mass, equal mass and different size, and different size and mass) over a range of mixture

parameters (diameter ratio, mass ratio, and volume fraction ratio), the details of which are listed in Table 2.1. Though this study focuses on a case of different- sized species with the same material density, similar trends were observed for all other cases analyzed. Results indicate that transport coefficients and equations of state predicted by GHD theory are substantially different than those predicted by dilute (GD) theory. Also, significant differences between predictions were reported for fairly dilute systems (ϕ = 0.1). In particular, the discrepancy between predictions was found to be as large as an order of magnitude. Certain coefficients, namely the mutual diffusion coefficient D_{11}, revealed that the magnitude and sign were different for the two theories. Naturally, the level of desired accuracy may vary between users of the theories. If, for example, 5% deviation between the GHD and GD predictions is deemed acceptable, then the need for a dense-phase correction is quite evident since the vast majority of quantities predicted by GHD theory are either larger or smaller than GD theory predictions by the 5% limit. Nonetheless, it is worthwhile to point that the comparison of dense- and dilute-phase predictions for a binary mixture presented here are independent of flow geometry. It is expected that is some flow geometries, one or more of the transport coefficients may dominate, while in other geometries another coefficient(s) may dominate. Such differences are system-dependent and should be taken into account when using the results contained herein.

Given the importance of the dense-phase corrections on the equations of state and transport coefficients, several follow-on studies are warranted: application of the theory to segregating systems in order to better understand the dominant segregation mechanisms (some previous studies have been carried in the tracer limit [7-9]), comparison with experimental and/or molecular-dynamics simulation data for purposes of validation, and application of the theory to a continuous particle size distribution. It is worthwhile to note that the GHD theory has been

incorporated recently into the open-source, public MFIX code (https://mfix.netl.doe.gov/) for the case of binary mixtures, thereby increasing its availability to a wider class of researchers.

Literature Cited

1. Garzó, V., J.W. Dufty, and C.M. Hrenya, *Enskog theory for polydisperse granular mixtures. I. Navier–Stokes order transport*. Physical Review E, 2007 **76**: 031303.
2. Garzó, V., C.M. Hrenya, and J.W. Dufty, *Enskog theory for polydisperse granular mixtures. II. Sonine polynomial approximation*. Physical Review E, 2007 **76**: 031304.
3. Garzó, V. and J.W. Dufty, *Hydrodynamics for a granular mixture at low density*. Physics of Fluids, 2002 **14**: 1476–1490.
4. Murray, J.A., V. Garzó, and C.M. Hrenya, *Enskog theory for polydisperse granular mixtures. III. Comparison of dense and dilute transpornt coefficients and equations of state for a binary mixture.* Powder Technology, 2012. **220**: p. 24-36.
5. Brey, J. J., M.J. Ruiz-Montero, and F. Moreno, *Energy partition and segregation for an intruder in a vibrated granular system under gravity*. Physical Review Letters, 2005 **95**: 098001.
6. Garzó, V. *Segregation in granular binary mixtures: thermal diffusion*. Europhysics Letters, 2006 **75**: p. 521–527.
7. Garzó, V. *Brazil-nut effect versus reverse Brazil-nut effect in a moderately granular dense gas*. Physical Review E, 2008 **78**: 020301(R).
8. Garzó, V. *Segregation by thermal diffusion in moderately dense granular mixtures*, European Physical Journal E: Soft Matter, 2009 **29**: p. 261–274.
9. Garzó, V. and F. Vega Reyes, *Mass transport of impurities in a moderately dense granular gas*, Physical Review E, 2009 **79**: 041303.

CHAPTER 3

CONTINUUM REPRESENTATION OF A CONTINUOUS SIZE DISTRIBUTION OF PARTICLES ENGAGED IN RAPID GRANULAR FLOW: NON-SEGREGATING SYSTEM[b]

3.1 Introduction

Granular materials are often comprised of particles of different sizes and/or material properties. Such polydispersity gives rise to a phenomenon known as species segregation or de-mixing, and has no monodisperse counterpart [1-4]. Though the majority of work on polydisperse kinetic theory of granular materials is limited to the binary case, it is more common that the distribution of particle sizes within a granular mixture is essentially continuous. Such continuous particle size distributions (PSDs) are prevalent in both nature (e.g., sandstorms, avalanches) and industry (e.g., grain processing, coal gasification), though not well understood.

Unlike the previous chapter, the focus here is on rapid granular flows of particles with a *continuous* distribution of sizes. Rapid flows are those in which particles engage in binary, instantaneous collisions. Such flows can be described mathematically via a kinetic theory analogy, which shares the same assumptions. As mentioned in Section 1.2.2 of this thesis, the starting single-particle velocity distribution function assumed in the initial kinetic equations of current kinetic-theory-based models is restricted to a *discrete* number, s, of particle species. Therefore, a discrete approximation is needed to examine the behavior of a continuous PSD using a kinetic-theory-based model. Unlike hydrodynamic models, moment models have been developed using a starting kinetic equation that incorporates a continuous PSD (e.g., Fox and Vedula [5]). The continuous PSD in moment models, however, is ultimately represented by a

[b] Murray, J.A., S. Benyahia , P. Metzger, and C.M. Hrenya. "Continuum Representation of a Continuous Size Distribution of Particles engaged in Rapid Granular Flow " *Physics of Fluids*, in press (2012).

fixed number of nodes (Fan and Fox [6]) which is determined by re-running simulations in a given geometry with an increasing number of nodes until the predictions are no longer sensitive to further increases.

Collectively, this work introduces a universal methodology for representing a continuous PSD in models based on the kinetic theory analogy, which can be carried out prior to simulation of a particular geometry. In particular, the mathematical technique developed and validated here uses as its foundation the explicit dependency of transport coefficients on the continuous PSD and its discrete approximation. From a physical standpoint, such information is critical for the prediction of practical flows, particularly since recent experiments exhibit qualitative differences between binary mixtures and continuous PSDs [7, 8].

To build on previous studies, the aim of the current work is to determine the suitability of polydisperse, hydrodynamic models to predict the flow behavior of a continuous size distribution of solids. In particular, the objective of this effort is twofold: (i) to determine the number of *discrete* species required to accurately approximate a *continuous* PSD, and (ii) to validate these results via a comparison with molecular dynamics (MD) simulations of continuous PSDs. The kinetic-theory-based model used in this study was proposed by Garzó, Hrenya, and Dufty [9, 10] (with corrections provided by Murray, Hrenya, and Garzó [11]) and is applicable to any number of finite species (s). A review of existing kinetic-theory-based models of polydisperse flows is given in Ref. [4]. Hereafter, this model will be referred to as GHD theory.

With regard to the first objective, transport coefficients given by GHD theory are evaluated over a range of restitution coefficients and volume fractions (dilute to moderately dense). It is important to note that the coefficient of restitution is denoted by e instead of α in Chapter 3 only. A discrete approximation for the continuous PSD (as is needed for use in the

kinetic-theory-based model) is accomplished via the matching of moments of the given continuous distribution and its discrete approximation. As the number of species used to approximate a continuous PSD increases, the number of moments matched increases as well. To determine the appropriate number of species (s_{min}) needed for the discrete approximation, both the desired accuracy and corresponding computational costs are considered. Specifically, transport coefficients of GHD theory are evaluated for increasing values of s until the desired accuracy is reached. The resulting s_{min} value is determined for a variety of Gaussian and lognormal PSDs of various widths, as well as for two experimentally-obtained continuous PSDs, namely coal particles used for gasification and simulants of lunar regolith (i.e., lunar soil). Results of this effort indicate that wider continuous PSDs require a larger number of particle species for an accurate discrete approximation, though the appropriate number of species can be fairly low overall ($s_{min} = 5$) for the widest lognormal PSD analyzed.

With regard to the accuracy of GHD theory applied to continuous PSDs (objective 2), a comparison between previous MD simulations of continuous PSDs engaged in simple shear [12] and GHD predictions of granular pressure and shear viscosity is conducted. The results not only confirm the earlier determination of s_{min} for various Gaussian and lognormal PSDs, but also provide validation of the GHD theory as well as the use of a moment-based discrete approximation for continuous PSDs.

3.2 Methods

As previously mentioned, a continuous PSD must be approximated as a discrete number of particle sizes (and associated volume fractions) in order to utilize existing kinetic-theory-based models. In the paragraphs below, the continuous PSDs examined in this work (Section 3.2.1), the method used to obtain discrete approximation to continuous PSDs (Section 3.2.2), as

well as the technique used to evaluate the accuracy of the discrete approximations (Section 3.2.3) are discussed.

3.2.1 Continuous PSDs Investigated

In this work, four types of continuous size distributions are investigated: (i) Gaussian distributions, (ii) lognormal distributions, (iii) a bidisperse PSD of coal particles used for gasification provided by the Department of Energy National Energy Technology Laboratory (DOE NETL), and (iv) a simulant of lunar soil provided by National Aeronautics and Space Administration Kennedy Space Center (NASA KSC). Figure 3.1 shows the number-based frequency distribution, f_n, for each of these size distributions. For the Gaussian and lognormal distributions, a range of distribution widths, σ/d_{ave}, where σ denotes the standard deviation of the PSD and d_{ave} denotes its arithmetic mean, are examined. Accordingly, $\sigma/d_{ave} = 0$ corresponds to the monodisperse limit. For Gaussian distributions, the maximum distribution width is $\sigma/d_{ave} =$ 30% since a further increase would result in negative (unphysical) particle diameters [13]. Due to the extended right tail of lognormal distributions, a similar limit does not exist, and here lognormal distributions with σ/d_{ave} = 0-90% are considered. Figures 3.1a and 3.1b show lognormal and Gaussian distributions, respectively, in which the average diameter (d_{ave} = 72.6 microns) is held constant, whereas Figures 3.1c and 3.1d show distributions with a constant root-mean-cube diameter (d_{rmc} = 72.6 microns). The former distributions were used in analyzing the discrete approximation of continuous PSDs (Sections 3.3.1), and the latter were used for direct comparison with the MD simulations of Dahl *et al*. [12; see Section 3.3.4]. The PSD of coal particles provided by DOE NETL was obtained via sieving and thus was provided in a mass-based form in Figure 3.1e. Note that the bidisperse nature of this distribution is no longer apparent when it is converted to a number-based distribution (Figure 3.1f), which is used to

obtain a discrete approximation (see Section 3.3.2). Lastly, the PSD of a simulant of lunar soil known as OB-1 and measured by NASA is shown, with the measured mass-based distribution in Figure 3.1g, and the associated number-based distribution in Figure 3.1h. For purposes of direct comparison, the bidisperse coal PSD (DOE NETL) and a lognormal distribution with the same average diameter as the OB-1 and a distribution width of σ/d_{ave} = 90% are also shown on these log-log plots. Relative distribution widths are revealed in Figures 3.1g and 3.1h. The lognormal distribution exhibits a high frequency of particles with diameters near the average diameter (d_{ave} = 0.57); however, the frequency quickly approaches zero as the particle diameter is increased. On the other hand, the lunar soil simulant distribution (OB-1) and coal PSD exhibit moderate frequencies for a larger range of particle diameters. Thus, the experimental distributions contain a larger "width" of particle diameters. Because the OB-1 distribution and the coal PSD have different average diameters, the relative width of these distributions is not so obvious. However, by approximating each experimental PSD with a lognormal distribution of appropriate width, it was determined that the lunar soil simulant distributions are much wider than the coal PSD. For the sake of brevity, the OB-1 lunar soil simulant [14] is the only shown lunar PSD. It is worth noting that distributions of several other lunar soil simulants (OB-1, JSC-1a, LHT-2M, BP-1) and a sample of lunar soil were investigated; the resulting trends are similar to those of OB-1 and thus only the representative results of OB-1 are included below for the sake of brevity.

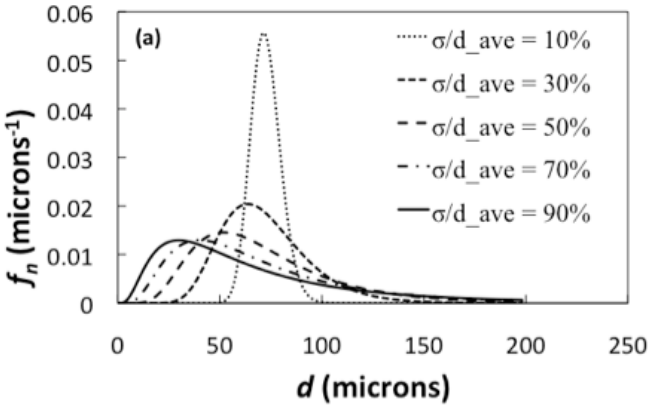

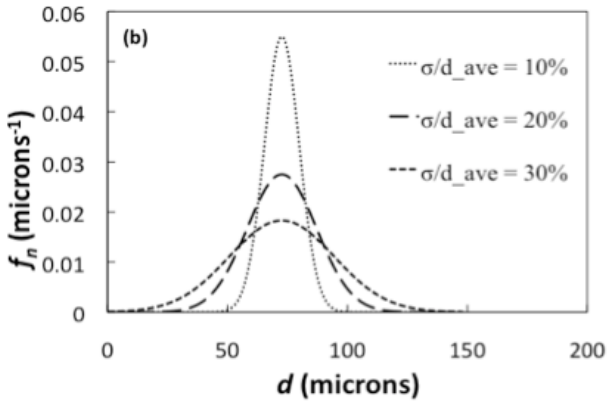

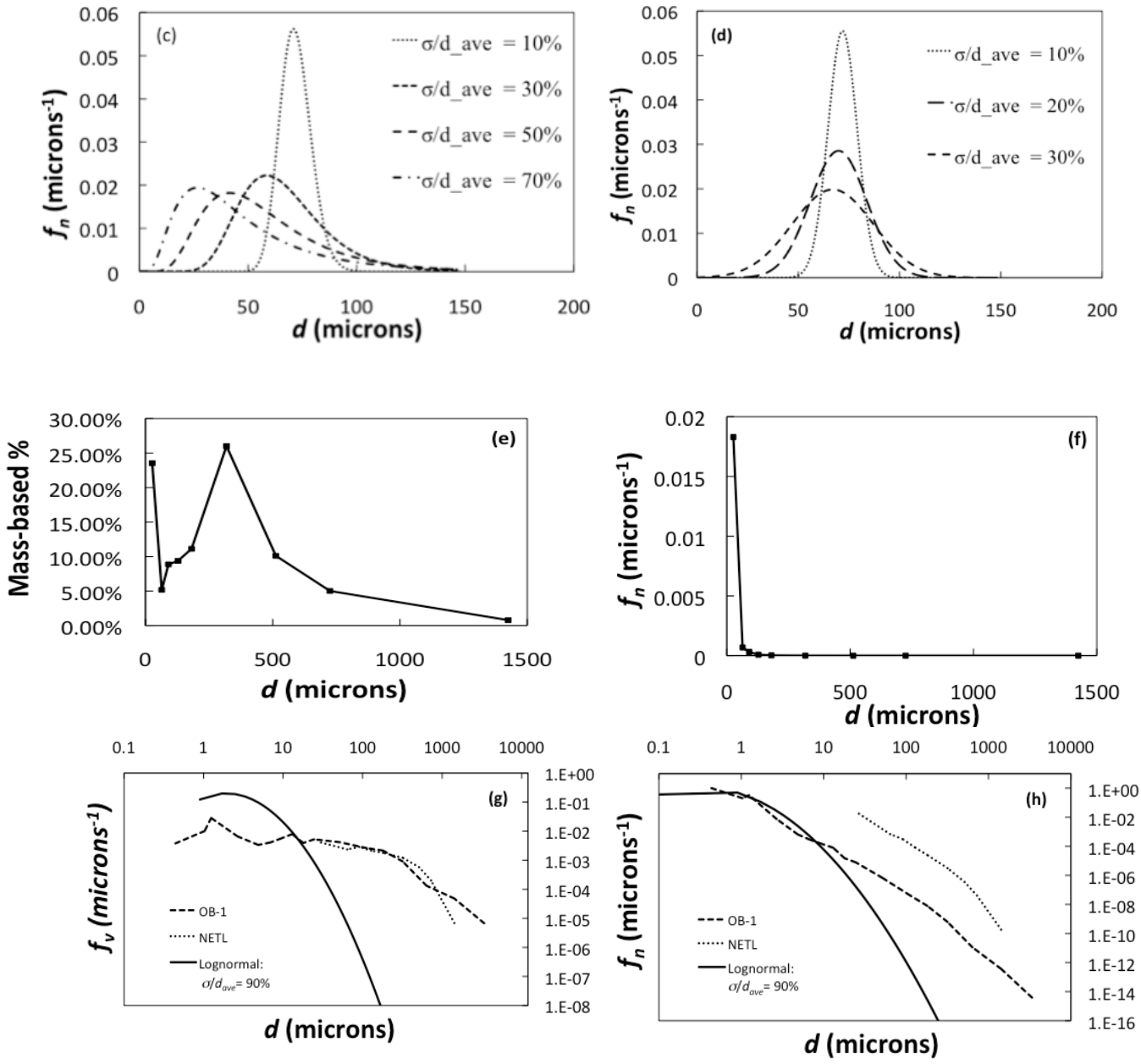

Figure 3.1: Number-based frequency (f_n) for **(a)** lognormal PSD with constant d_{ave}, **(b)** Gaussian PSD with constant d_{ave}, **(c)** lognormal PSD with constant d_{rmc}, and **(d)** Gaussian PSD with constant d_{rmc}. Frequency distributions of coal particles in terms of a **(e)** mass and **(f)** number basis. Frequency distributions of lunar soil simulant (OB-1) in terms of a **(g)** mass and **(h)** number basis.

3.2.2 Discrete, Moment-Based Approximation of Continuous PSDs

Though continuous PSDs can be discretized using a variety of methods, a logical choice involves the matching of moments between the continuous PSD and its discrete approximation. The method of matching moments has been previously utilized by Fan and Fox [6] for application to fluidized beds. Specifically, the i^{th} moment of a continuous PSD (μ_i) is defined by:

$$\mu_i = \int_0^\infty d^i f_n d(d) \qquad \textbf{Eq. 3.1}$$

where f_n denotes the number-based frequency distribution of particle diameter (d). The first several moments are familiar quantities: the zeroth moment (μ_0) is equal to unity, the first moment (μ_1) is equal to the number-based average diameter, and the second and third moments are the variance and skewness, respectively.

For Gaussian and lognormal distributions, analytic expressions for the moments are available and take the following forms, respectively [6]:

$$\mu_{i,Gaussian} = \sum_{r=0}^{i} \sigma^{i-r} d_{ave}^{r} \frac{i! \cdot 1 \cdot 3 \cdots (i-r-1)}{(i-r)!r!} \qquad \textbf{Eq. 3.2}$$

$$\mu_{i,Lognormal} = d_{ave}^{i} \exp\left(\frac{i^2\sigma^2}{2}\right) \qquad \textbf{Eq. 3.3}$$

In these equations $r = 0,2,\ldots$ for even values of i and $r = 1,3,\ldots$for odd values of i.

Unlike Gaussian and lognormal distributions, analytic forms of the moments for the experimentally obtained distributions are not available. Accordingly, numerical means are instead used to determine the moments of these continuous distributions, as given by Eq. 3.1. In other words, continuous PSDs can be divided into "bins" of width Δd, where smaller widths results in higher accuracy:

$$\mu_i \sim \sum_{b=1}^{k} d_b^i f_n \Delta d \qquad \textbf{Eq. 3.4}$$

where k is the number of bins and d_b is the diameter of particles associated with bin b.

Once the moments of a given *continuous* PSD have been obtained either analytically or numerically (via Eq. 3.3 or 3.4, respectively), a corresponding *discrete* approximation can be determined by matching the desired number of moments between the two distributions. The number of size species, s, contained in this discrete approximation is chosen independently, and with an increase in the number of species comes an increase in the number of moments matched. More specifically, for a discrete approximation with s species, the first $2s$ moments are matched between the distributions, where the moments of the discrete approximation are obtained via:

$$\mu_i = \sum_{j=1}^{s} d_j^i w_j \qquad \textbf{Eq. 3.5}$$

where d_j are the particle sizes and w_j are the corresponding number-based fractions or "weights" of particles with size d_j. Accordingly, the first $2s$ moments result a system of $2s$ equations, with s unknown diameters and s unknown weights. Furthermore, in order to relate the particle size and associated weight (number fraction) to the volume fraction of species j, the following relationship is used:

$$\frac{\phi_j}{\phi} = \frac{\phi_j}{\sum_{j=1}^{s} \phi_j} = \frac{d_j^3 w_j}{\sum_{j=1}^{s} d_j^3 w_j} \qquad \textbf{Eq. 3.6}$$

where the species volume fraction is denoted by ϕ_j and the overall volume fraction is denoted by ϕ. For example, for a discrete approximation using $s = 2$, the first four moments of the distribution are matched to that of the continuous distribution. Calculating the first four moments

of the discrete approximation will allow for the determination of the two particle species diameters (d_1, d_2) and associated volume fraction ratios (ϕ_1/ϕ, ϕ_2/ϕ). Generally speaking, the resulting set of $2s$ nonlinear equations is quite stiff; therefore, a method known as the product-difference algorithm is used to solve for the s particle diameters and associated species weights [6, 15].

It is important to note that a tradeoff exists between the number of species s chosen for the discrete approximation and the computational power required to solve the resulting kinetic-theory-based equations (described below and presented in Table 1.1). Matching a greater number of moments (i.e., larger s) results in a more accurate approximation. Figure 3.2 shows an example of a continuous PSD (d_{ave} = 894 μm) that has been discretized using both two and four discrete species. Note that the discretization using s = 4 more accurately mimics the shape of the actual distribution than does the discretization using s = 2. However, because s + 2 governing differential equations need to be solved for a mixture with s species (1 momentum, 1 granular energy, and s mass balances), choosing a larger number of species will increase the complexity of the resulting expressions given in Table 1.1 as well as the computational power required.

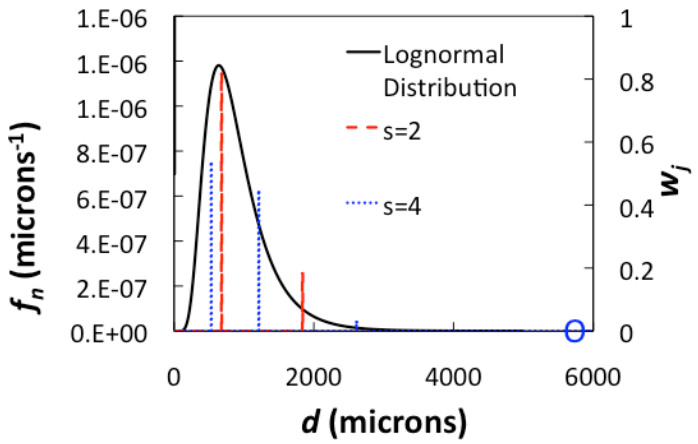

Figure 3.2: Discrete approximation of lognormal distribution (d_{ave} = 894 microns, σ/d_{ave} = 50%) using two particle species (s = 2) and four particle species (s = 4), corresponding to the red and blue lines, respectively. The left hand y-axis corresponds to the number-based frequency of the

lognormal distribution, whereas the right hand y-axis corresponds to the number-based fractions of the discrete approximations. The fourth particle species has such a low number-based fraction that the line is not visible at the given scale and its location is circled instead.

3.2.3 Evaluation of the Discrete Approximation to a Continuous PSD

To determine the impact of the choice of s on the accuracy of the discrete approximations to continuous PSDs, such approximations are obtained for various values of s (Section 3.2.2) for each of the PSDs considered here (Section 3.2.1). Then, kinetic theory predictions of transport coefficients are evaluated for each of the discrete approximations. By comparing predictions for discrete distributions at various values of s, the minimum number of species (s_{min}) needed to achieve the desired accuracy can be determined. Using these values, kinetic theory predictions of discrete distributions are then compared to MD simulations of simple shear flows with continuous size distributions.

For purposes of this work, the kinetic-theory-based model considered here is that proposed by Garzó, Hrenya, and Dufty [9, 10] (with corrections provided by Murray, Hrenya, and Garzó [11]). This theory, referred to as GHD hereafter, is used since it contains the fewest assumptions of existing polydisperse theories; it accounts for non-equipartition and non-Maxwellian effects and is applicable up to moderately dense flows and over a wide range of restitution coefficients [see Ref. 4 for a review of various polydisperse, kinetic-theory-based models]. The mass, momentum, and granular energy balances for the GHD theory are cast in terms of the species number density (n_i), mass-based mixture velocity ($\underline{U}$), and number-based mixture granular temperature (T), as shown in Table 1.1. Each balance equation is expressed in terms of these hydrodynamic variables (n_i, $\underline{U}$, T) along with the following constitutive quantities: cooling rate (ζ), mass flux of species i ($\underline{j_{oi}}$), heat flux ($\underline{q}$), and pressure tensor ($\underline{\underline{P}}$). Constitutive expressions for these quantities are also given in Table 1.1 in terms of the transport coefficients ζ

$^{(0)}$ (zeroth-order cooling rate), ζ_u (transport coefficient associated with first-order cooling rate), D_{ij} (mutual diffusivity), D_i^T (thermal diffusivity), D_{ij}^F (mass mobility), λ (conductivity), $D_{q,i}$ (Dufour coefficient), L_{ij} (thermal mobility), p (pressure), η (shear viscosity), and κ (bulk viscosity). These transport coefficients depend on the particle properties (species diameters, species masses, species restitution coefficients) as well as the hydrodynamic variables, thereby resulting in a closed set of equations (see Table 1.1 with additional expression in Appendix A).

To determine the number of species needed for the discrete approximation to accurately capture the given continuous PSD, the transport coefficients from the GHD theory are evaluated using the moment-based discrete approximation for increasing number of particle species (s). Namely, once the continuous PSD has been discretized for a given s (as described in Section 3.2.2), the particle sizes and associated volume fractions ($\phi_i = n_i \pi d_i^3/6$) can be used in the GHD expressions of transport coefficients. More specifically, the transport coefficients $\zeta^{(0)}$, ζ_u, p, η, and κ given by GHD theory are compared for s = 1, s = 2, etc. over a range of restitution coefficients and overall solids fractions to determine at what value of s the predictions essentially collapse on one another (as detailed below). Results of this study provide a basis for using the least computational power (i.e., lowest value of s) while achieving an accurate approximation.

It is worthwhile to note that some transport coefficients (i.e., $\zeta^{(0)}$, ζ_u , p, η, κ, λ; see Table 1.1) are calculated as summations over each species, but exist as a single-valued quantity regardless of the number of species chosen. Because the remaining transport coefficients (i.e., D_{ij}, D_i^T, D_{ij}^F, $D_{q,i}$, L_{ij}) are calculated for each species (e.g., D_i^T) or for a species pairing (e.g., D_{ij}), a one-to-one comparison between approximations with different s is not possible. For instance, the prediction of D_1^T using an s = 1 approximation cannot be compared to the prediction of D_1^T for the s = 2 approximation since species 1 has a different size for each approximation. Though

conductivity (λ) does not fall under this category, its summation includes D_i^T, a term that has been found to be discontinuous under certain conditions. Therefore, analyses of conductivity are omitted from this study.

The specific range of input parameters (solids fraction, restitution coefficient, etc.) used for each of the distributions considered here is given in Table 3.1. When three consecutive predictions of a transport coefficient, using increasing values of s (i.e., $s_{\min}$, $s_{\min}+1$, $s_{\min}+2$), lie within 2% of one another for the parameter space considered here (Table 3.1), the minimum number of discrete species is considered to be reached. An example of this methodology is displayed in Figure 3.3, which shows the dimensionless zeroth-order cooling rate as a function of restitution coefficient (e) for increasing values of s from 1-10. The zeroth-order cooling rate ($\zeta^{(0)}$) is non-dimensionalized by the average diameter of the distribution (d_{ave}), material density (ρ), and granular temperature (T). It is quite evident that the curves collapse when two or more discrete species are used in the approximation, which is a relatively small number. It is worthwhile to note that the minimum number of discrete species ($s_{\min}$) deemed necessary may be different depending on the specific transport coefficient analyzed.

As further verification of the $s_{\min}$ needed for the discrete approximation and for validation of the GHD theory itself, predictions from the theory for *discrete* approximations are also compared to molecular dynamics (MD) data of *continuous* size distributions undergoing simple shear flow [12]. The distributions examined in this MD-theory comparison are also contained in Table 3.1, along with the corresponding range of input parameters.

Table 3.1: Parameter space used to assess the number of discrete species needed to accurately represent a continuous PSD.

Type of Comparison	Continuous Distribution	Coefficient of Restitution	Volume Fraction	Distribution Width (σ/μ)
Kinetic theory (GHD) predictions of $\zeta^{(0)}$, ζ_u, p, η, and κ for increasing values of s in the discrete approximation	Lognormal	0.50-0.99	10^{-8}-0.50	0, 0.1, 0.3, 0.5, 0.7, 0.9
	Gaussian	0.50-0.99	10^{-8}-0.50	0, 0.05, 0.1, 0.2, 0.3
	Coal Particles	0.50-0.99	10^{-8}-0.50	**N/A**
	Lunar Soil Simulant, OB-1	0.50-0.99	0.1	**N/A**
MD vs. kinetic theory (GHD) predictions	Lognormal	0.85, 0.95	0.1, 0.3, 0.5	0, 0.1, 0.3, 0.5, 0.7
	Gaussian	0.85, 0.95	0.1, 0.3, 0.5	0, 0.05, 0.1, 0.2, 0.3

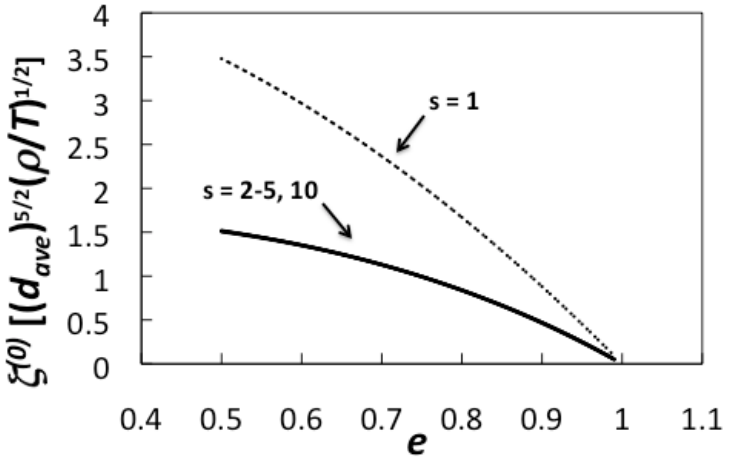

Figure 3.3:. GHD predictions of the dimensionless zeroth-order cooling rate as a function of restitution coefficient (***e***) for various values of s. The discrete distributions shown here are approximations of a lognormal PSD with a distribution width σ/d_{ave} = 50% and an overall volume fraction $\phi = 0.3$.

3.3 Results and Discussion

To determine the appropriateness of a (*discrete*) kinetic-theory-based prediction of a *continuous* PSD, the number of discrete species needed for the "collapse" of various transport coefficients ($\zeta^{(0)}$, ζ_u, p, η, and κ) over a range of parameters is first pursued for Gaussian and lognormal PSDs of different widths (Section 3.3.1), as well as each experimentally-obtained PSD (Section 3.3.2). A summary of the results is given in the following section (Section 3.3.3). Second, predictions of pressure and shear viscosity in a simple shear flow system obtained from (discrete) GHD theory is compared with MD simulations of continuous PSDs (Section 3.3.4).

3.3.1 Discrete Approximation of Gaussian and Lognormal PSDs

To determine the number of species needed in kinetic-theory-based models to appropriately mimic continuous PSDs, the following transport coefficients were evaluated using GHD theory, the following transport coefficients are examined: zeroth-order cooling rate ($\zeta^{(0)}$), first-order cooling rate (ζ_u), pressure (p), shear viscosity (η), and bulk viscosity (κ). In particular, these quantities were evaluated for each continuous PSD using an increasing number of discrete species (s) to approximate the given PSD (as described in Section 3.2.3). These evaluations were carried out over a range of restitution coefficients (e) and overall volume fractions (ϕ). Representative plots of the dimensionless pressure and shear viscosity are included in Figures 3.4 – 3.9; the remaining results are summarized in Table 3.2 for the sake of brevity. Both pressure and shear viscosity have been non-dimensionalized, where m is the particle mass associated with the average diameter of the distribution (d_{ave}).

Similar to Figure 3.3 for the dimensionless zeroth-order cooling rate, Figures 3.4 and 3.5 show how the pressure and shear viscosity vs. restitution coefficient, respectively, change with the number of species for *lognormal distributions* with $\phi = 0.3$ and distribution widths of $\sigma/d_{ave} =$

10% (Figures 3.4a and 3.5a) and σ/d_{ave} = 70% (Figures 3.4b and 3.5b). Expectedly, as the number of discrete species s used to approximate the continuous distribution increases, the curves begin to collapse on one another. As described in Section 3.2.3, once a 2% or less error is established among three consecutive approximations (e.g., s = 2, 3, 4) of a transport coefficient over the entire range of restitution coefficients shown, the minimum number of species for desired accuracy ($s_{\min}$) has been determined. For instance, Figure 3.4a indicates that predictions of pressure using s = 2, 3, or 4 are extremely close to one another (< 2% change). Therefore, only 2 species are deemed necessary to approximate the pressure of a lognormal PSD with σ/d_{ave} = 10% and ϕ = 0.3. Comparing Figure 3.4a to Figure 3.4b, it is evident that the number of species used in the discrete approximation of a lognormal PSD has a larger effect for wider distributions. Specifically, Figure 3.4a shows that the monodisperse prediction of pressure agrees qualitatively and quantitatively well with the polydisperse predictions (s = 1-10) for a narrow lognormal distribution (σ/d_{ave} = 10%). However, for the wider continuous lognormal PSD (σ/d_{ave} = 70%) of Figure 3.4b, the pressure predictions for s > 1 are quite different quantitatively than the monodisperse counterpart (s = 1). Moreover, Figure 3.4b shows that pressure predicted using s = 2-10 is slightly non-monotonic, whereas the monodisperse prediction increases monotonically with restitution coefficient. Nevertheless, both discretizations require 2 particles species for the established criterion to be met for granular pressure (i.e., $s_{\min}$ = 2), regardless of vast differences in distribution width. Finally, as seen when comparing the shear viscosity of different distribution widths in Figures 3.5a and 3.5b, the trends are similar to those of pressure (Figures 3.4a and 3.4b), though $s_{\min}$ = 3 for σ/d_{ave} = 70%.

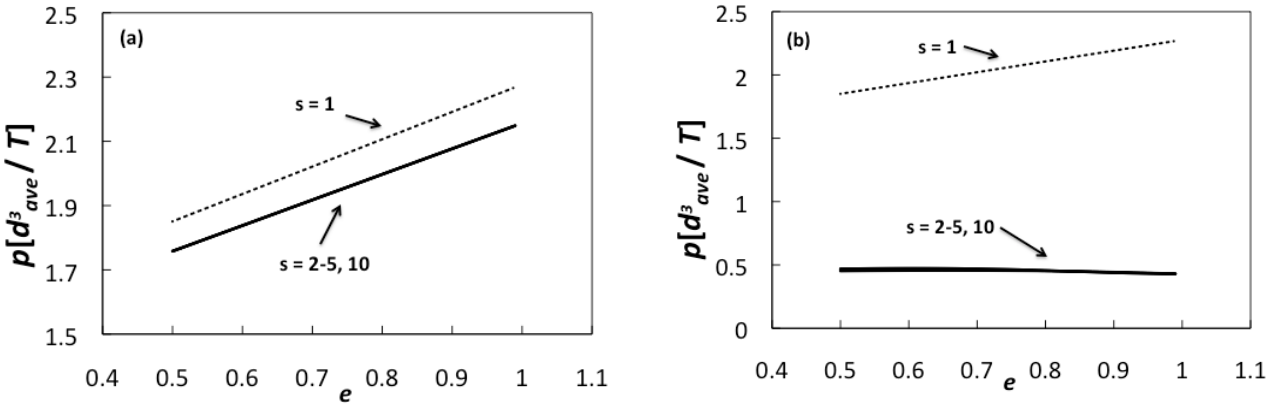

Figure 3.4: Predictions of granular pressure as a function of coefficient of restitution (***e***) for *lognormal* distributions with σ/d_{ave} of (a) 10% and (b) 70% using GHD theory. The overall volume fraction of the system is $\phi = 0.3$.

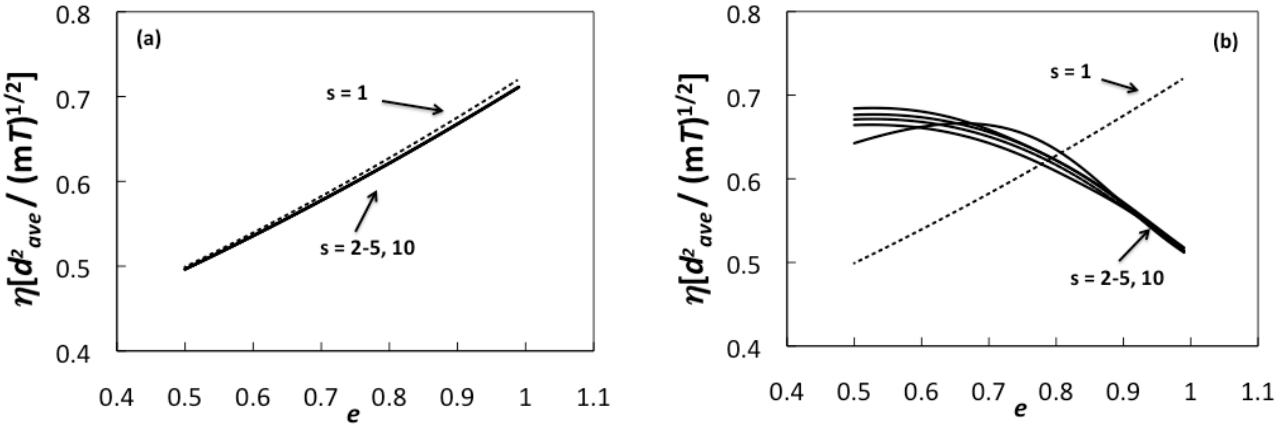

Figure 3.5: Predictions of shear stress as a function of coefficient of restitution (***e***) for *lognormal* distributions with σ/d_{ave} of (a) 10% and (b) 70% using GHD theory. The overall volume fraction of the system is $\phi = 0.3$.

Analogous to Figures 3.4 and 3.5, Figures 3.6 and 3.7 show predictions of dimensionless pressure and shear viscosity for *Gaussian distributions* of σ/d_{ave} = 10% (Figures 3.6a and 3.7a) and σ/d_{ave} = 30% (Figures 3.6b and 3.7b). Lognormal and Gaussian distributions behave quite similarly for σ/d_{ave} = 10-30%, as the asymmetries of lognormal distributions are not prominent for such small distribution widths (see Figures 3.1a and 3.1c). Therefore, it is not surprising that Figures 3.4a and 3.6a for pressure and Figures 3.5a and 3.7a for shear viscosity are similar for

the different distributions. Since Gaussian distributions are limited to a maximum σ/d_{ave} of 30% (otherwise unphysical negative diameters result), however, Figures 3.6b and 3.7b (σ/d_{ave} = 30%) do differ slightly from Figures 3.6a and 3.7a, respectively, though not nearly as much when comparing lognormal distributions over a wider range of distributions widths (e.g., comparing Figures 3.4a and 3.4b). It is also important to note that for pressure and shear viscosity, the widest Gaussian distribution (σ/d_{ave} = 30%) requires only $s_{\min}$ = 2 and the widest lognormal distribution requires $s_{\min}$ = 3. In sum, very few particle species can be used to describe fairly wide continuous distributions.

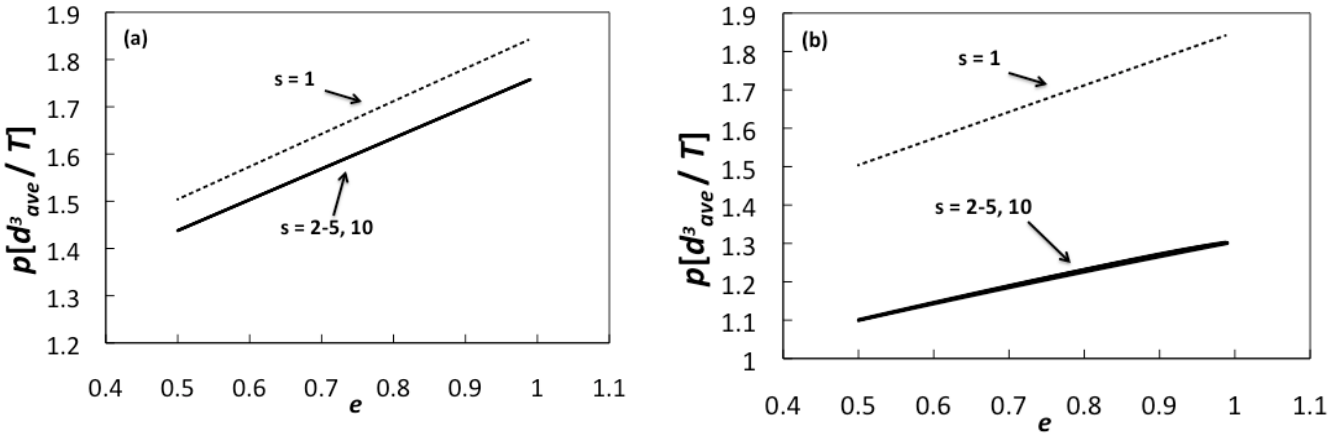

Figure 3.6: Predictions of granular pressure as a function of coefficient of restitution (***e***) for *Gaussian* distributions with σ/d_{ave} of (a) 10% and (b) 30% using GHD theory. The overall volume fraction of the system is ϕ = 0.3.

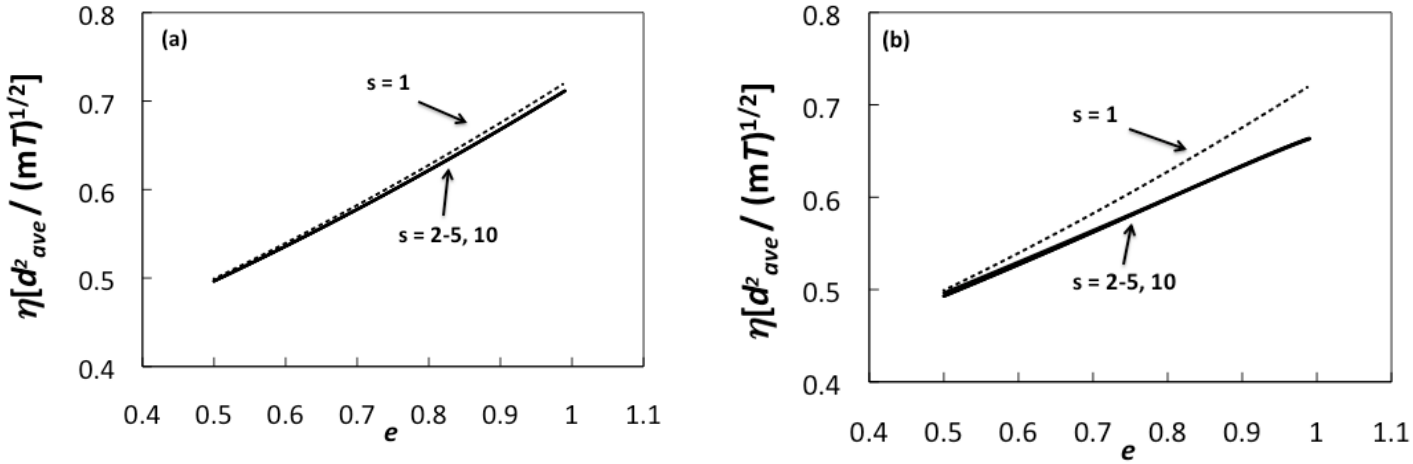

Figure 3.7: Predictions of shear stress as a function of coefficient of restitution (***e***) for *Gaussian* distributions with σ/d_{ave} of (a) 10% and (b) 30% using GHD theory. The overall volume fraction of the system is $\phi = 0.3$.

3.3.2 Discrete Approximation of Experimental PSDs

Results of dimensionless pressure and shear viscosity are also given for the *bidisperse NETL distribution of coal particles* (Figure 3.8). When the bidisperse mass-based distribution is converted to a number-based PSD, the resulting distribution is extremely right-skewed (Figure 3.1f), similar to a very wide lognormal distribution. Figure 3.8a shows that the monodisperse approximation (s = 1) of pressure is both qualitatively and quantitatively different than the polydisperse (s > 2) approximations. More notable is the discrepancy among discrete approximations for the shear viscosity (Figure 3.8b). The predictions using s = 3 and s = 4 are almost indistinguishable; however, adding a fifth particle species causes a significant change in the prediction of shear viscosity. Predictions of this NETL distribution are obtained to s = 10 to ensure this pattern does not continue. Accordingly, the number of species required to accurately capture the pressure and shear viscosity of the NETL distribution is $s_{\min} = 6$ for both quantities. The need for a larger number of species to accurately approximate the NETL distribution comes about from the width of the PSD. Specifically, Figures 3.1g and 3.1h show the large width of the NETL distribution relative to a lognormal distribution with σ/d_{ave} = 90%. Because the frequencies associated with the NETL distribution remains moderate over a larger range of particle diameters than those in the lognormal distribution, the coal PSD contains a larger width of particle diameters. Therefore, it is reasonable that the values of s_{min} for the NETL distribution are greater than or equal to the values of s_{min} for the Gaussian and lognormal distributions investigated here.

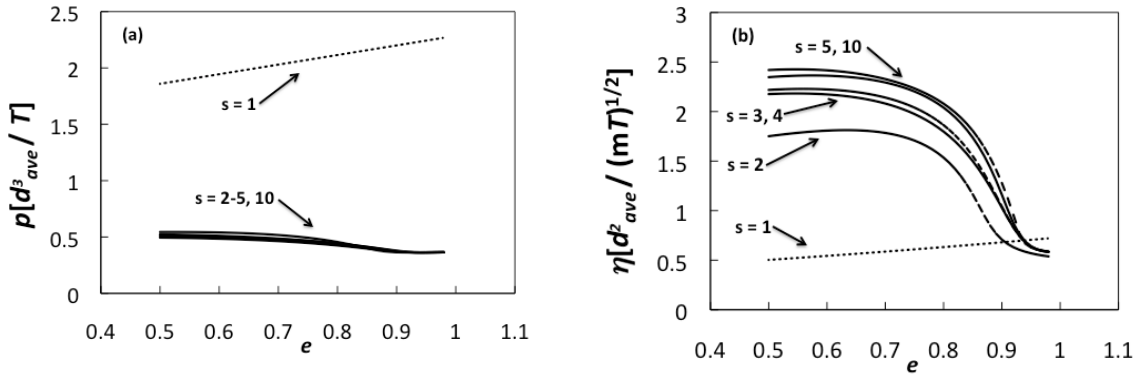

Figure 3.8: Predictions of (a) granular pressure and (b) shear stress as a function of coefficient of restitution (***e***) for *NETL distribution of coal feedstock* for gasification. The overall volume fraction of the system is $\phi = 0.3$.

Referring back to Figures 3.1g and 3.1h, the width of the *NASA lunar soil simulant OB-1* is compared to that of a lognormal distribution with a similar arithmetic mean and a distribution width of σ/d_{ave} = 90%, showing that OB-1 distribution is much wider than the lognormal distributions examined. Mimicking the lunar PSD with an extremely wide lognormal distribution, it was determined that the corresponding lognormal PSD has a width of about σ/d_{ave} = 250%. For this lunar PSD, matching more than 9 moments does not change the discrete approximation; therefore, only predictions for $s = 1 – 9$ are shown in Figure 3.9. Due to the large width of lunar PSDs, a large number of species is required to accurately predict each of the transport coefficients compared to the other PSDs investigated here. The pressure predicted using only one particle species to approximate the lunar simulant OB-1 is orders of magnitude larger than the predictions for $s = 2 – 9$. Including the $s = 1$ prediction of dimensionless pressure in Figure 3.9a would cause the $s = 2 – 9$ predictions to be nearly indistinguishable, so it is omitted from the plot. Though only predictions up to $s = 9$ are reported, collapse of curves occurs at $s_{\min} = 7$ for pressure (Figure 3.9a) and begins at $s_{\min} = 8$ for shear viscosity (Figure 3.9b). Each transport coefficient examined here, with the exception of pressure, requires at least eight

particle species to obtain an accurate prediction (s_{min} = 8), as is the case for the lunar soil itself and other lunar soil simulants (figures not shown).

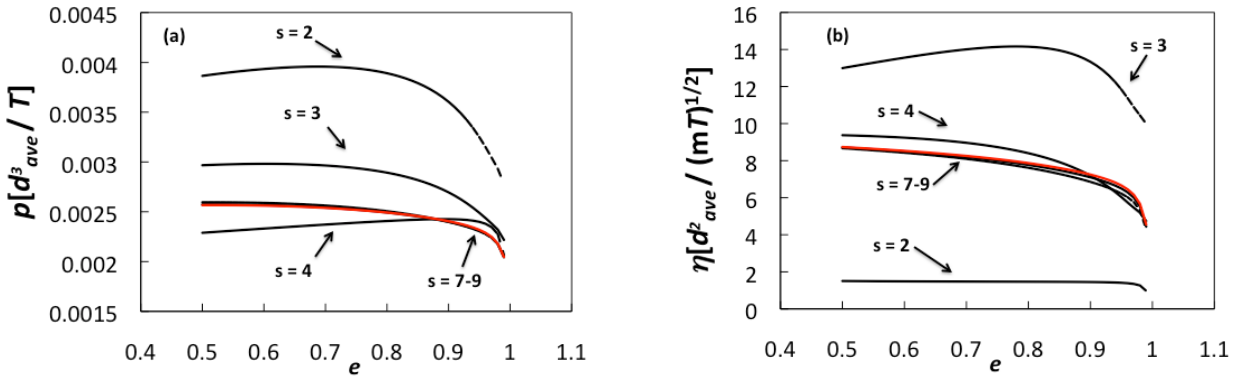

Figure 3.9: Predictions of (a) granular pressure and (b) shear stress as a function of coefficient of restitution (***e***) for the *OB-1* lunar PSD. The overall volume fraction of the system is $\phi = 0.1$. The $s = 9$ approximation is given by the solid red line, for color versions.

3.3.3 Summary of discrete approximations

For the sake of brevity, only figures for pressure and shear viscosity were shown above for each of the continuous PSDs investigated. The results obtained for the remaining transport coefficients ($\zeta^{(0)}$, ξ_u, and κ) behave in a similar fashion. A summary of these results over the parameter space evaluated is given in Table 3.2. Each value in Table 3.2 corresponds to the minimum number of species (s_{min}), as determined by the 2% criterion established in Section 3.2.2. It is important to note that the number of species required to accurately represent a continuous PSD with σ/d_{ave} = 0-90% is generally quite low (s_{min} = 1 – 5). However, the much wider distributions (i.e., lunar soil simulant) may require as many as 8 particle species (s_{min} = 8).

Table 3.2: Summary of minimum number of species (s_{min}) required to accurately approximate Gaussian, lognormal, bidisperse coal (NETL), and lunar soil (OB-1) size distributions with a discrete number of species.

		Gaussian			Lognormal					NETL	OB-1
	σ / d_{ave}	10%	20%	30%	10%	30%	50%	70%	90%		
	ϕ										
Zeroth-Order Cooling Rate	0.05	2	2	3	2	2	3	4	4	5	
	0.1	2	2	2	2	2	3	4	4	5	8
	0.3	2	2	2	2	2	3	4	4	5	
	0.5	2	2	2	2	2	3	4	4	3	
First-Order Cooling Rate	0.05	1	2	2	2	2	2	4	4	6	
	0.1	1	2	2	2	2	2	4	4	6	8
	0.3	2	2	2	2	2	2	4	4	5	
	0.5	2	2	2	2	2	2	3	3	6	
Pressure	0.05	2	2	2	2	2	2	2	2	2	
	0.1	2	2	2	2	2	2	2	3	3	7
	0.3	2	2	2	2	2	2	3	4	5	
	0.5	2	2	2	2	2	2	3	4	6	
Shear Viscosity	0.05	1	2	2	1	2	4	5	5	5	
	0.1	1	2	2	1	2	4	4	4	5	8
	0.3	1	2	2	1	2	3	3	4	6	
	0.5	1	2	2	1	2	2	3	5	6	
Bulk Viscosity	0.05	2	2	2	2	2	2	4	4	5	
	0.1	1	2	2	1	2	2	4	4	5	8
	0.3	1	2	2	1	2	2	3	4	6	
	0.5	1	2	2	1	2	2	3	5	6	

Another notable trend that is revealed in Table 3.2 is that distribution width generally has a larger effect on the number of species required for an accurate discretization ($s_{\min}$) of a given continuous PSD than does the volume fraction. More specifically, the values in Table 3.2 increase more within rows (varying σ/d_{ave}) than within columns (varying ϕ). To better illustrate this trend, Figure 3.10 displays the dependency of number of discrete species required on both distribution width (Figure 3.10a) and overall volume fraction (Figure 3.10b). A sufficient increase in distribution width (σ/d_{ave} = 0-90%) always shows an increase to the number of species required, whereas the increases volume fraction may decrease (η) or not affect ($\xi^{(0)}$, ξ_u , p, κ) the number of species needed. For instance, Figure 3.10b shows that predictions for shear stress require fewer species at higher volume fractions, whereas the remaining transport coefficients require the same number of species regardless of the volume fraction ($\phi = 10^{-8}$ - 0.5).

In sum, for all but one coefficient (η), s is independent of ϕ, though the same is not true for σ/d_{ave}.

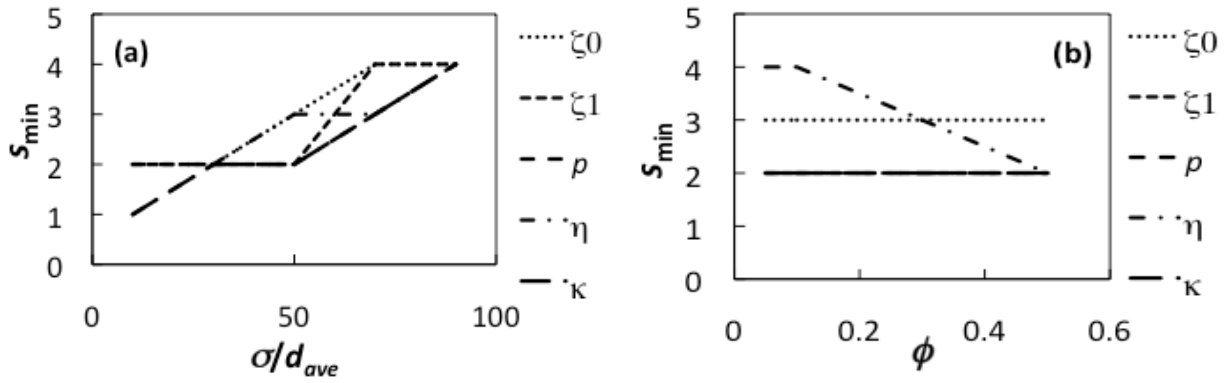

Figure 3.10: Minimum number of species required ($s_{\min}$) for a (a) lognormal distribution with a volume fraction of $\phi = 0.3$ and varying σ/d_{ave} and (b) a lognormal distribution with $\sigma/d_{ave} = 50\%$ and varying ϕ.

Finally, Table 3.2 can be used as a guide for determining how many species are needed for a specific flow system. For instance, if a specific flow geometry is dominated by the granular pressure and contains a Gaussian PSD with σ/d_{ave} = 30% and the overall volume fraction is predominantly ϕ = 0.05, only two particle species are necessary for the level of accuracy described here (2%). However, if a different flow geometry with the same PSD and overall ϕ is dominated by the zeroth-order cooling rate, three particle species are necessary for a similarly accurate approximation. Thus, in order to use these results in a practical application, some information must be known about the dominating effects of a system *a priori*. Alternatively, the maximum value of $s_{\min}$ among all transport coefficients examined may be used as a guide. Further discussion on the pros and cons of the use of Table 3.2 (or a similar analysis for other distributions) as a guide for determining the appropriate number of discrete species for a given application is included in Concluding Remarks (Section 3.4).

3.3.4 Comparison with molecular dynamics (MD) simulations

Molecular dynamics (MD) simulations of lognormal and Gaussian distributions undergoing simple shear flow (SSF) have been performed by Dahl, Clelland, and Hrenya [12]. In the current work, the simulation data is used not only to confirm for the minimum number of species ($s_{\min}$) required for an accurate discrete approximation (as reported in previous section), but also to test the accuracy of the GHD theory. The parameters used as inputs for the MD simulations are included in Table 3.1; the outputs include both pressure and viscosity. This MD data is displayed in Figures 3.11 and 3.12 for lognormal and Gaussian distributions of various widths, respectively. Also shown in Figures 3.11 and 3.12 are the predictions obtained from GHD theory for several discrete approximations (various s) of the given continuous PSDs. Note that these predictions were obtained by first solving the energy equation (the only nontrivial equation for SSF) for granular temperature (T) using the appropriate discrete approximation, and then using this value of T to evaluate the pressure and shear viscosity. The DOE-based code MFIX (Multiphase Flow with Interphase Exchanges, www.mfix.netl.doe.gov), which contains the GHD theory, was used for these purposes.

The results displayed in Figures 3.11 and 3.12 demonstrate that the number of species required for an accurate approximation of pressure and shear viscosity is correctly predicted by the approach described in the previous section. More specifically, a value of $s = 3$ is sufficient in each case, as consistent with the values given in Table 3.2 (whereas smaller values of s do not achieve the desired accuracy). Figures 3.11 and 3.12 clearly show drastic differences between the monodisperse approximation and the ternary approximation ($s = 3$), where the ternary prediction using GHD theory is far more accurate. However, increasing the number of species to $s = 5$ in

the discrete approximation shows little to no change at all, which further supports the predictions summarized in Table 3.2.

Though the monodisperse approximation of pressure and shear viscosity using GHD theory is appropriate in the monodispesre limit (i.e., $\sigma/d_{ave} = 0$), a larger number of particle species is required as the width of the PSD increases. Recall that for the MD data, the root mean cube of the continuous distribution was held constant (d_{rmc} = 72.6 microns). However, the dimensionless pressure and shear viscosity are plotted with respect to σ/d_{ave}. In order to maintain a constant d_{rmc} while increasing σ/d_{ave}, d_{ave} decreases accordingly, and thus the monodisperse approximations (i.e., $s = 1$) do not remain constant along the x-axis in Figures 3.11 and 3.12.

Regarding the validity of the GHD theory to predict properties of a continuous PSD, it is clear from Figures 3.11 and 3.12 that the GHD predictions using $s = 3$ and MD data are in close qualitative, as well as quantitative, agreement. From a qualitative perspective, the MD data displayed in Figures 3.11 and 3.12 indicate that the quantities behave non-monotonically with respect to the distribution width. This qualitative trend is captured by the polydisperse (s = 3, 5) GHD predictions, but not the monodisperse counterparts (s=1). Perhaps more importantly is the quantitative agreement between GHD predictions and MD data. For instance, Figure 3.12b shows a maximum percent difference between the s = 3 prediction and the MD data of 4%. For the widest distributions, GHD predictions have similar accuracy when compared to MD data as in the monodisperse limit ($\sigma/d_{ave} = 0$). Therefore, no loss of accuracy arises from the polydisperse theory itself (relative to monodisperse), nor due to the discrete approximations of continuous PSDs.

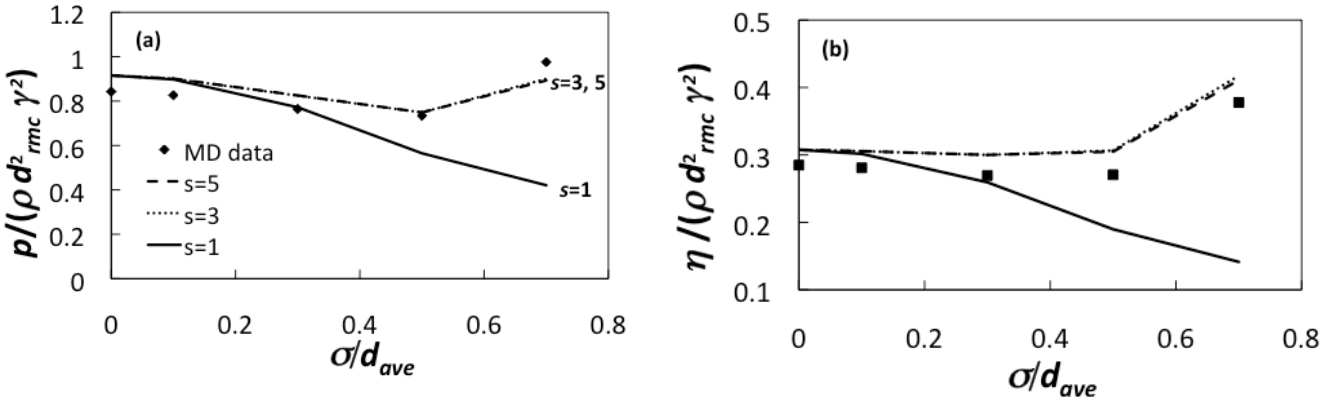

Figure 3.11: Dimensionless (a) pressure and (b) shear stress as a function of σ/d_{ave} for *lognormal* distributions. Comparison of MD simulation data to GHD theory predictions using an increasing number of particle species. Overall volume fraction: $\phi = 0.3$, restitution coefficient: $e = 0.85$.

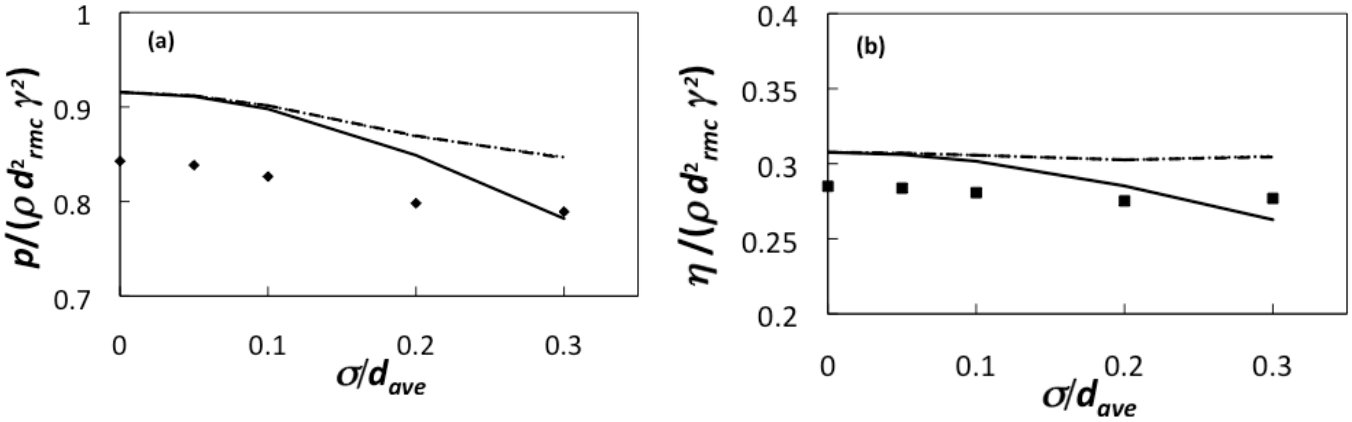

Figure 3.12: Dimensionless (a) pressure and (b) shear stress as a function of σ/d_{ave} for *Gaussian* distributions. Comparison of MD simulation data to GHD theory predictions using an increasing number of particle species. Overall volume fraction: $\phi = 0.3$, restitution coefficient: $e = 0.85$. See Figure 3.11a for legend.

3.4 Concluding Remarks

The overall aim of this work is to assess the ability of polydisperse, kinetic-theory-based, hydrodynamic models to describe continuous size distributions. In particular, the objective of this effort is twofold: (i) to determine the number of *discrete* species (s) required to accurately approximate a *continuous* PSD, and (ii) to validate the theoretical predictions via a comparison with molecular dynamics (MD) simulations of continuous PSDs. With regards to the first

objective, the moments of the discrete approximation are first matched with moments of the given continuous PSD. Next, five transport coefficients ($\zeta^{(0)}$, ζ_u , p, η, κ) given by GHD theory [9, 10], with corrections in Murray, Garzó, and Hrenya [11], are evaluated for the discrete approximations with various s, and the minimum number of species ($s_{\min}$) required to accurately capture the continuous PSD is identified via the "collapse" of these transport coefficients at higher values of s. It is worthwhile to note that this approach, unlike previous works [16-19], does not involve the computational fluid dynamics (CFD) simulations of specific systems thereby making it more universal and computationally efficient than previous works. With regard to the second objective, a comparison between MD data [12] and theoretical predictions at $s = s_{\min}$ is presented to determine the validity of GHD predictions of pressure and shear viscosity.

Regarding the number of species required to accurately represent a continuous PSD, the transport coefficients $\zeta^{(0)}$, ζ_u , p, η, and κ given by GHD theory are examined over a range of coefficient of restitution (e), overall volume fraction (ϕ), and distribution width (σ/d_{ave}). Both ideal (Gaussian and lognormal) and experimental (bidisperse coal particles and lunar soil simulants) continuous PSDs are considered. The number of species required for an accurate approximation depends on the transport coefficient of interest. For the Gaussian distributions analyzed, the maximum number of species required is typically 2 regardless of transport coefficient. However, the wider lognormal distributions require more species for the same accuracy level. For example, $s_{\min} = 5$ for the shear and bulk viscosities of lognormal distributions with a width of $\sigma/d_{ave} = 90\%$. Because the number-based frequency distribution of the NETL distribution is wider than the lognormal distributions analyzed, it is found that a greater number of species is needed for an accurate approximation ($s_{\min} = 6$). Even wider than the NETL distribution are the distributions of the lunar soil simulants. An examination of the lunar PSD

known as OB-1 shows that at least 8 particle species need to be considered in the discrete approximation for accurate predictions.

The aforementioned results indicate that an increase in distribution width leads to a corresponding increase in the number of species required to accurately approximate the PSD. However, the same is not true for volume fraction of the granular mixture. Increasing overall volume fraction may lead to a decrease or no change to the number of required species.

The second portion of this work focuses on the comparison of GHD predictions of pressure and shear viscosity with those given by previous MD simulations [12] for continuous PSDs. GHD predictions utilize a discrete approximation to the Gaussian and lognormal PSDs present in the MD simulations. Results indicate that the polydisperse prediction (s = 3) is qualitatively and quantitatively more accurate than the s = 1 counterpart, which is in agreement with the results of the former analysis on the discretization of continuous PSDs. The comparison also reveals that the level of accuracy (~5%) between MD and GHD predictions in distributions of increasing widths is similar to that of monodisperse systems. Accordingly, the results provide validation for both the moment-based approximation to continuous PSDs and the polydisperse theory itself. Furthermore, because the GHD theory uses the Enskog equation as its starting point, the good match obtained between MD and GHD theory displayed here provides support for the applicability of the Enskog equation to moderately dense flows.

Finally, a benefit of the current effort is that the analysis of some transport coefficients ($\xi^{(0)}$, ζ_u, p, η, κ) is system-independent - i.e., it does not depend on the flow geometry under consideration since the most general form of the transport coefficients is utilized. Nonetheless, it is worthwhile to note that the analysis here is restricted to the transport coefficients that are not indexed to specific species or species pairs (ie., $\xi^{(0)}$, ζ_u , p, η, κ). Because some transport

coefficients are indexed to specific species or species pairs (ie., D_{ij}, D_i^T, D_{ij}^F, $D_{q,i}$, L_{ij}), a one-to-one comparison of these quantities for successive values of s is not possible. For example, the s = 2 prediction of D_{12} cannot be compared to the s = 3 approximation of D_{12} because species 1 and 2 have different sizes for each approximation. Accordingly, the results of this work may be used differently depending on the system under analysis. If the system is dominated by one or more of the transport coefficients investigated here, then this analysis provides a method for determining the number of species needed for the discrete approximation. An example of such a system is simple shear flow, in which the only constitutive quantities that are included in the governing equations are $\xi^{(0)}$, p, and η. Otherwise, results of this effort should be used as a guide until further work is done to determine the effects of the remaining transport coefficients. An example of such a system is one which segregates, since the governing equations of a segregating system would include D_{ij}. Nonetheless, because the discrepancy between the number of species required amongst the transport coefficients considered here is relatively small, it is possible that the same may be true for the transport coefficients not examined here (ie., D_{ij}, D_i^T, D_{ij}^F, $D_{q,i}$, L_{ij}). However, this matter remains to be tested and will be the focus of future work.

Literature Cited

1. Curtis, J.S. and B. van Wachem, *Modeling particle-laden flows: A research outlook.* AIChE Journal, 2004. **50**(11): p. 2638-2645.
2. Muzzio, F.J., T. Shinbrot, and B.J. Glasser, *Powder technology in the pharmaceutical industry: the need to catch up fast.* Powder Technology, 2002. **124**(1-2): p. 1-7.
3. Sundaresan, S., *Some outstanding questions in handling of cohesionless particles.* Powder Technology, 2001. **115**(1): p. 2-7.
4. Hrenya, C.M., *Kinetic theory for granular materials: Polydispersity*, in *Computational Gas-Solids Flows and Reacting Systems: Theory, Methods and Practice*, S.P., M. Syamlal, and T. O'Brien, Editor. 2011, IGI Global: Hershey, PA.
5. Fox, R.O., P. Vedula, *Quadrature-based moment model for moderately dense polydisperse gas-particle flows*. Industrial and Engineering Chemistry Research, 2010. **49**(11): p. 5174-5187.
6. Fan, R. and R.O. Fox, *Segregation in polydisperse fluidized beds: Validation of a multi-*

fluid model. Chemical Engineering Science, 2008. **63**(1): p. 272-285.
7. Chew, J. W., J. Wolz, and C. M. Hrenya, *Axial segregation in bubbling gas-fluidized beds with Gaussian and lognormal Distributions of Geldart group B particles*. AIChE Journal, 2010. **56**: p. 3049-3061.
8. Chew, J. W. and C. M. Hrenya, *Link between bubbling and segregation patterns in gas-fluidized beds with continuous size distributions*. AIChE Journal, 2011. **57**: p. 3003-3011.
9. Garzó, V., C.M. Hrenya, and J.W. Dufty, *Enskog theory for polydisperse granular mixtures. II. Sonine polynomial approximation.* Physical Review E, 2007. **76**(3): p. 031304.
10. Garzó, V., J.W. Dufty, and C.M. Hrenya, *Enskog theory for polydisperse granular mixtures. I. Navier-Stokes order transport.* Physical Review E, 2007. **76**(3): p. 031303.
11. Murray, J.A., V. Garzó, and C.M. Hrenya, *Enskog theory for polydisperse granular mixtures. III. Comparison of dense and dilute transpornt coefficients and equations of state for a binary mixture.* Powder Technology, 2012. **220**: p. 24-36.
12. Dahl, S., R. Clelland, and C.M. Hrenya, *Three-dimensional, rapid shear flow of particles with continuous size distributions.* Powder Technology, 2003. **138**(1): p. 7-12.
13. Dahl, S., R. Clelland, and C.M. Hrenya, *The effects of continuous size distributions on the rapid flow of inelastic particles.* Physics of Fluids, 2002. **14**: p. 1972.
14. Battler, M.M. and J.G. Spray, *The Shawmere anorthosite and OB-1 as lunar highland regolith simulants.* Planetary and Space Science, 2009. **57**(14-15): p. 2128-2131.17.
15. Gordon, R.G., *Error bounds in spectroscopy and nonequilibrium statistical mechanics.* Journal of Mathematical Physics, 1968. **9**: p. 1087-1092.
16. Fan, R., D.L. Marchisio, and R.O. Fox, *Application of the direct quadrature method of moments to polydisperse gas-solid fluidized beds.* Powder Technology, 2004. **139**(1): p. 7-20.
17. Isben, C.H., E. Helland, B.H. Hjertager, T. Solberg, L. Tadrist, and R. Occelli, *Comparison of multi-fluid and discrete particle modeling in numerical predictions of gas particle flow in circulating fluidized beds.* Powder Technology, 2004. **149**(1): p. 29-41.
18. Mathiesen, V., T. Solberg, and B.H. Hjertager, *Predictions of gas/particle flow with an Eulerian model including a realistic particle size distribution.* Powder Technology, 2000. **112**(1-2): p. 34-45.
19. Sanyal, J., D.L. Marchisio, R.O. Fox, and K. Dhanasekharan, *On the comparison between population balance models for CFD simulation of bubble columns.* Industrial & Engineering Chemistry Research, 2005. **44**(14): p. 5063-5072.

CHAPTER 4

REPRESENTATION OF A CONTINUOUS SIZE DISTRIBUTION IN A SEGREGATING SYSTEM USING A KINETIC THEORY MODEL

4.1 Introduction

As mentioned in Section 1.2.2, several studies and theories have been proposed for polydisperse, rapid solids flows [1-10]. Because of the increasing complexity of introducing additional particle species in a kinetic-theory-based model, only a few studies have been conducted for mixtures with more than two discrete particle species [6] and even fewer that investigate continuous PSDs. Nevertheless, several MD simulations and experimental data are available for comparison with polydisperse KT [8-14]. Specifically, the focus of this effort is to quantify the number of species necessary to approximate a continuous particle size distribution (PSD), while obtaining an accurate comparison between MD and KT predictions of solids fraction and granular temperature profiles for a *segregating system*. Though MD data exists for polydisperse mixtures in bounded conduction [10, 11], a comparison with KT predictions has not yet been performed; this task is the focus of this chapter. The kinetic theory considered here (GHD theory [1, 2] with corrections by Murray *et al*. [15]) is restricted to rapid granular flows (binary, instantaneous particle interactions) for any finite number of species. For this study, GHD theory was used in conjunction with the standard Enskog theory rather than the revised Enskog theory. Motivation for this change is described in Section 4.4.1.

In the previous chapter (Chapter 3), the focus was an examination of single-valued transport coefficients for increasing values of s in order to determine the appropriate number of species to capture a continuous PSD. This discrete approximation was then used in a comparison with MD simulations for a non-segregating system, specifically simple shear flow. The focus of this section is to show how discrete approximations of continuous PSDs can be used to

accurately predict behavior in a *segregating system*, specifically bounded conduction. Examining a segregating system provides a more comprehensive understanding of the sensitivity of transport coefficients that do not exist as a single value (thermal diffusion, ordinary diffusion, etc.) to discrete approximations of continuous PSDs.

4.2 Methods

4.2.1 System Description

Continuous size distributions are examined for a bounded conduction system, known to exhibit species segregation. The physical parameters and continuous distributions considered for a segregating system are given in Table 4.1; the distributions examined include both lognormal and Gaussian distributions of varying widths. It is important to note that for a lognormal distribution of $\sigma/d_{ave} = 0.3$, the coefficient of restitution is also varied in order to demonstrate its effect on species segregation. Figure 4.1 shows a two-dimensional slice of a continuous PSD engaged in bounded conduction in a three-dimensional system. The bounded conduction system is characterized by "hot" and "cold" boundaries at the left and right side, respectively, with periodic boundaries at top, bottom, front, and back. Moreover, this system is characterized by no external forces and zero mean flow, such that a gradient in temperature and solids fraction develops between the fixed-temperature walls. A general property of a granular mixture in bounded conduction is that all particles segregate in the region of lowest granular temperature, with the more massive particles segregating preferentially (resulting in species segregation, or de-mixing) [9-12]. The profiles of solids fraction and granular temperature of several continuous PSDs in bounded conduction are compared for both KT and MD simulations later in this chapter.

Table 4.1: Parameter space used in determination and validation of s_{min} values, as well as in the comparison of KT and MD simulations for a bounded conduction system. The granular temperature ratio used in each MD simulation is $T_h/T_c = 2$.

Type of Comparison	Continuous Distribution	Coefficient of Restitution	Volume Fraction	Distribution Width (σ/d_{ave})
Molecular Dynamics	Lognormal	0.99	0.05	0.1, 0.3, 0.5
		0.90, 0.80	0.05	0.3
	Gaussian	0.99	0.05	0.1, 0.2, 0.3
Kinetic Theory	Lognormal	0.99	0.05	0.1, 0.3, 0.5
		0.90, 0.80	0.05	0.3
	Gaussian	0.99	0.05	0.1, 0.2, 0.3

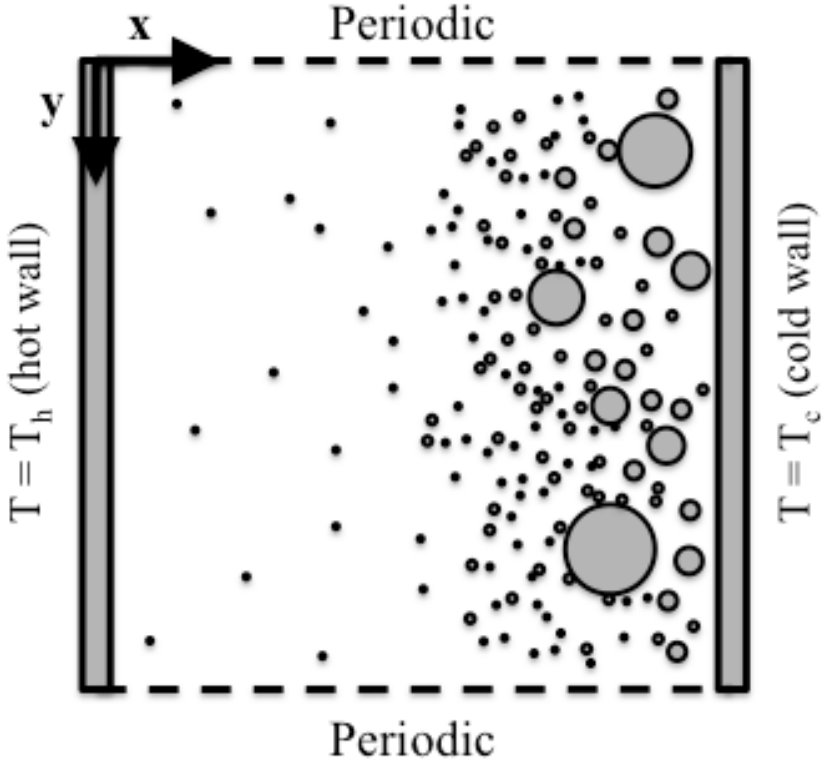

Figure 4.1: Two-dimensional cross-section of a continuous PSD engaged in bounded conduction. The system is assumed periodic in both the *y*- and *z*-directions, where the *z*-component runs perpendicular to the *xy*-plane.

4.2.2 Molecular Dynamics Description

For the molecular dynamics simulation conducted, particles were considered spherical and inelastic (see Table 4.1 for parameter space evaluated). A hard-sphere, event-driven algorithm is used, meaning that collisions are binary and instantaneous in nature. Linear trajectories are assumed between collisions due to the lack of external forces. Lastly, 500 collisions per particle are used in order to achieve a statistical steady state for each simulation. The MD code used for analysis of continuous PSDs in bounded conduction here is the same as used in the work of Dahl and Hrenya [10]; however, the parameter space evaluated here is different than that evaluated by Dahl and Hrenya [10].

4.2.3 Continuum Model Description

Referring back to Table 1.1, the governing equations applied to a specific system provide valuable insight about the behavior of the system. For the bounded conduction studies presented in this thesis work, it is assumed that there is zero mean flow, steady-state conditions, and no external forces. Therefore, the balance of momentum for a granular mixture (Eq. 1.2) indicates that pressure (p), which is defined as

$$p = nT + \frac{2\pi}{3}\sum_{i=1}^{s}\sum_{j=1}^{s}\mu_{ji}\left(1+\alpha_{ij}\right)d_{ij}^{3}\,\chi_{ij}^{(0)}n_i\,n_j\,T_i\ , \qquad \textbf{Eq. 4.1}$$

is constant throughout the system, where n denotes number density, T denotes granular temperature, $\mu_{ij} = (m_i/(m_i + m_j))$, α_{ij} denotes coefficient of restitution, d_{ij} denotes the average diameter of species i and j, and $\chi_{ij}^{(0)}$ denotes the pair-correlation function. From the balance of mass (Eq. 1.1), it is clear that the mass flux equals zero (ie., $j_{oi} = 0$, Eq. 1.4), which includes ordinary (D_{ij}) and thermal (D_i^T) diffusion coefficients as follows

$$\underline{j}_{oi} = -\sum_{j=1}^{s} m_i m_j \frac{n_j}{\rho} D_{ij} \underline{\nabla} \ell n(n_j) - \rho D_i^T \underline{\nabla} \ell n(T) = 0 \qquad \textbf{Eq. 4.2}$$

Lastly, the balance of granular energy (Eq. 1.3) reveals that the heat flux ($\underline{q}$) and cooling rate terms remain. Considering the heat flux expression (Eq. 1.5), it is evident that the conductivity (λ), cooling rate (ζ), and Dufour coefficient ($D_{q,ij}$) also play an important role in determining the granular temperature and solids fraction profiles for a bounded conduction system as shown in the equation below

$$\nabla \cdot \underline{q} = \nabla \cdot [-\lambda \underline{\nabla} T - \sum_{i=1}^{s} \sum_{j=1}^{s} T^2 D_{q,ij} \underline{\nabla} \ln(n_i)] = -\frac{3}{2} n \zeta T \qquad \textbf{Eq. 4.3}$$

Though the cooling rate and conductivity are single-valued transport coefficients (and thus were examined in Chapter 3), the Dufour coefficient, ordinary diffusion coefficient, and thermal diffusion coefficient exist as a matrix of values, the size of which depends upon the number of particle species used in the discrete approximation (see Table 1.1). Therefore, it was not possible to directly compare these quantities for increasing values of s as done for the single-valued transport coefficients (Chapter 3).

The set of governing equations shown in Eqs. 4.1 – 4.3 are solved using MFIX software (https://mfix.netl.doe.gov/) applied to a bounded conduction system. Simulations were run for a maximum of 150 seconds, with a time-step between 10^{-3} – 10^{-8} seconds. It is worthwhile to note that the constant-temperature wall used in the MD simulations is only applied to those particles that have collided with the the wall, such that the prescribed wall temperature is not representative of the averaging strip next to the wall. Therefore, the MD values of granular temperature one averaging strip removed from the wall (ie., x/L = 0.15 and x/L = 0.85) were used as the boundary conditions for the KT model. For purposes of direct comparison with MD simulations, a modified grid-size of 7x10 in the xy-plane was used (ie., x/L = 0-0.7) in the KT

model. Because the modified grid-size used in the KT model spans a domain of $x/L = 0 – 0.7$, the solids fraction and granular temperature profiles obtained using MFIX were then shifted $x/L = 0.15$ to the right, allowing for discrete approximations of KT predictions for increasing values of s over the range of $x/L = 0.15 – 0.85$. Consequently, the values of s_{min} determined using KT predictions of solids fraction and granular temperature are restricted to this domain.

Similar to the rule-of-thumb used in Section 3.2.3, when two consecutive predictions of both solids fraction and granular temperature profiles, using increasing values of s (i.e., $s_{\min}$ and $s_{\min}+1$), lie within 2% of one another for the bounded conduction domain (Table 4.2), the minimum number of discrete species is considered to be reached.

4.3 Results and Discussion

The figures below show KT predictions of Gaussian and lognormal distributions having widths between $\sigma/d_{ave} = 0.1 – 0.3$, using discrete approximations of $s = 1$, 2, and 3. For the wider lognormal distribution, $\sigma/d_{ave} = 0.5$, discrete approximations were compared for $s = 1$, 2, 3, and 4. Discrete approximations of continuous PSDs were obtained by matching distribution moments as described in Section 3.2.2. Also, a comparison between MD and KT predictions of overall solids fraction and granular temperature is carried out for each system presented in Table 4.1.

The results presented in Figures 4.2-4.9, and summarized in Table 4.2, are laid out systematically below. More specifically, predictions of (a) solids fraction, (b) reduced granular temperature, and (c) species volume fraction ratios are shown across the domain for Gaussian (Figures 4.2 – 4.4) and lognormal (Figures 4.5 – 4.9) having widths of $\sigma/d_{ave} = 0.1 – 0.3$ and $\sigma/d_{ave} = 0.1 – 0.5$, respectively. The coefficient of restitution and solids fraction considered for each case are $\alpha = 0.99$ and $\phi = 0.05$, and the temperature ratio of the hot wall to the cold wall is $T_h/T_c = 2$. For a lognormal distribution with $\sigma/d_{ave} = 0.3$, coefficients of restitution of $\alpha = 0.90$

and $\alpha = 0.80$ are also considered as shown in Figures 4.8 and 4.9, respectively. Subplots (a) and (b) of Figures 4.2 – 4.9 show both the comparison of KT predictions for increasing values of s (solid lines), as well as the comparison with MD simulations (data points). Subplot (c) for Figures 4.2 – 4.9 shows the ratio of each species volume fraction (ϕ_i) to average species volume fraction ($\phi_{uniform,i}$), again plotted against the domain length. Therefore, a ratio $\phi_i / \phi_{uniform,i} > 1$ corresponds to a high density region with respect to species i, and $\phi_i / \phi_{uniform,i} < 1$ corresponds to a dilute region with respect to species i. Accordingly, species segregation can be detected in a system when one or more species begins to become increasingly dense/dilute compared to other species. Because a large coefficient of restitution and a low volume fraction were considered in this study, species segregation did not occur significantly except for the widest distribution (lognormal with $\sigma/d_{ave} = 0.5$) and the more inelastic systems (lognormal with $\sigma/d_{ave} = 0.3$, $\alpha =$ 0.90, 0.80). Examples of species segregation is shown in Figures 4.7c – 4.9c, where all species segregation toward the cold wall (ie., $\phi_i / \phi_{uniform,i} > 1$), and the largest species segregates in this region preferentially (since its $\phi_i / \phi_{uniform,i}$ is larger than other species).

As mentioned previously, subplots (a) and (b) of Figures 4.2 – 4.9 show the comparison of KT predictions and MD data. For narrow Gaussian ($\sigma/d_{ave} = 0.1 – 0.3$) and lognormal ($\sigma/d_{ave}$ = 0.1) distributions, MD simulations and discrete approximations of solids fraction and granular temperature agree within a few percent (< 5%) throughout the entire domain. However, for the wider lognormal distributions analyzed ($\sigma/d_{ave} = 0.3, 0.5$), agreement between KT and MD predictions worsen, with a maximum discrepancy between solids fraction profiles of 12%; however, this level of agreement is still promising. It is important to note that as the continuous distribution of interest increases in width, the associated size discrepancy amongst species of the discrete approximation increases, leading to a greater level of species segregation (Figure 4.7c).

Also, lower coefficients of restitution create larger gradients in granular temperature, leading to species segregation (Figures 4.8c and 4.9c). Because the parameter space evaluated here is limited here, the range of physical parameters and width of distributions must be more widely varied in order to assess the effect of species segregation on the accuracy of continuum models.

As evident from Table 4.2 and the results shown below, very few species are required to achieve an accurate discrete approximation of the Gaussian and lognormal distributions examined, even for less elastic systems. Due to restrictions of current KT models, as discussed in Section 4.4, a large coefficient of restitution ($\alpha = 0.99$) and a low volume fraction ($\phi = 0.05$) are considered for these bounded conduction studies, limiting the applicability of the results to nearly elastic, relatively dilute systems. Though wider distributions are limited with respect to coefficient of restitution, moderate-width distributions are not; therefore, an analysis of restitution coefficient on species segregation is conducted for a lognormal PSD with $\sigma/d_{ave} = 0.3$. It is worthwhile to compare the values of s_{min} between the study of segregating systems (this Chapter) and the study of single-valued transport coefficients (Chapter 3) given in Table 1.1. The value of s_{min} determined for a segregating system always matches at least one of the transport coefficient predictions. Also, the value of s_{min} was not affected by changes in coefficient of restitution. For a lognormal distribution with $\sigma/d_{ave} = 0.3$, $s_{min} = 2$ regardless the coefficient of restitution input (ie., $\alpha = 0.99, 0.90, 0.80$). Though a wider parameter space (eg., less elastic, more dense, etc.) must be evaluated before definitive conclusions can be drawn, the results presented in Table 4.2 suggest the values of s_{min} determined in the study of single-valued transport coefficients are applicable to segregating systems and non-segregating systems.

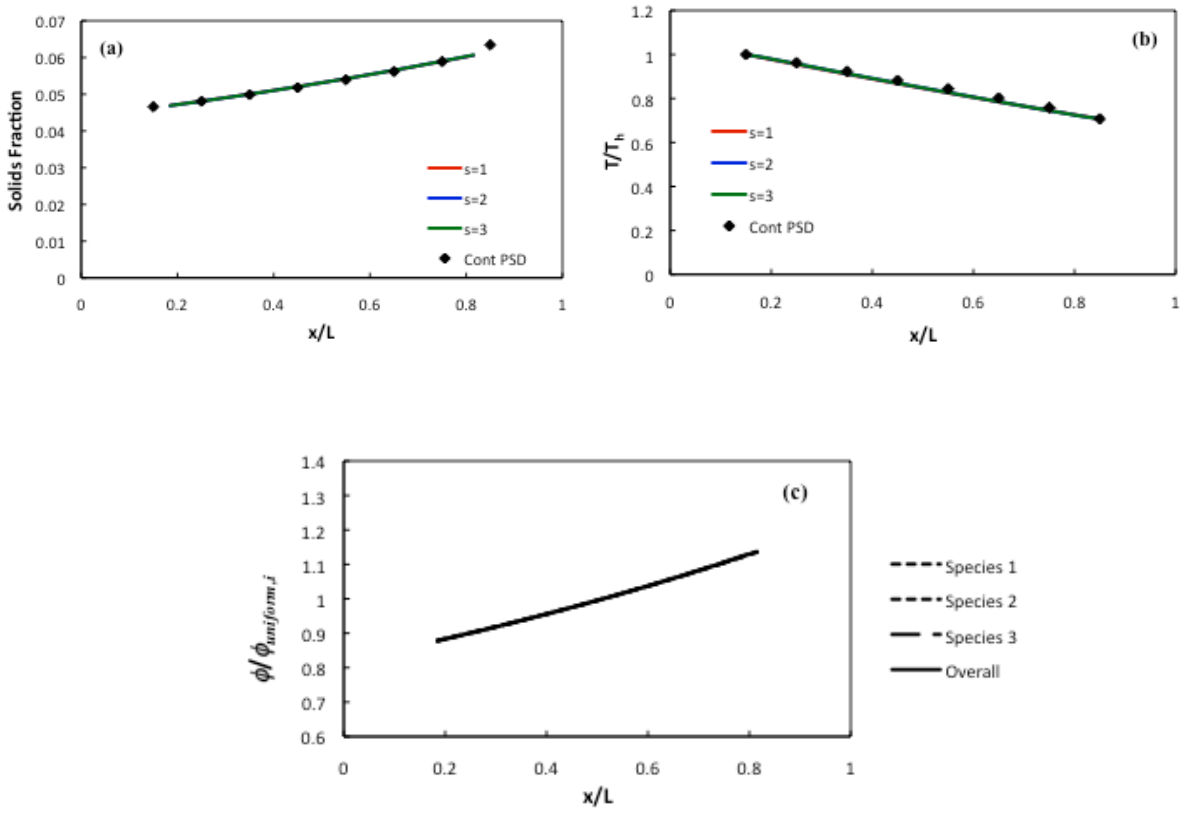

Figure 4.2: (a) MD and KT predictions of overall solids fraction, (b) MD and KT predictions of reduced granular temperature and (c) KT predictions of species solids fraction ratio for an $s = 3$ approximation as a function of domain length for a ***Gaussian*** distribution having a width of $\boldsymbol{\sigma/d_{ave} = 0.1}$. For (a) and (b) the data points correspond to the MD simulations run for the continuous PSD, whereas the solid lines correspond to KT predictions. For the $s = 3$ approximation, the diameter ratios and species volume fraction ratios are $d_3/d_1 = 1.490$, $d_3/d_2 = 1.1732$ and $\phi_1/\phi = 0.0915$, $\phi_2/\phi = 0.6472$, $\phi_3/\phi = 0.2613$. Also, the following physical parameters were used: $\phi = 0.05$, $\alpha = 0.99$, $T_h/T_c = 2$.

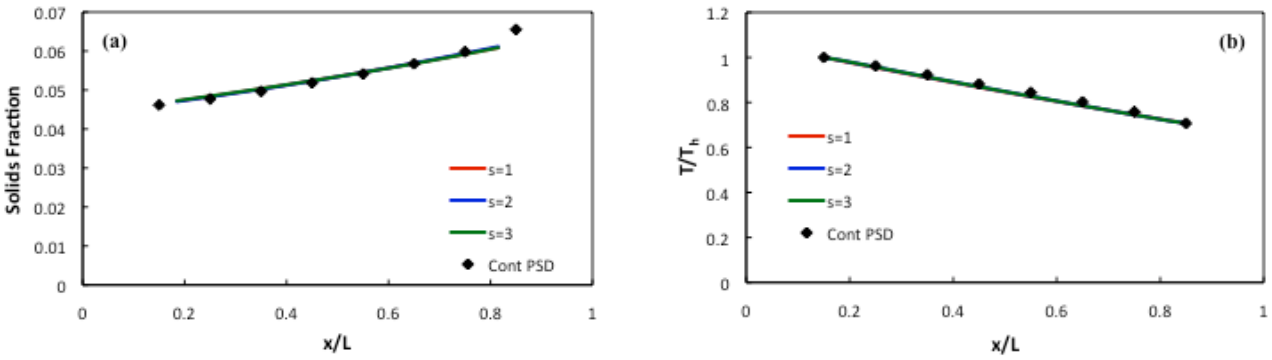

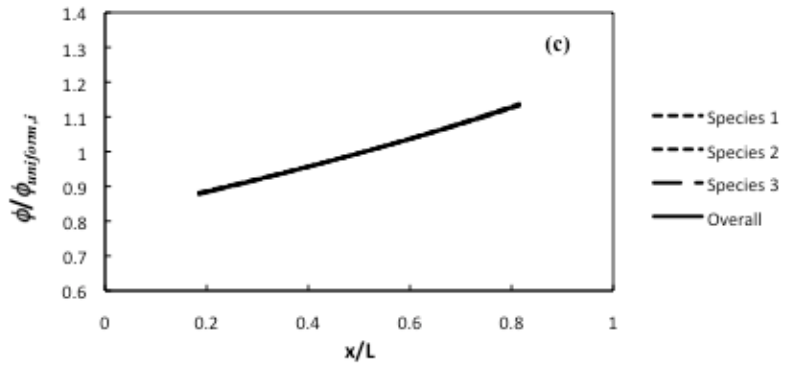

Figure 4.3: (a) MD and KT predictions of overall solids fraction, (b) MD and KT predictions of reduced granular temperature and (c) KT predictions of species solids fraction ratio for an $s = 3$ approximation as a function of domain length for a ***Gaussian*** distribution having a width of $\boldsymbol{\sigma/d_{ave} = 0.2}$. For (a) and (b) the data points correspond to the MD simulations run for the continuous PSD, whereas the solid lines correspond to KT predictions. For the $s = 3$ approximation, the diameter ratios and species volume fraction ratios are $d_3/d_1 = 2.060$, $d_3/d_2 = 1.3464$ and $\phi_1/\phi = 0.0415$, $\phi_2/\phi = 0.5952$, $\phi_3/\phi = 0.3633$. Also, the following physical parameters were used: $\phi = 0.05$, $\alpha = 0.99$, $T_h/T_c = 2$.

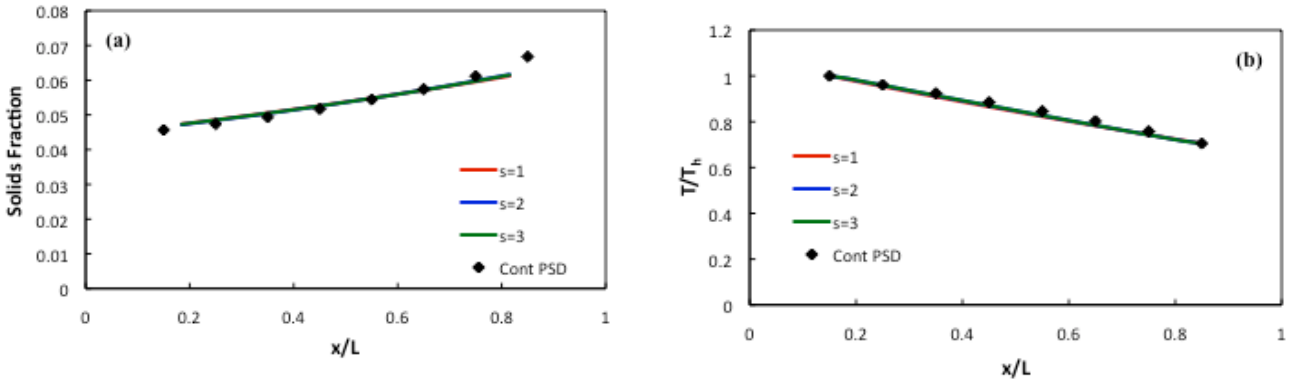

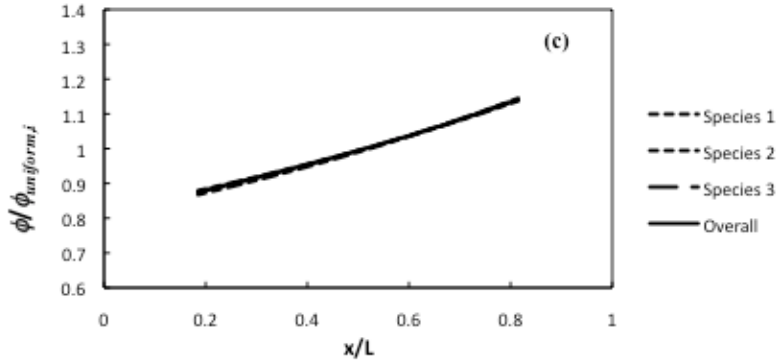

Figure 4.4: (a) MD and KT predictions of overall solids fraction, (b) MD and KT predictions of reduced granular temperature and (c) KT predictions of species solids fraction ratio for an $s = 3$ approximation as a function of domain length for a ***Gaussian*** distribution having a width of $\boldsymbol{\sigma/d_{ave} = 0.3}$. For (a) and (b) the data points correspond to the MD simulations run for the continuous PSD, whereas the solid lines correspond to KT predictions. For the $s = 3$ approximation, the diameter ratios and species volume fraction ratios are $d_3/d_1 = 3.1633$, $d_3/d_2 = 1.5196$ and $\phi_1/\phi = 0.0146$, $\phi_2/\phi = 0.5249$, $\phi_3/\phi = 0.4605$. Also, the following physical parameters were used: $\phi = 0.05$, $\alpha = 0.99$, $T_h/T_c = 2$.

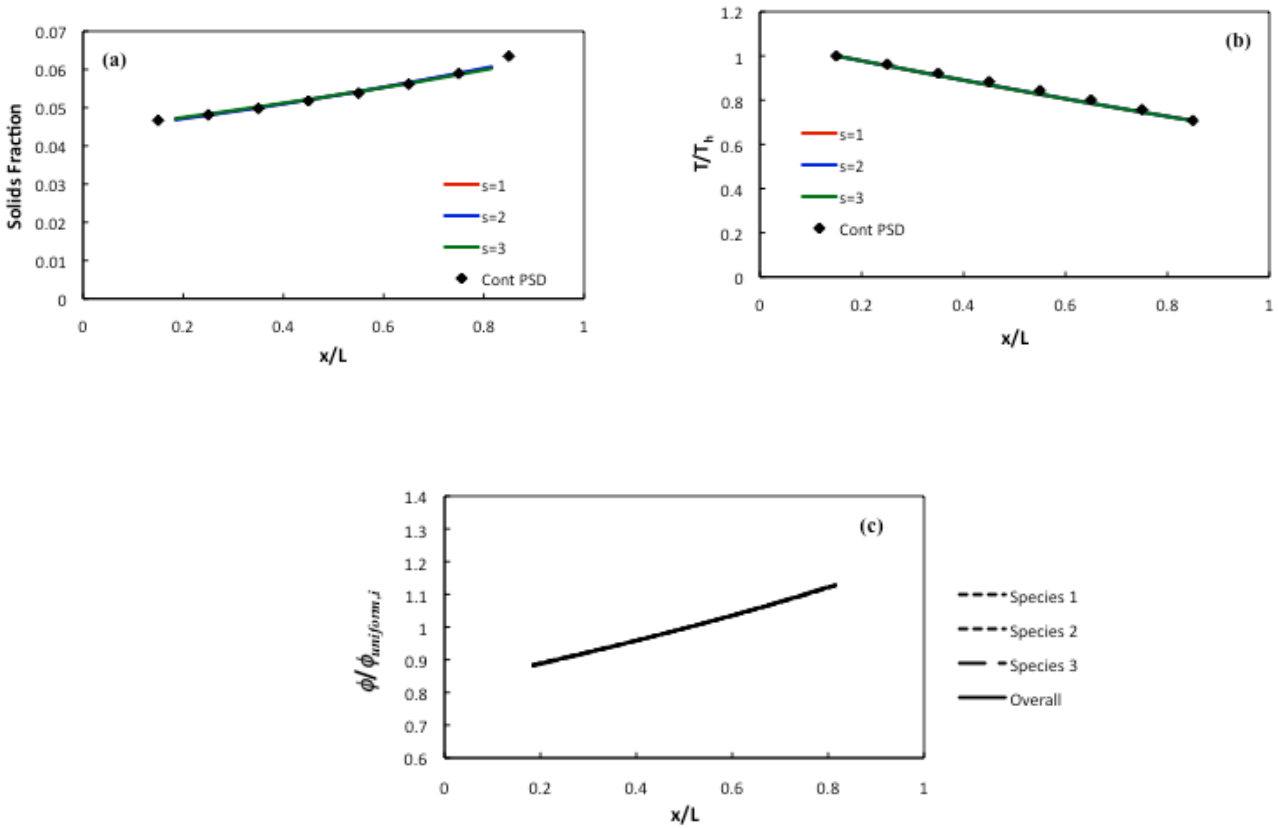

Figure 4.5: (a) MD and KT predictions of overall solids fraction, (b) MD and KT predictions of reduced granular temperature and (c) KT predictions of species solids fraction ratios for an $s = 3$ approximation as a function of domain length for a ***lognormal*** distribution having a width of $\boldsymbol{\sigma/d_{ave} = 0.1}$. For (a) and (b) the data points correspond to the MD simulations run for the continuous PSD, whereas the solid lines correspond to KT predictions. For the $s = 3$ approximation, the diameter ratios and species volume fraction ratios are $d_3/d_1 = 1.4142$, $d_3/d_2 =$

1.1892 and $\phi_1/\phi = 0.1518$, $\phi_2/\phi = 0.6677$, $\phi_3/\phi = 0.1805$. Also, the following physical parameters were used: $\phi = 0.05$, $\alpha = 0.99$, $T_h/T_c = 2$.

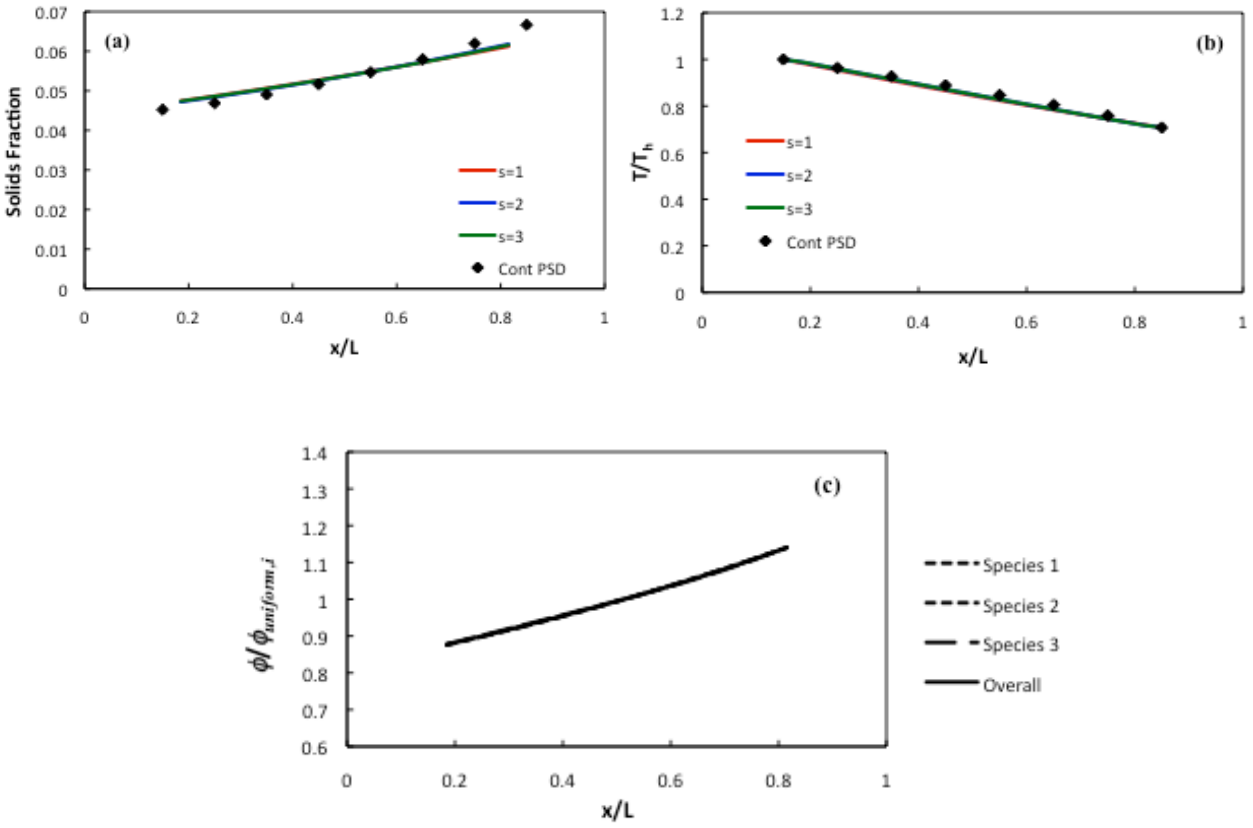

Figure 4.6: (a) MD and KT predictions of overall solids fraction, (b) MD and KT predictions of reduced granular temperature and (c) KT predictions of species solids fraction ratios for an $s = 3$ approximation as a function of domain length for a ***lognormal*** distribution having a width of $\boldsymbol{\sigma/d_{ave} = 0.3}$. For (a) and (b) the data points correspond to the MD simulations run for the continuous PSD, whereas the solid lines correspond to KT predictions. For the $s = 3$ approximation, the diameter ratios and species volume fraction ratios are $d_3/d_1 = 2.8373$, $d_3/d_2 = 1.6844$ and $\phi_1/\phi = 0.1206$, $\phi_2/\phi = 0.6764$, $\phi_3/\phi = 0.2030$. Also, the following physical parameters were used: $\phi = 0.05$, $\alpha = 0.99$, $T_h/T_c = 2$.

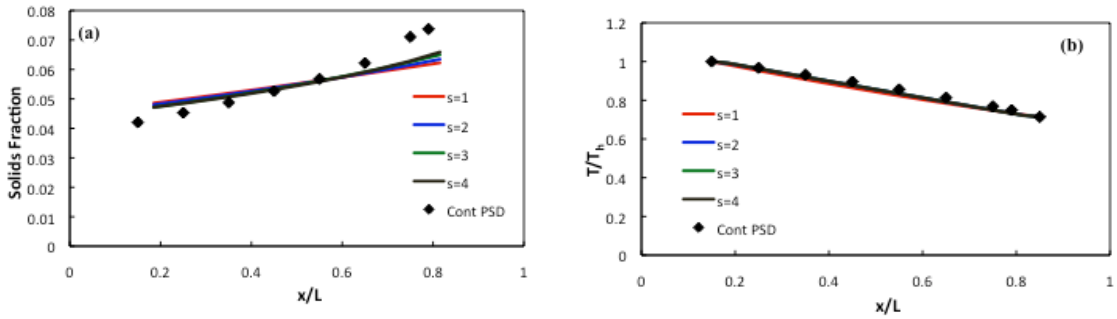

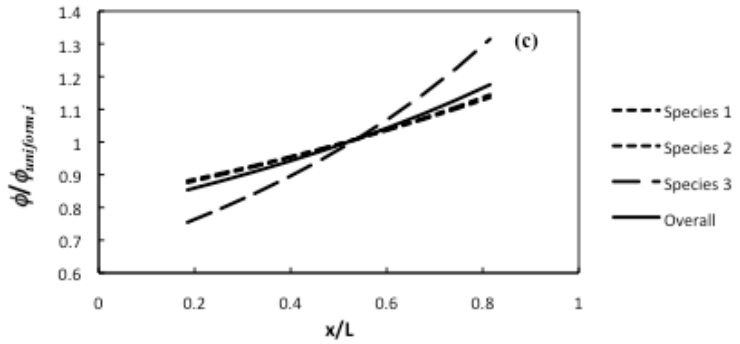

Figure 4.7: (a) MD and KT predictions of overall solids fraction, (b) MD and KT predictions of reduced granular temperature and (c) KT predictions of species solids fraction ratios for an $s = 3$ approximation as a function of domain length for a ***lognormal*** distribution having a width of $\boldsymbol{\sigma/d_{ave} = 0.5}$. For (a) and (b) the data points correspond to the MD simulations run for the continuous PSD, whereas the solid lines correspond to KT predictions. For the $s = 3$ approximation, the diameter ratios and species volume fraction ratios are $d_3/d_1 = 5.7358$, $d_3/d_2 = 2.3950$ and $\phi_1/\phi = 0.0906$, $\phi_2/\phi = 0.6923$, $\phi_3/\phi = 0.2171$. Also, the following physical parameters were used: $\phi = 0.05$, $\alpha = 0.99$, $T_h/T_c = 2$.

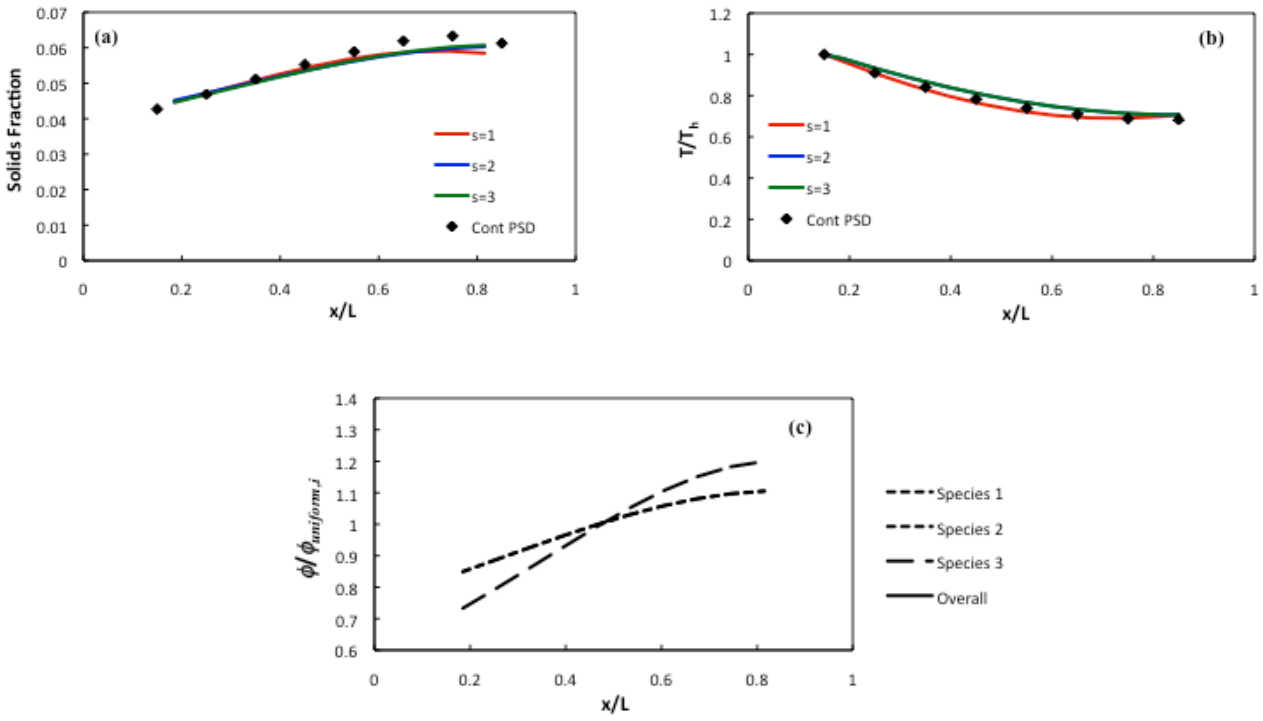

Figure 4.8: (a) MD and KT predictions of overall solids fraction, (b) MD and KT predictions of reduced granular temperature and (c) KT predictions of species solids fraction ratios for an $s = 3$ approximation as a function of domain length for a ***lognormal*** distribution having a width of $\boldsymbol{\sigma/d_{ave} = 0.3}$. For (a) and (b) the data points correspond to the MD simulations run for the continuous PSD, whereas the solid lines correspond to KT predictions. For the $s = 3$ approximation, the diameter ratios and species volume fraction ratios are $d_3/d_1 = 2.8373$, $d_3/d_2 = 1.6844$ and $\phi_1/\phi = 0.1206$, $\phi_2/\phi = 0.6764$, $\phi_3/\phi = 0.2030$. Also, the following physical parameters were used: $\phi = 0.05$, $\boldsymbol{\alpha = 0.90}$, $T_h/T_c = 2$.

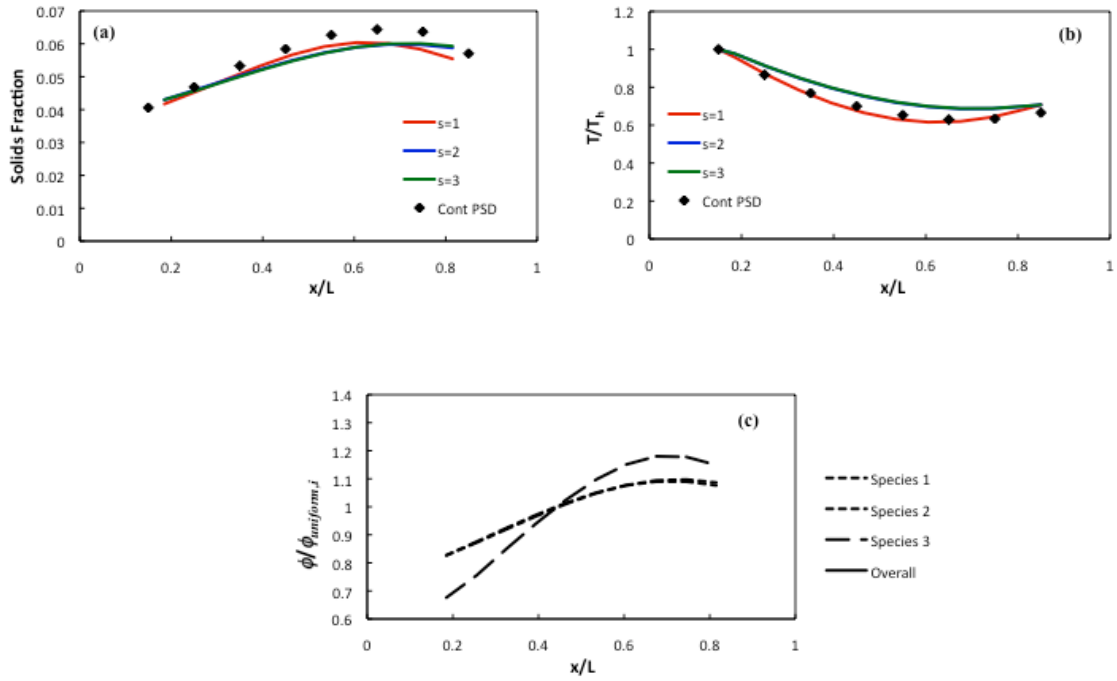

Figure 4.9: (a) MD and KT predictions of overall solids fraction, (b) MD and KT predictions of reduced granular temperature and (c) KT predictions of species solids fraction ratios for an $s = 3$ approximation as a function of domain length for a ***lognormal*** distribution having a width of $\boldsymbol{\sigma/d_{ave} = 0.3}$. For (a) and (b) the data points correspond to the MD simulations run for the continuous PSD, whereas the solid lines correspond to KT predictions. For the $s = 3$ approximation, the diameter ratios and species volume fraction ratios are $d_3/d_1 = 2.8373$, $d_3/d_2 = 1.6844$ and $\phi_1/\phi = 0.1206$, $\phi_2/\phi = 0.6764$, $\phi_3/\phi = 0.2030$. Also, the following physical parameters were used: $\phi = 0.05$, $\boldsymbol{\alpha = 0.80}$, $T_h/T_c = 2$.

Table 4.2: Summary of minimum number of species (s_{min}) required to accurately approximate Gaussian and lognormal size distributions with a discrete number of species *for a segregating system*. Also, comparisons with predictions from Chapter 3 are shown. The following inputs were used throughout all KT and MD simulations: $\alpha = 0.99$, $\phi = 0.05$, $T_h/T_c = 2$, $L/d_{rmc} = 1/0.0725566$. L/d_{rmc} refers to the ratio of domain length to the root-mean-cube diameter of the continuous size distribution. For each distribution analyzed here, the root-mean-cube diameter and associated particle mass were held constant at $d_{rmc} = 0.0725566$ and $m_{rmc} = 1$, respectively.

		Bounded Conduction	System-Independent Analysis (Chapter 3)				
			Zeroth-Order Cooling Rate	First-Order Cooling Rate	Pressure	Shear Viscosity	Bulk Viscosity
	σ / d_{ave}	s_{min}	s_{min}				
Gaussian PSDs	0.1	1	2	1	2	1	2
	0.2	1	2	2	2	2	2
	0.3	2	3	2	2	2	2
Lognormal PSDs	0.1	1	2	2	2	1	2
	0.3	2	2	2	2	2	2
	0.5	3	3	2	2	4	2

4.4 Issues Encountered Using KT Predictions

4.4.1 SET vs RET

The standard and revised Enskog theories differ in the treatment of the radial distribution function. Specifically, standard Enskog theory (SET) treats the radial distribution function as a function of the local value of solids concentration, whereas the revised Enskog theory (RET) is a functional of the local value of solids concentration and its gradient. Consequently, SET has been shown to be contradictory to irreversible thermodynamics, whereas RET is in agreement with irreversible thermodynamics [16]. The term I_{ilj}, which appears in the KT expression for ordinary diffusion coefficient (Eq. 1.22), is the main difference between SET- and RET-derived equations, where $I_{ilj} = 0$ for SET but $I_{ilj} \neq 0$ for RET. Due to the rigor involved in its derivation and increased computational power required for discrete approximations with $s > 2$, I_{ilj} has only been determined rigorously for $s = 1$ and 2; therefore KT predictions beyond $s = 2$ are not currently possible using RET. A formal methodology for developing the expression for I_{ilj} has

been established for any value of s by J. Dufty [17], though as implied above, the evaluation is too complicated for incorporation into a computational fluid dynamics model. Therefore, the term I_{ilj} was set to zero and SET was used for all KT predictions, allowing for an evaluation of a larger number of species. Figures 4.10a and 4.10b show the solids fraction and granular temperature profiles for a binary mixture of particles in bounded conduction with a size ratio of $d_1/d_2 = 3$. Figures 4.11a and 4.11b show data for an analogous system, but with a size ratio of $d_1/d_2 = 2$. These preliminary results indicate that the differences between SET and RET are fairly small for binary systems in bounded conduction, though the parameter space evaluated is limited.

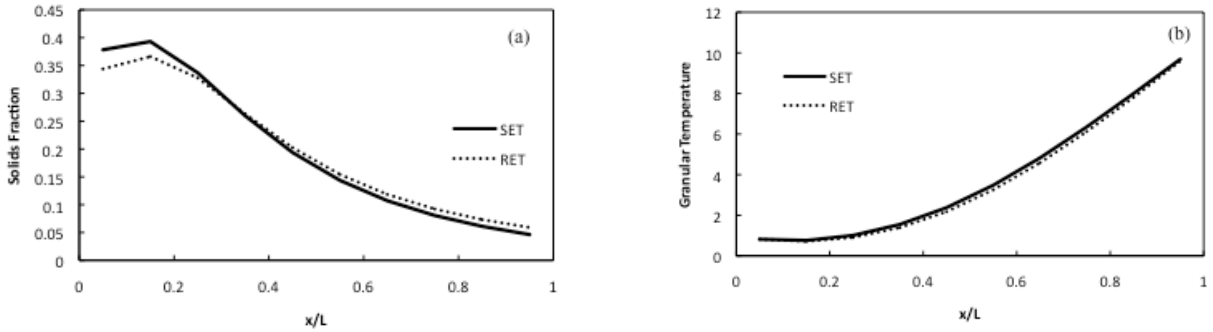

Figure 4.10: Comparison of (a) solids fraction and (b) granular temperature using SET and RET for a binary system in bounded conduction with the following physical parameters: $\phi = 0.2$, $\alpha = 0.9$, $d_1/d_2 = 3$, $\rho_1/\rho_2 = 2$, $T_h/T_c = 10$.

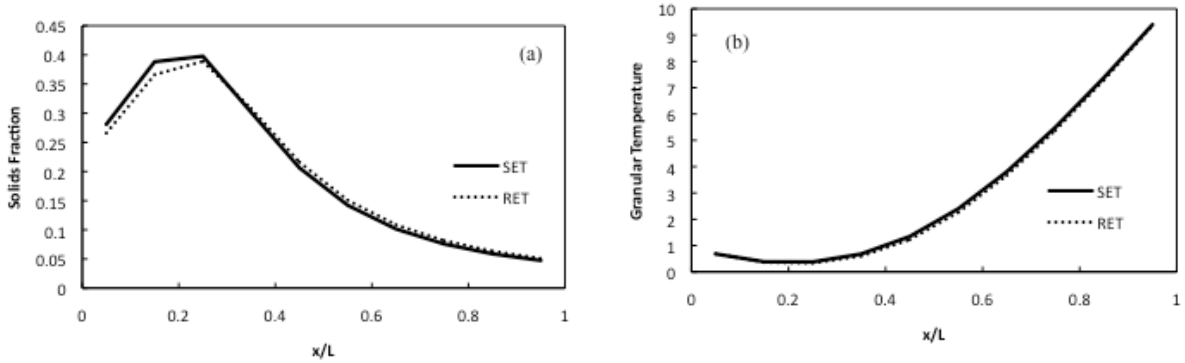

Figure 4.11: Comparison of (a) solids fraction and (b) granular temperature using SET and RET for a binary system in bounded conduction with the following physical parameters: $\phi = 0.2$, $\alpha = 0.9$, $d_1/d_2 = 2$, $\rho_1/\rho_2 = 2$, $T_h/T_c = 10$.

4.4.2 Thermal Diffusivity

During the study of discrete approximations of continuous PSDs using single-valued transport coefficients (Chapter 3), singularities were observed in the thermal conductivity, which were traced to the thermal diffusion coefficient. Figure 4.12 shows an example of the singularities observed in the thermal diffusion coefficient for polydisperse systems. Calculations revealed that the more inelastic the system and the larger the disparity in particle size, the more likely a singularity will occur. Singularities in thermal diffusion are not observed in the monodisperse or elastic limits. Specifically, the singularity occurs because the inverse of a matrix is needed for the solution of the thermal diffusion; however, this matrix is singular for certain combinations of physical parameters (coefficient of restitution, volume fraction, particle sizes, etc.). The observed singularities not only affect the analysis of conductivity with respect to the study of single-valued transport coefficients, but also limits the width of continuous PSDs and range of restitution coefficient for the study of bounded conduction.

Because the thermal diffusion coefficient is contained in the mass flux (Eq. 1.4), it was initially hypothesized that a more accurate approximation of the mass flux is required, namely, using a second-order Sonine polynomial approximation rather than first-order. The mass flux of a polydisperse mixture is established by solving the appropriate kinetic equation by means of the Chapman-Enskog method. The corresponding transport coefficients of the mass flux are given in terms of a set of coupled linear integral equations, approximately solved by considering the first and second Sonine approximations [18]. Using a larger number of terms in the Sonine approximation (eg., using a second-order approximation instead of a first-order) should increase

the accuracy of the prediction of transport coefficients, however, the singularities persisted even with an expanded Sonine approximation of the mass flux in the binary, dilute limit.

A recommendation for future work in this area would be to conduct a study on the conductivity to determine the associated s_{min} for different continuous PSDs, as was done for the other single-valued transport coefficients in Chapter 3. However, the expression for thermal diffusion in the elastic limit should be used to ensure that no singularities are present. Also, a study on bounded conduction, similar to Chapter 4, may be conducted for a larger parameter space using the elastic form of the thermal diffusion, while the remaining transport coefficients would be evaluated with inelasticity included. Using this methodology, it is possible to work around the issue with thermal diffusion while obtaining results having only a small expected sacrifice in quantitative error (due to elastic approximation for D_i^T only).

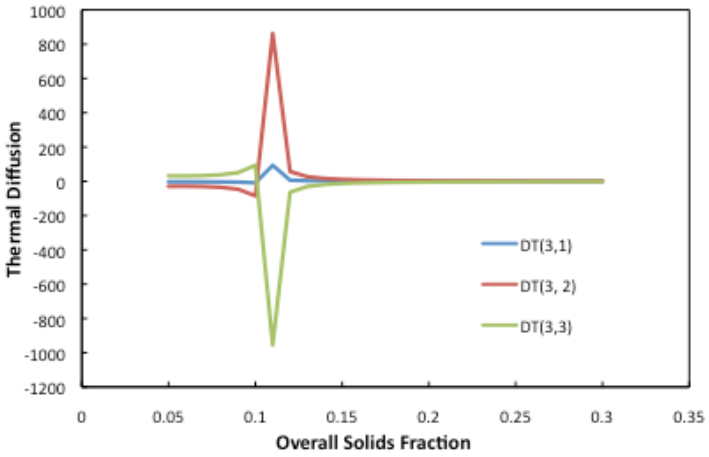

Figure 4.12: Thermal diffusion coefficient values for an $s = 3$ approximation of a lognormal distribution having a width of $\sigma/d_{ave} = 0.5$ and a coefficient of restitution of $\alpha = 0.7$.

4.5 Concluding Remarks

In Section 4.3, the values of s_{min} for a segregating system are determined for several Gaussian (σ/d_{ave} = 0.1 – 0.3) and lognormal (σ/d_{ave} = 0.1 – 0.5) distributions. These values are determined by comparing the solids fraction and granular temperature profiles for increasing values of s used in the discrete approximation. Though the parameter space is limited to a high coefficient of restitution and low solids fraction (Table 4.1), the results are still comparable to the values of s_{min} determined via study of single-valued transport coefficients (Chapter 3). Table 4.2 shows the comparison between predictions of s_{min} using the two different methods, which clearly shows agreement between two. Not only does this suggest the values of s_{min} determined using GHD predictions of transport coefficients are accurate, but also that these values are robust, applying to both segregating and non-segregating systems. For the parameter space evaluated (Table 4.1), the difference between KT predictions and MD data is generally below 10%.

Subplot (c) of Figures 4.2 – 4.9 shows the levels of species segregation for each s = 3 discrete approximation as described in Section 4.3. It is evident from these figures that discrete approximations of wider distributions exhibit a larger degree of species segregation, due to the increasing discrepancy in species sizes. Also, as the particles become less elastic, an increased leveal of species segregation is observed. Though the results shown in Figures 4.2 – 4.9 reveal interesting information about KT predictions of bounded conduction, a larger parameter space should be evaluated to determine the effect of species segregation on the accuracy of KT predictions.

Future work includes a larger parameter space with regard to volume fraction, coefficient of restitution, and distribution width, once outstanding issues with KT are resolved. Specifically, the revised Enskog theory (RET) is to be used in place of the standard Enskog theory (SET). Due

to complications in the derivation process of the mass flux for polydisperse mixtures, the current study uses SET for evaluation of discrete approximations, thereby limiting the scope of this study. Incorporating RET into the same study presented in this chapter will allow for the determination of the need for RET. Also, as in Section 4.4.2, outstanding issues exist with the solution of the thermal diffusion coefficient. Using the perfectly elastic form of the thermal diffusion coefficient, while allowing for inelasticity in the remaining transport coefficients, may allow for the investigation of a larger parameter space with respect to the study of continuous PSDs in bounded conduction.

Literature Cited

1. Garzó, V., C.M. Hrenya, and J.W. Dufty, *Enskog theory for polydisperse granular mixtures. II. Sonine polynomial approximation.* Physical Review E, 2007. **76**(3): p. 031304.
2. Garzó, V., J.W. Dufty, and C.M. Hrenya, *Enskog theory for polydisperse granular mixtures. I. Navier-Stokes order transport.* Physical Review E, 2007. **76**(3): p. 031303.
3. Zamankhan, P., *Kinetic theory of multicomponent dense mixtures of slightly inelastic spherical particles.* Physical Review E, 1995. **52**(5): p. 4877-4891.
4. Mathiesen, V., et al., *Experimental and computational study of multiphase gas/particle flow in a CFB riser.* AIChE Journal, 1999. **45**(12): p. 2503-2518.
5. Iddir, H. and H. Arastoopour, *Modeling of multitype particle flow using the kinetic theory approach.* AIChE Journal, 2005. **51**(6): p. 1620-1632.
6. Iddir, H., H. Arastoopour, and C.M. Hrenya, *Analysis of binary and ternary granular mixtures behavior using the kinetic theory approach.* Powder Technology, 2005. **151**(1- 3): p. 117-125.
7. Remy, B., J.G. Khinast, and B.J. Glasser, *Polydisperse granular flows in a bladed mixer: Experiments and simulations of cohesionless spheres.* Chemical Engineering Science, 2011. **66**(9): p. 1811-1824.
8. Dahl, S., R. Clelland, and C.M. Hrenya, *Three-dimensional, rapid shear flow of particles with continuous size distributions.* Powder Technology, 2003. **138**(1): p. 7-12.
9. Dahl, S., R. Clelland, and C.M. Hrenya, *The effects of continuous size distributions on the rapid flow of inelastic particles.* Physics of Fluids, 2002. **14**: p. 1972.
10. Dahl, S. and C.M. Hrenya, *Size segregation in rapid, granular flows with continuous size distributions.* Physics of Fluids, 2004. **16**: p. 1.
11. Galvin, J., S. Dahl, and C. Hrenya, *On the role of non-equipartition in the dynamics of rapidly flowing granular mixtures.* Journal of Fluid Mechanics, 2005. **528**: p. 207-232.
12. Hrenya, C.M., J. E. Galvin, and R.D. Wildman, *Evidence of higher-order effects in thermally driven rapid granular flows*. Jornal of Fluid Mechanics, 2007. **598**: p. 429-450.

13. Chew, J. W. and C. M. Hrenya, *Link between bubbling and segregation patterns in gas-fluidized beds with continuous size distributions*. AIChE Journal, 2011. **57**: p. 3003-3011.
14. Chew, J. W., J. Wolz, and C. M. Hrenya, *Axial segregation in bubbling gas-fluidized beds with Gaussian and lognormal Distributions of Geldart group B particles*. AIChE Journal, 2010. **56**: p. 3049-3061.
15. Murray, J.A., V. Garzó, and C.M. Hrenya, *Enskog theory for polydisperse granular mixtures. III. Comparison of dense and dilute transpornt coefficients and equations of state for a binary mixture.* Powder Technology, 2012. **220**: p. 24-36.
16. Hrenya, C.M., *Kinetic theory for granular materials: Polydispersity*, in *Computational Gas-Solids Flows and Reacting Systems: Theory, Methods and Practice*, S.P., M. Syamlal, and T. O'Brien, Editor. 2011, IGI Global: Hershey, PA.
17. Dufty, J.W., Personal Communication, July 2012.
18. Garzó, V., J.A. Murray, F.V. Reyes, *Diffusion transport coefficients for granular binary mixtures at low density. Second Sonine approximation*. In preparation.

CHAPTER 5

SUMMARY

5.1 Overview

A comprehensive study has been carried out with respect to the three objectives of this thesis: (i) to determine the importance of finite-volume (non-dilute) effects of solid particles in binary mixtures, (ii) to determine the minimum number of discrete particle species needed to accurately approximate a continuous PSD, and (iii) to validate discrete approximations of continuous PSDs in a kinetic-theory-based model via comparison of theoretical predictions with MD simulations for both segregating and non-segregating systems. The first objective is detailed in Chapter 2, and involves the comparison of dense and dilute kinetic-theory-based predictions of transport coefficients. The second objective is touched upon in Chapters 3 and 4, using both system-independent and system-dependent methods, respectively. The third objective, comparing MD and KT predictions, is also covered in Chapters 3 and 4.

5.2 Summary of Findings

5.2.1 Dense vs Dilute Treatment of KT Transport Coefficients (Chapter 2)

As described in Chapter 2, GHD theory [1, 2] (with modifications provided by Murray, Garzó, and Hrenya [3]) is applicable to dilute and moderately dense mixtures, whereas GD theory [4] is only applicable to dilute, binary systems of particles. All other assumptions used during the derivation of these two theories are identical. Therefore, by comparing the transport coefficients (see Table 1.1 with additional expressions in Appendix A) of the competing theories for binary mixtures, it is possible to determine the importance of dense-phase corrections in the theoretical treatment. As shown in the results presented in Chapter 2, the differences between dense- and dilute-phase predictions can be quite substantial, even for lower volume fractions. For

a granular mixture with a volume fraction $\phi = 0.1$, it is shown that the difference between GHD and GD predictions of some transport coefficients can be up to an order of magnitude. In a more densely packed system ($\phi = 0.5$), differences between theories can be up to two orders of magnitude. More importantly, this study provides a basis for choosing the appropriate model given physical parameters such as solids fraction and coefficient of restitution.

5.2.2 Discrete Approximations of Continuous PSDs (Chapters 3 and 4)

The number of *discrete* particle species (s) to accurately approximate a *continuous* PSD for use in kinetic-theory-based models is determined using two methods. The first method is a system-independent or "universal" study. By comparing the single-valued transport coefficients of GHD theory for increasing values of s, the minimum number of species (s_{min}) needed for an accurate prediction can be determined by establishing at which s the predictions begin to collapse on one another. Because the discrete approximations of these single-valued transport coefficients do not depend on system geometry, but only physical input parameters, the study is system-independent or universal in nature. Several Gaussian and lognormal distributions of different widths, as well as coal and lunar regolith PSDs, were analyzed in this study. For more narrow distributions (eg., Gaussian $\sigma/d_{ave} = 0.2$) the critical number of species for use in GHD theory can be as low as $s_{min} = 2$. For wider distributions (eg., lunar regolith, Figure 1.1) the critical number of species is shown to be about $s_{min} = 8$, which is relatively low for the wide range of particle sizes (~ 2 orders of magnitude between smallest and largest particle size) covered by the lunar regolith PSDs. Overall, this system-independent study provides a guide for determining the number of discrete species to use with GHD theory [1, 2].

The second approach to determining appropriate discrete approximations of continuous PSDs for use in KT models involves a segregating system, namely bounded conduction. Using

GHD expressions modified for a standard Enskog theory, solids fraction and granular temperature profiles are compared for increased values of s. As mentioned in Section 3.4, the previous approach involves the comparison amongst discrete approximations of only the single-valued transport coefficients. However, several transport coefficients do not exist as a single-valued (ie., D_{ij}, D_i^T, D_{ij}^F, $D_{q,i}$, L_{ij}), and thus the sensitivity of these quantities to physical parameters must be examined for specific system geometries. The KT predictions of bounded conduction systems were used to determine the critical number of species for a given PSD and compared to the s_{min} value to results of the study on single-valued transport coefficients. The results indicate that the number of particle species predicted for a segregating system match the values determined in the "universal" study of discrete approximations, suggesting that both single-valued and non-single-valued transport coefficients lead to a similar discrete approximation.

5.2.3 Comparison of KT and MD simulations (Chapters 3 and 4)

In order to gage the accuracy of the discrete approximations of continuous PSDs previously established, comparison with MD simulations of continuous PSDs [5] is carried out. Using s_{min} values determined in the system-independent study (Table 3.2), kinetic-theory-based predictions of pressure and shear viscosity are compared to MD simulations of a non-segregating system, namely, simple shear flow. As shown in the comparison between theoretical predictions and MD predictions of pressure and shear viscosity, the accuracy level is about the same regardless the distribution width. Therefore, no substantive loss of accuracy is traceable to the discrete approximation or polydisperse theory used. Also, the accuracy of the theoretical predictions of solids fraction and granular temperature profiles (Table 4.2) is determined via comparison with MD simulations for continuous PSDs in bounded conduction. Once again,

discrete KT predictions agree very well with MD data for all Gaussian and lognormal distributions analyzed, with a maximum observed error of only 12%.

5.3 Recommendations for Future Work

As pointed out in the system-*independent* study of discrete approximations of continuous PSDs (Chapter 3), the thermal conductivity could not be determined for the entire parameter space evaluated. Discontinuities were observed for given physical parameters and discrete approximations for thermal conductivity, but not for the other single-valued transport coefficients. Because the thermal conductivity depends on the thermal diffusion, which also shows discontinuities, it was determined that the source of the singularity stems from the thermal diffusion coefficient. The second Sonine polynomial approximation of the mass flux was examined to resolve the singularities in the thermal diffusion, however the singularities persisted. Further analysis is required to determine the source of error associated with the thermal diffusion given by GHD theory [1, 2]. Once the singularities associated with the thermal diffusion have been corrected, it will be possible to determine the number of species required for an accurate discrete approximation of various continuous PSDs with respect to the thermal conductivity. Therefore, all single-valued transport coefficients will have been examined, allowing for a more complete study. Nevertheless, a simplified analysis of the conductivity is currently possible. In particular, the elastic form of the thermal diffusion coefficient can be used rather than its inelastic form, as the former does not exhibit singularities. Although such an approach is expected to come at the cost of a fairly small quantitative error, using the elastic form of the thermal diffusion coefficient allows for a sound preliminary analysis of conductivity with regard to discrete approximations of continuous PSDs.

As pointed out in the system-*dependent* study of discrete approximations of continuous PSDs (Chapter 4), the solids fraction and granular temperature profiles were determined using GHD theory, modified to include standard Enskog theory (SET) rather than revised Enskog theory (RET). The reason for this being that the term I_{ilj} has only been developed for $s = 1$ and 2 (i.e., restricted to binary mixtures), whereas SET is achieved by setting I_{ilj} to zero regardless of the value of s. Differences between predictions using RET and SET are minimal for a bounded conduction system with the physical parameters indicated in Figures 4.8 and 4.9. Though the predictions using SET are accurate with respect to MD data, the extension of the term I_{ilj} for any value of s is of great interest. Once a general s-component expression for I_{ilj} has been determined for practical use, it will be possible to compare predictions between RET and SET for a bounded conduction system using increasing values of s in discrete approximations of continuous PSDs. Though the results of such a study are not universal, it is also possible to conduct analogous studies for other system geometries (eg., simple shear flow). The comparison between RET and SET shown is restricted to binary mixtures, so the impact of increased polydispersity on the discrepancy between RET and SET predictions should be pursued. Also, as pointed out in the system-*dependent* study of discrete approximations of continuous PSDs, the parameter space was somewhat restricted due to issues with the thermal diffusion coefficient. Therefore, the comparison of kinetic-theory-based predictions and MD simulations of solids fraction and granular temperature was limited to a volume fraction and coefficient of restitution of $\phi = 0.05$ and $\alpha = 0.99$. The widest distribution that was successfully approximated with more than 2 particle species was a lognormal distribution with $\sigma/d_{ave} = 0.5$. Expanding the parameter space with respect to the volume fraction, coefficient of restitution, and width of distributions analyzed

is the next step in gaining a better understanding of continuous PSDs engaged in the bounded conduction system.

Lastly, it is important to note that only one segregating system was analyzed in this thesis work with regard to continuous PSDs. However, by analyzing a larger number of system geometries, each dominated by a unique set of transport coefficients, it will be possible to achieve a more comprehensive understanding of the effects of each hydrodynamic quantity on the discrete approximation of a continuous PSD. Due to the seemingly infinite number of system geometries, it is also of interest to determine a method for establishing discrete approximations *a priori*. In other words, a method to determine s_{min} for any specific system and continuous PSD without actually analyzing the system itself (similar to the work in Chapter 3) would drastically minimize the computational effort involved in the investigation of several different system geometries.

Though each of the proposed works are of interest to a variety of scientists and engineers, the impact and effort required of each study varies. The singularities involved with the thermal diffusion coefficient and the evaluation of the term I_{ilj} will require a significant amount of technical derivation. However, the analysis of different system geometries, while isolating specific transport coefficients, can be accomplished more readily using computational fluid dynamics programs. In order to temporarily overcome the issues noted with the thermal diffusion coefficient, the elastic limit should be considered for this quantity, as singularities are not noted for this case. The remaining transport coefficients may consider inelasticity. Overall, the former recommendations require rigorous investigation with an impact that is uncertain, whereas the latter recommendation will certainly reveal additional information about the discrete approximations of continuous PSDs.

Literature Cited

1. Garzó, V., J.W. Dufty, and C.M. Hrenya, *Enskog theory for polydisperse granular mixtures. I. Navier-Stokes order transport.* Physical Review E, 2007. **76**(3): p. 031303.
2. Garzó, V., C.M. Hrenya, and J.W. Dufty, *Enskog theory for polydisperse granular mixtures. II. Sonine polynomial approximation.* Physical Review E, 2007. **76**(3): p. 031304.
3. Murray, J.A., V. Garzó, and C.M. Hrenya, *Enskog theory for polydisperse granular mixtures. III. Comparison of dense and dilute transpornt coefficients and equations of state for a binary mixture.* Powder Technology, 2012. **220**: p. 24-36.
4. Garzó, V. and J.W. Dufty, *Hydrodynamics for a granular mixture at low density*. Physics of Fluids, 2002 **14**: 1476–1490.
5. Dahl, S., R. Clelland, and C.M. Hrenya, *Three-dimensional, rapid shear flow of particles with continuous size distributions.* Powder Technology, 2003. **138**(1): p. 7-12.

BIBLIOGRAPHY

Arnarson, B. and J. Willits, *Thermal diffusion in binary mixtures of smooth, nearly elastic spheres with and without gravity.* Physics of Fluids, 1998. **10**: p. 1324.

Battler, M.M. and J.G. Spray, *The Shawmere anorthosite and OB-1 as lunar highland regolith simulants.* Planetary and Space Science, 2009. **57**(14-15): p. 2128-2131.17.

Brey, J., M. Ruiz-Montero, and F. Moreno, *Energy partition and segregation for an intruder in a vibrated granular system under gravity.* Physical Review Letters, 2005. **95**(9): p. 98001.

Chapman, S. and T. Cowling, *The mathematical theory of non-uniform gases.* Cambridge: Cambridge University, 1970.

Chew, J. W. and C. M. Hrenya, *Link between bubbling and segregation patterns in gas-fluidized beds with continuous size distributions*. AIChE Journal, 2011. **57**: p. 3003-3011.

Chew, J. W., J. Wolz, and C. M. Hrenya, *Axial segregation in bubbling gas-fluidized beds with Gaussian and lognormal Distributions of Geldart group B particles*. AIChE Journal, 2010. **56**: p. 3049-3061.

Curtis, J.S. and B. van Wachem, *Modeling particle-laden flows: A research outlook.* AIChE Journal, 2004. **50**(11): p. 2638-2645.

Dahl, S., R. Clelland, and C.M. Hrenya, *Three-dimensional, rapid shear flow of particles with continuous size distributions.* Powder Technology, 2003. **138**(1): p. 7-12.

Dahl, S., R. Clelland, and C.M. Hrenya, *The effects of continuous size distributions on the rapid flow of inelastic particles.* Physics of Fluids, 2002. **14**: p. 1972.

Dahl, S. and C.M. Hrenya, *Size segregation in rapid, granular flows with continuous size distributions.* Physics of Fluids, 2004. **16**: p. 1.

Dufty, J.W., Personal Communication, July 2012.

Fan, R. and R.O. Fox, *Segregation in polydisperse fluidized beds: Validation of a multi- fluid model.* Chemical Engineering Science, 2008. **63**(1): p. 272-285.

Fan, R., D.L. Marchisio, and R.O. Fox, *Application of the direct quadrature method of moments to polydisperse gas-solid fluidized beds.* Powder Technology, 2004. **139**(1): p. 7-20.

Fox, R.O., P. Vedula, *Quadrature-based moment model for moderately dense polydisperse gas-particle flows*. Industrial and Engineering Chemistry Research, 2010. **49**(11): p. 5174-5187.

Galvin, J., S. Dahl, and C. Hrenya, *On the role of non-equipartition in the dynamics of rapidly flowing granular mixtures.* Journal of Fluid Mechanics, 2005. **528**: p. 207-232.

Garzó, V. *Brazil-nut effect versus reverse Brazil-nut effect in a moderately granular dense gas*. Physical Review E, 2008 **78**: 020301(R).

Garzó, V. *Segregation by thermal diffusion in moderately dense granular mixtures*, European Physical Journal E: Soft Matter, 2009 **29**: p. 261–274.

Garzó, V., *Segregation in granular binary mixtures: Thermal diffusion.* Europhysics Letters, 2006. **75**: p. 521.

Garzó, V. and J.W. Dufty, *Hydrodynamics for a granular mixture at low density*. Physics of Fluids, 2002 **14**: 1476–1490.

Garzó, V., J.W. Dufty, and C.M. Hrenya, *Enskog theory for polydisperse granular mixtures. I. Navier-Stokes order transport.* Physical Review E, 2007. **76**(3): p. 031303.

Garzó, V., C.M. Hrenya, and J.W. Dufty, *Enskog theory for polydisperse granular mixtures. II. Sonine polynomial approximation.* Physical Review E, 2007. **76**(3): p. 031304.

Garzó, V. and J.M. Montanero, *Navier–Stokes transport coefficients of d-dimensional granular binary mixtures at low density.* Journal of Statistical Physics, 2007 **129**: p. 27.

Garzó, V., J.M. Montanero, and J.W. Dufty, *Mass and heat fluxes for a binary granular mixture at low density*. Physics of Fluids, 2006 **18**: 083305.
Garzó, V., J.A. Murray, F.V. Reyes, *Diffusion transport coefficients for granular binary mixtures at low density. Second Sonine approximation*. In preparation.
Garzó, V. and F. Vega Reyes, *Mass transport of impurities in a moderately dense granular gas*, Physical Review E, 2009 **79**: 041303.
Gordon, R.G., *Error bounds in spectroscopy and nonequilibrium statistical mechanics.* Journal of Mathematical Physics, 1968. **9**: p. 1087-1092.
Hrenya, C.M., *Kinetic theory for granular materials: Polydispersity*, in *Computational Gas-Solids Flows and Reacting Systems: Theory, Methods and Practice*, S.P., M. Syamlal, and T. O'Brien, Editor. 2011, IGI Global: Hershey, PA.
Hrenya, C.M., J. E. Galvin, and R.D. Wildman, *Evidence of higher-order effects in thermally driven rapid granular flows*. Jornal of Fluid Mechanics, 2007. **598**: p. 429-450.
Hsiau, S. and M. Hunt, *Granular thermal diffusion in flows of binary-sized mixtures.* Acta Mechanica, 1996. **114**(1): p. 121-137.
Huilin, L., D. Gidaspow, and E. Manger, *Kinetic theory of fluidized binary granular mixtures.* Physical Review E, 2001. **64**(6): p. 61301.
Iddir, H. and H. Arastoopour, *Modeling of multitype particle flow using the kinetic theory approach.* AIChE Journal, 2005. **51**(6): p. 1620-1632.
Iddir, H., H. Arastoopour, and C.M. Hrenya, *Analysis of binary and ternary granular mixtures behavior using the kinetic theory approach.* Powder Technology, 2005. **151**(1- 3): p. 117-125.
Isben, C.H., E. Helland, B.H. Hjertager, T. Solberg, L. Tadrist, and R. Occelli, *Comparison of multi-fluid and discrete particle modeling in numerical predictions of gas particle flow in circulating fluidized beds.* Powder Technology, 2004. **149**(1): p. 29-41.
Jenkins, J. and F. Mancini, *Balance laws and constitutive relations for plane flows of a dense, binary mixture of smooth, nearly elastic, circular disks.* Journal of Applied Mechanics, 1987. **54**: p. 27.
Jenkins, J. and F. Mancini, *Kinetic theory for binary mixtures of smooth, nearly elastic spheres.* Physics of Fluids A: Fluid Dynamics, 1989. **1**: p. 2050.
Liu, X., M. Metzger, and B. Glasser, *Couette flow with a bidisperse particle mixture.* Physics of Fluids, 2007. **19**: p. 073301.
Mathiesen, V., et al., *Experimental and computational study of multiphase gas/particle flow in a CFB riser.* AIChE Journal, 1999. **45**(12): p. 2503-2518.
Mathiesen, V., T. Solberg, and B.H. Hjertager, *Predictions of gas/particle flow with an Eulerian model including a realistic particle size distribution.* Powder Technology, 2000. **112**(1-2): p. 34-45.
Murray, J.A., V. Garzó, and C.M. Hrenya, *Enskog theory for polydisperse granular mixtures. III. Comparison of dense and dilute transpornt coefficients and equations of state for a binary mixture.* Powder Technology, 2012. **220**: p. 24-36.
Muzzio, F.J., T. Shinbrot, and B.J. Glasser, *Powder technology in the pharmaceutical industry: the need to catch up fast.* Powder Technology, 2002. **124**(1-2): p. 1-7.
Ottino, J. and D. Khakhar, *Mixing and segregation of granular materials.* Annual Review of Fluid Mechanics, 2000. **32**(1): p. 55-91.

Rahaman, M.F., J. Naser, and P.J. Witt, *An unequal granular temperature kinetic theory: description of granular flow with multiple particle classes.* Powder Technology, 2003. **138**(2-3): p. 82-92.
Remy, B., J.G. Khinast, and B.J. Glasser, *Polydisperse granular flows in a bladed mixer: Experiments and simulations of cohesionless spheres.* Chemical Engineering Science, 2011. **66**(9): p. 1811-1824.
Sanyal, J., D.L. Marchisio, R.O. Fox, and K. Dhanasekharan, *On the comparison between population balance models for CFD simulation of bubble columns.* Industrial & Engineering Chemistry Research, 2005. **44**(14): p. 5063-5072.
Schröter, M., et al., *Mechanisms in the size segregation of a binary granular mixture.* Physical Review E, 2006. **74**(1): p. 11307.
Sundaresan, S., *Some outstanding questions in handling of cohesionless particles.* Powder Technology, 2001. **115**(1): p. 2-7.
Wildman, R., et al., *A comparison of the predictions of a simple kinetic theory with experimental and numerical results for a vibrated granular bed consisting of nearly elastic particles of two sizes.* Physics of Fluids, 2006. **18**: p. 073301.
Yoon, D. and J. Jenkins, *The influence of different species granular temperatures on segregation in a binary mixture of dissipative grains.* Physics of Fluids, 2006. **18**: p. 073303.
Zamankhan, P., *Kinetic theory of multicomponent dense mixtures of slightly inelastic spherical particles.* Physical Review E, 1995. **52**(5): p. 4877-4891.

APPENDIX A

ADDITIONAL EXPRESSIONS FOR GHD THEORY

The expressions listed below refer to quantities not explicitly expressed in Table 1.1. For additional information as to the solution method, see Garzó, Hrenya, and Dufty [Phys. Rev. E 76, 31303 and 031304 (2007)], with correction in Murray, Garzó, and Hrenya [Powder Technology, Vol. 202, p. 24-36 (2012)].

For $i = 1 - s$ and $j = 1 - s$

$$\chi_{ij}^{(0)} = \frac{1}{1-\phi} + \frac{3}{2}\frac{\beta}{(1-\phi)^2}\frac{d_i d_j}{d_{ij}} + \frac{1}{2}\frac{\beta^2}{(1-\phi)^3}\left(\frac{d_i d_j}{d_{ij}}\right)^2 \qquad \textbf{Eq. A.1}$$

$$\beta = \frac{\pi}{6}\sum_{i=1}^{s} n_i d_i^2 \,,\; \phi = \frac{\pi}{6}\sum_{i=1}^{s} n_i d_i^3 \qquad \textbf{Eq. A.2}$$

For $i = 1 - s$

$$\sum_{j=1}^{s}\left(\psi_{ij} - \frac{3}{2}\xi^{(0)}\delta_{ij}\right)e_{j,D} = \frac{-\pi}{45 n_i}\sum_{j=1}^{s} n_i n_j \chi_{ij}^{(0)} d_{ij}^3 \mu_{ji}(1+\alpha_{ij})\Big[40(\mu_{ij}-1) + 4(19+9\alpha_{ij})\mu_{ji}$$
$$-48\mu_{ji}^2\frac{(\theta_i+\theta_j)}{\theta_j}(1+\alpha_{ij})^2 + 15\mu_{ji}^3\frac{(\theta_i+\theta_j)^2}{\theta_j^2}(1+\alpha_{ij})^3\Big] \qquad \textbf{Eq. A.3}$$

For $i = j$

$$\psi_{ii} = -\frac{2}{15 n_i}\Bigg[\Bigg(\sum_{j=1}^{s}\frac{\sqrt{\pi}}{2} n_i n_j \chi_{ij}^{(0)} d_{ij}^2\sqrt{\frac{2T}{m}}\frac{\mu_{ji}(1+\alpha_{ij})}{(\theta_i\theta_j)^{1/2}(\theta_i+\theta_j)^{5/2}}\Big\{-2\left[90\theta_j^3 + 231\theta_i\theta_j^2 + 40\theta_i^3\right]$$
$$+3\mu_{ji}(1+\alpha_{ij})(\theta_i+\theta_j)\left[70\theta_j^2 + 117\theta_i\theta_j + 44\theta_i^2\right] - 24\mu_{ji}^2(1+\alpha_{ij})^2(\theta_i+\theta_j)^2(5\theta_j+4\theta_i)$$
$$+30\mu_{ji}^3(1+\alpha_{ij})^3(\theta_i+\theta_j)^3 + 5\theta_j(\theta_i+\theta_j)\left[2(4\theta_i+3\theta_j) - 3\mu_{ji}(1+\alpha_{ij})(\theta_i+\theta_j)\right]\Big\}\Bigg) + \frac{\sqrt{2\pi}}{32} n_i^2 \chi_{ii}^{(0)} d_i^2 \frac{(1+\alpha_{ii})}{\theta_i^{1/2}}\sqrt{\frac{2T}{m}}$$
$$\left[30\alpha_{ii}^3 - 126\alpha_{ii}^2 + 177\alpha_{ii} + 48(3\alpha_{ii}-7) - 137\right] + \frac{3}{32}\sqrt{2\pi} n_i^2 \chi_{ii}^{(0)} d_i^2 \frac{(1+\alpha_{ii})}{\theta_i^{1/2}}\sqrt{\frac{2T}{m}}\left[10\alpha_{ii}^3 + 22\alpha_{ii}^2 + 11\alpha_{ii} - 3\right]\Bigg]$$
Eq. A.4

For $i \neq j$

$$\psi_{ij} = -\frac{2}{15 n_i}\Bigg[\frac{\sqrt{\pi}}{2} n_i n_j \chi_{ij}^{(0)} d_{ij}^2\sqrt{\frac{2T}{m}}\mu_{ji}\frac{(1+\alpha_{ij})\theta_i^{3/2}}{\theta_j^{3/2}(\theta_i+\theta_j)^{5/2}}$$
$$\Big\{\left[2\theta_j + 5\theta_i\right]\left[2\theta_j + 3\mu_{ji}(1+\alpha_{ij})(\theta_i+\theta_j)\right] - 24\mu_{ji}^2(1+\alpha_{ij})^2(\theta_i+\theta_j)^2$$

$$+30\mu_{ji}^3\left(1+\alpha_{ij}\right)^3\frac{\left(\theta_i+\theta_j\right)^3}{\theta_j}-5\left(\theta_i+\theta_j\right)\left[2\theta_j+3\mu_{ji}\left(1+\alpha_{ij}\right)\left(\theta_i+\theta_j\right)\right]\Bigg\} \qquad \textbf{Eq. A.5}$$

For $i = 1-s$ and $j = 1-s$

$$I_{i\ell j}=\left\{\frac{3}{2\pi}\left[\delta_{j\ell}\frac{n_\ell}{T}\left(\frac{\partial\mu_i}{\partial n_\ell}\right)_{n,T}-\frac{n_\ell}{n_i}\delta_{j\ell}\delta_{ij}-\frac{4\pi}{3}\delta_{j\ell}n_\ell\chi_{ij}^{(0)}d_{ij}^3\right]-n_\ell^2d_{i\ell}^3\frac{\partial\chi_{i\ell}^{(0)}}{\partial n_j}\right\}\left(\frac{1}{n_\ell\chi_{i\ell}^{(0)}d_{i\ell}^3}\right) \qquad \textbf{Eq. A.6}$$

For $i = 1-s$

$$\frac{\mu_i}{T}=\ell n(n_i)+\ell n(\lambda_i^3)-\ell n(1-\phi)+3\frac{M_2}{M_3}\frac{\phi}{1-\phi}d_i+3\left[\frac{M_2^2}{M_3^2}\frac{\phi}{(1-\phi)}+\frac{M_2^2}{M_3^2}\ell n(1-\phi)\right]d_i^2$$
$$-\left[\frac{M_2^3}{M_3^3}\frac{\phi(2-5\phi+\phi^2)}{(1-\phi)^3}-\frac{3M_1M_2}{M_3^2}\frac{\phi^2}{(1-\phi)^2}-\frac{\phi}{M_3(1-\phi)}+\frac{2M_2^3}{M_3^3}\ell n(1-\phi)\right]d_i^3 \qquad \textbf{Eq. A.7}$$

$$M_x=\frac{1}{n}\sum_{i=1}^{s}n_id_i^x \qquad \textbf{Eq. A.8}$$

For $i = j$

$$\nu_{ii}=\frac{4\sqrt{\pi}}{3}\sum_{i\neq j}^{s}n_jd_{ij}^2\chi_{ij}^{(0)}\mu_{ij}\sqrt{\frac{2T}{m}}(1+\alpha_{ij})\left(\frac{\theta_i+\theta_j}{\theta_i\theta_j}\right)^{1/2} \qquad \textbf{Eq. A.9}$$

For $i \neq j$

$$\nu_{ij}=-\frac{4\sqrt{\pi}}{3}n_id_{ij}^2\chi_{ij}^{(0)}\mu_{ij}\sqrt{\frac{2T}{m}}(1+\alpha_{ij})\left(\frac{\theta_i+\theta_j}{\theta_i\theta_j}\right)^{1/2} \qquad \textbf{Eq. A.10}$$

For $i = j$

$$\tau_{ii}=\frac{4\sqrt{\pi}}{15}\sqrt{\frac{2T}{m}}\Bigg\{n_id_i^2\chi_{ii}^{(0)}(2\theta_i)^{-1/2}(9-3\alpha_{ii})(1+\alpha_{ii})+2\sum_{j\neq i}^{s}n_j\chi_{ij}^{(0)}d_{ij}^2\mu_{ji}(1+\alpha_{ij})\theta_i^{3/2}\theta_j^{-1/2}$$
$$\left[6\beta_{ij}\theta_i^{-2}(\theta_i+\theta_j)^{-1/2}+\frac{(9-3\alpha_{ij})}{2}\mu_{ji}\theta_i^{-2}(\theta_i+\theta_j)^{1/2}+5\theta_i^{-1}(\theta_i+\theta_j)^{-1/2}\right]\Bigg\} \qquad \textbf{Eq. A.11}$$

For $i \neq j$

$$\tau_{ij}=\frac{8\sqrt{\pi}}{15}\sqrt{\frac{2T}{m}}n_i\chi_{ij}^{(0)}d_{ij}^2\mu_{ij}\theta_j^{3/2}\theta_i^{-1/2}(1+\alpha_{ij})\left[6\beta_{ij}\theta_j^{-2}(\theta_i+\theta_j)^{-1/2}\right.$$

$$+\frac{(9-3\alpha_{ij})}{2}\mu_{ji}\theta_j^{-2}(\theta_i+\theta_j)^{1/2}-5\theta_j^{-1}(\theta_i+\theta_j)^{-1/2}\Bigg] \quad \textbf{Eq. A.12}$$

$$\beta_{ij}=\mu_{ij}\theta_j-\mu_{ji}\theta_i \quad \textbf{Eq. A.13}$$

For $i=j$

$$\gamma_{ii}=\frac{16\sqrt{\pi}}{15}d_i^2 n_i\chi_{ii}^{(0)}\sqrt{\frac{2T}{m}}(2\theta_i)^{-1/2}(1+\alpha_{ii})\left[1+\frac{33}{16}(1-\alpha_{ii})\right]+\frac{2\sqrt{\pi}}{15}\sum_{j\neq i}^{s}n_j\chi_{ij}^{(0)}d_{ij}^2\sqrt{\frac{2T}{m}}\mu_{ji}(1+\alpha_{ij})$$
$$\left[\frac{\theta_i}{\theta_j(\theta_i+\theta_j)}\right]^{3/2}\left[E_{ij}-5\left(\frac{\theta_i+\theta_j}{\theta_i}\right)A_{ij}\right] \quad \textbf{Eq. A.14}$$

For $i\neq j$

$$\gamma_{ij}=-\frac{2\sqrt{\pi}}{15}n_i\chi_{ij}^{(0)}d_{ij}^2\sqrt{\frac{2T}{m}}\mu_{ij}(1+\alpha_{ij})\left[\frac{\theta_j}{\theta_i(\theta_i+\theta_j)}\right]^{3/2}\left[F_{ij}+5\left(\frac{\theta_i+\theta_j}{\theta_j}\right)C_{ij}\right] \quad \textbf{Eq. A.15}$$

For $i=1-s$ and $j=1-s$

$$E_{ij}=\frac{2\mu_{ji}}{\theta_i^2}(\theta_i+\theta_j)^2(2\alpha_{ij}^2-3\alpha_{ij}+4)\left[5\theta_i+8\theta_j\right]-\mu_{ji}(\theta_i+\theta_j)$$
$$\left\{\frac{\beta_{ij}}{\theta_i^2}\left[5\theta_i+8\theta_j\right]\left[14\alpha_{ij}-22\right]-\frac{\theta_j}{\theta_i}\left[20+3(15-7\alpha_{ij})+9(1-\alpha_{ij})-28\alpha_{ij}\right]-25(1-\alpha_{ij})\right\}$$
$$+18\frac{\beta_{ij}^2}{\theta_i^2}\left[5\theta_i+8\theta_j\right]+2\frac{\beta_{ij}}{\theta_i}\left[25\theta_i+66\theta_j\right]+5\frac{\theta_j}{\theta_i}\left[11\theta_i+6\theta_j\right]-\frac{5(\theta_i+\theta_j)\theta_j}{\theta_i^2}\left[5\theta_i+6\theta_j\right] \quad \textbf{Eq. A.16}$$

For $i=1-s$ and $j=1-s$

$$A_{ij}=5(2\beta_{ij}+\theta_j)+\mu_{ji}(\theta_i+\theta_j)\left\{5(1-\alpha_{ij})-\left[14\alpha_{ij}-22\right]\frac{\beta_{ij}}{\theta_i}\right\}+18\frac{\beta_{ij}^2}{\theta_i}$$
$$+2\mu_{ji}^2(2\alpha_{ij}^2-3\alpha_{ij}+4)\frac{(\theta_i+\theta_j)^2}{\theta_i}-5\frac{\theta_i}{\theta_j}(\theta_i+\theta_j) \quad \textbf{Eq. A.17}$$

For $i=1-s$ and $j=1-s$

$$C_{ij}=5(2\beta_{ij}-\theta_i)+\mu_{ji}(\theta_i+\theta_j)\left\{5(1-\alpha_{ij})+\left[14\alpha_{ij}-22\right]\frac{\beta_{ij}}{\theta_j}\right\}-18\frac{\beta_{ij}^2}{\theta_j}$$
$$-2\mu_{ji}^2(2\alpha_{ij}^2-3\alpha_{ij}+4)\frac{(\theta_i+\theta_j)^2}{\theta_j}+5(\theta_i+\theta_j) \quad \textbf{Eq. A.18}$$

For $i=1-s$ and $j=1-s$

$$F_{ij} = \frac{2\mu_{ji}^2}{\theta_j^2}(\theta_i+\theta_j)^2(2\alpha_{ij}^2-3\alpha_{ij}+4)\Big[8\theta_i+5\theta_j\Big]-\mu_{ji}(\theta_i+\theta_j)$$
$$\left\{\frac{\beta_{ij}}{\theta_j^2}\Big[8\theta_i+5\theta_j\Big]\Big[14\alpha_{ij}-22\Big]+\frac{\theta_i}{\theta_j}\Big[20+3(15-7\alpha_{ij})+9(1-\alpha_{ij})-28\alpha_{ij}\Big]+25(1-\alpha_{ij})\right\}$$
$$+18\frac{\beta_{ij}^2}{\theta_j^2}\Big[6\theta_i+5\theta_j\Big]-2\frac{\beta_{ij}}{\theta_j}\Big[66\theta_i+25\theta_j\Big]+5\frac{\theta_i}{\theta_j}\Big[6\theta_i+11\theta_j\Big]-\frac{5(\theta_i+\theta_j)}{\theta_j}\Big[6\theta_i+5\theta_j\Big] \qquad \textbf{Eq. A.19}$$

For $i = 1-s$

$$\bar{\lambda}_i = -\frac{5}{2}\frac{\rho}{T_i}\frac{n_iT_i^3}{Tm_i}\sum_{j=1}^{s}\left(\frac{\omega_{ij}-\xi^{(0)}\delta_{ij}}{n_jT_j}\right)D_j^T+\frac{5}{2}\frac{n_iT_i^2}{m_iT}+\frac{1}{6T}\sum_{j=1}^{s}2\pi n_in_j\mu_{ij}\chi_{ij}^{(0)}d_{ij}^3T_j(1+\alpha_{ij})$$
$$\left\{\frac{T_i}{m_i}\Big[5(\mu_{ij}^2-1)+(1-9\alpha_{ij})\mu_{ij}\mu_{ji}+(2+3\alpha_{ij}+6\alpha_{ij}^2)\mu_{ji}^2\Big]+6\frac{T_j}{m_j}\mu_{ji}^2(1+\alpha_{ij})^2\right\} \qquad \textbf{Eq. A.20}$$

For $i = j$

$$\omega_{ii} = \frac{4\sqrt{\pi}}{3\sqrt{2}}d_i^2n_i\chi_{ii}^{(0)}\sqrt{\frac{2T}{m}}\frac{(1-\alpha_{ii}^2)}{\theta_i^{1/2}}+\frac{4\sqrt{\pi}}{15}\sum_{j\neq i}^{s}n_j\chi_{ij}^{(0)}d_{ij}^2\sqrt{\frac{2T}{m}}\mu_{ji}(1+\alpha_{ij})\frac{\theta_i^{1/2}}{(\theta_i+\theta_j)^{1/2}\theta_j^{3/2}}A_{ij} \qquad \textbf{Eq. A.21}$$

For $i \neq j$

$$\omega_{ij} = \frac{4\sqrt{\pi}}{15}n_j\chi_{ij}^{(0)}d_{ij}^2\sqrt{\frac{2T}{m}}\mu_{ji}(1+\alpha_{ij})\frac{\theta_i^{1/2}}{(\theta_i+\theta_j)^{1/2}\theta_j^{3/2}}C_{ij} \qquad \textbf{Eq. A.22}$$

For $i = 1-s$ and $j = 1-s$

$$C_{ij}^T = -\frac{4\sqrt{\pi}}{3}n_in_j\left(\frac{2T}{m}\right)^{3/2}\frac{1}{(\theta_i+\theta_j)^{1/2}(\theta_i\theta_j)^{3/2}}\Big\{2\beta_{ij}^2+\theta_i\theta_j+(\theta_i+\theta_j)\Big[(\theta_i+\theta_j)\mu_{ij}\mu_{ji}+\beta_{ij}(1+\mu_{ji})\Big]\Big\}$$
$$-\sqrt{\pi}n_in_j\left(\frac{2T}{m}\right)^{3/2}(1-\alpha_{ij})(\mu_{ji}-\mu_{ij})\left(\frac{\theta_i+\theta_j}{\theta_i\theta_j}\right)^{3/2}\left[\mu_{ji}+\frac{\beta_{ij}}{(\theta_i+\theta_j)}\right] \qquad \textbf{Eq. A.23}$$

For $i = 1-s$ and $j = 1-s$

$$\bar{d}_{q,ij} = -\frac{5}{2}\frac{n_in_jT_i^3}{m_iT^2}\left\{\frac{m_j}{\rho T_i}\sum_{\ell=1}^{s}m_\ell\left(\frac{\omega_{i\ell}-\xi^{(0)}\delta_{i\ell}}{n_\ell T_\ell}\right)D_{\ell j}-\frac{2}{5}\frac{m_iT}{n_iT_i^3}\frac{\partial\xi^{(0)}}{\partial n_j}\lambda_i-\frac{1}{3T_i}\frac{\partial\ell n(T_i)}{\partial n_j}+\frac{1}{3T^2}\Big[S_1+S_2\Big]\right\} \qquad \textbf{Eq. A.24}$$

For $i = 1-s$ and $j = 1-s$

$$S_1 = \left[\delta_{\ell j}+\frac{1}{2}\left(n_\ell\frac{\partial\ell n\chi_{ij}^{(0)}}{\partial n_j}+I_{i\ell j}\right)\right]\pi\, m_in_in_\ell\chi_{i\ell}^{(0)}d_{i\ell}^3\mu_{\ell i}(1+\alpha_{i\ell})\Big\{[11\mu_{i\ell}^2+(13-9\alpha_{i\ell})\mu_{i\ell}\mu_{\ell i}$$

$$+(5+3\alpha_{i\ell}^2-3\alpha_{i\ell})\mu_{\ell i}^2]\frac{T_i^2}{m_i^2}+3\mu_{\ell i}^2(1+\alpha_{i\ell})^2\frac{T_\ell^2}{m_\ell^2}+[5\mu_{i\ell}^2+(1-9\alpha_{i\ell})\mu_{i\ell}\mu_{\ell i}$$

$$+(2+3\alpha_{i\ell}+6\alpha_{i\ell}^2)\mu_{\ell i}^2]\frac{T_iT_\ell}{m_im_\ell}-5\left(\frac{T_i}{m_i}+\frac{T_\ell}{m_\ell}\right)\frac{T_i}{m_i}\Bigg\} \qquad \textbf{Eq. A.25}$$

For $i = 1 - s$ and $j = 1 - s$

$$S_2=\frac{\partial\ell n(T_\ell/T)}{\partial\ell n(n_j)}\pi\ n_in_\ell\mu_{i\ell}\chi_{i\ell}^{(0)}d_{i\ell}^3T_\ell(1+\alpha_{i\ell})\Bigg\{\frac{T_i}{m_i}\Big[5(\mu_{i\ell}^2-1)+(1-9\alpha_{i\ell})\mu_{i\ell}\mu_{\ell i}+(2+3\alpha_{i\ell}+6\alpha_{i\ell}^2)\mu_{\ell i}^2\Big]$$

$$+6\frac{T_\ell}{m_\ell}\mu_{\ell i}^2(1+\alpha_{i\ell})^2\Bigg\} \qquad \textbf{Eq. A.26}$$

For $i = 1 - s$ and $j = 1 - s$

$$C_{ipj}^T=\frac{8\sqrt{\pi}}{3}n_in_p\left(\frac{2T}{m}\right)^{3/2}\frac{1}{(\theta_i+\theta_p)^{1/2}(\theta_i\theta_p)^{3/2}}$$

$$\left\{\delta_{jp}\beta_{ip}(\theta_i+\theta_p)-\frac{1}{2}\theta_i\theta_p\left[1+\frac{\mu_{pi}(\theta_i+\theta_p)-2\beta_{ip}}{\theta_p}\right]\frac{n_j}{T_p}\frac{\partial T_p}{\partial n_j}\right\}$$

$$+\frac{2\sqrt{\pi}}{3}n_in_p\left(\frac{2T}{m}\right)^{3/2}(1-\alpha_{ip})(\mu_{pi}-\mu_{ip})\left(\frac{\theta_i+\theta_p}{\theta_i\theta_p}\right)^{3/2}\left(\delta_{jp}+\frac{3}{2}\frac{\theta_i}{(\theta_i+\theta_p)}\frac{n_j}{T_p}\frac{\partial T_p}{\partial n_j}\right) \qquad \textbf{Eq. A.27}$$